Novel Developments of Brain-Computer Interfaces for Smart Home Control

Francisco Laport López

PhD Thesis UDC / 2022

Advisors: Adriana Dapena Janeiro
Paula María Castro Castro

PhD Program in Information Technology and Mobile Network Communication

UNIVERSIDADE DA CORUÑA

Novos Desenvolvementos de Interfaces Cerebro-Ordenador para o Control dun Fogar Intelixente

Francisco Laport López

Tese de Doutoramento UDC / 2022

Directoras: Adriana Dapena Janeiro
Paula María Castro Castro

Programa de Doutoramento en Tecnoloxías da Información e das Comunicacións en Redes Móbiles

Nuevos Desarrollos de Interfaces Cerebro-Ordenador para el Control de un Hogar Inteligente

Francisco Laport López

Tesis Doctoral UDC / 2022

Directoras: Adriana Dapena Janeiro
Paula María Castro Castro

Programa de Doctorado en Tecnologías de la Información y de las Comunicaciones en Redes Móviles

UNIVERSIDADE DA CORUÑA

Francisco Laport López

CERTIFICA / *CERTIFICA* / *CERTIFIES*

Que a presente memoria é o resultado do meu propio traballo de investigación e que o traballo doutros autores está citado axeitadamente.

Que la presente memoria es el resultado de mi propio trabajo de investigación y que el trabajo de otros autores está citado apropiadamente.

That the present report is the result of my own research work and that the work done by other authors is appropriately cited.

A Coruña, 13 de outubro de 2021 / *13 de octubre de 2021* / *October 13, 2021*.

Francisco Laport López

Adriana Dapena Janeiro
Paula María Castro Castro

CERTIFICAN / *CERTIFICAN* / *CERTIFY*

Que a presente tese titulada "Novos desenvolvementos de interfaces cerebro-ordenador para o control dun fogar intelixente" foi realizada por Francisco Laport López baixo a nosa dirección no Departamento de Enxeñaría de Computadores da Universidade da Coruña e preséntase para obter o grao de Doutor con Mención Internacional.

Que la presente tesis titulada "Nuevos desarrollos de interfaces cerebro-ordenador para el control de un hogar inteligente" fue realizada por Francisco Laport López bajo nuestra dirección en el Departamento de Ingeniería de Computadores de la Universidade da Coruña y se presenta para obtener el grado de Doctor con Mención Internacional.

That the present thesis titled "Novel developments of brain-computer interfaces for smart home control" was done by Francisco Laport López under our supervision in the Department of Computer Engineering at the University of A Coruña and it is submitted to obtain the Ph.D. degree with International Mention.

As directoras da tese / *Las directoras de la tesis* / *The Ph.D. supervisors*.
A Coruña, 13 de outubro de 2021 / *13 de octubre de 2021* / *October 13, 2021*.

Dra. Adriana Dapena Janeiro
Catedrática de Universidade
Dpto. de Enxeñaría de Computadores
Universidade da Coruña

Full Professor
Dept. of Computer Engineering
University of A Coruña

Dra. Paula María Castro Castro
Prof. Contratada Doutora
Dpto. de Enxeñaría de Computadores
Universidade da Coruña

Ph.D. Associate Professor
Dept. of Computer Engineering
University of A Coruña

Tese de Doutoramento / *Tesis Doctoral / Doctoral Thesis*

Título:	Novos desenvolvementos de interfaces cerebro-ordenador para o control dun fogar intelixente
***Título*:**	*Nuevos desarrollos de interfaces cerebro-ordenador para el control de un hogar inteligente*
***Title*:**	*Novel developments of brain-computer interfaces for smart home control*
Autor / *Autor* / *Author*:	Francisco Laport López
Directores / *Directores* / *Supervisors*:	Adriana Dapena Janeiro Paula María Castro Castro
Data / *Fecha* / *Date*:	xaneiro de 2022 / *enero de 2022* / *January 2022*

Tribunal / *Tribunal / Evaluation Committee*

Presidente / *Presidente* / *President*:	Begoña García-Zapirain Soto
Vogal / *Vocal* / *Member*:	Sérgio Ivan Fernandes Lopes
Secretario / *Secretario* / *Secretary*:	Francisco Javier Vázquez Araújo

Acknowledgements

First of all, I would like to thank my two thesis supervisors, Adriana and Paula. Without your dedication, time, ideas and initiative this work would not have been possible. You have always had time and kind words to assist me, guide me and support me, which is of great importance for a novice researcher like me. For all this, my sincere thanks.

I would also like to thank Luis Castedo for giving me the opportunity to belong to the GTEC and supporting my research work and thesis during all these years.

I want to especially thank Dr. Vicente Zarzoso from the Université Côte d'Azur for allowing me to work with him and the great team at I3S. My research stay was a great experience, both academically and personally, so thank you very much for giving me that opportunity.

I would also like to thank Fran, Óscar and Dani for their help and collaboration in the work developed over these years. I have learned a lot from you and without your help this thesis would not have been possible either. Of course, I am not forgetting the rest of the GTEC colleagues, with whom I have shared wonderful moments and have made this whole journey more bearable.

Finally, I want to thank my family for their unconditional support throughout my life. I also want to remember my friends, who have accompanied and helped me during all these years, either being close or from a distance. In particular, I want to thank my partner, Ale, who has always had the right words to advise and encourage me. She has lived through all the good and bad moments of this trip, always with kind words and a positive look. Since we were teenagers, you have supported and inspired me to get here, so sincerely, thank you, I dedicate this thesis to you.

This thesis has been funded by the Xunta de Galicia and the European Social Fund by the predoctoral grant No. ED481A-2018/156.

Resumo

Neste traballo analizamos e desenvolvemos novas Interfaces Home-Máquina (HMI) que faciliten a comunicación e a interacción de persoas que sofren problemas motrices severos, coa súa contorna e dispositivos cotiáns a través dun fogar intelixente. Unha casa intelixente pode definirse coma unha residencia equipada cunha rede de comunicación, sensores, dispositivos e electrodomésticos que os residentes poden controlar, acceder e monitorar de forma remota para satisfacer as súas necesidades da vida diaria. Representa un sistema sensible ao contexto que, utilizando tecnoloxías coma Internet das cousas (IoT) e técnicas de intelixencia artificial, pode detectar, anticipar e responder ás actividades no fogar.

As HMI ofrecen novas canles de comunicación que permiten aos seus usuarios interactuar con dispositivos da súa contorna empregando os sinais biolóxicos provenientes de diferentes partes do seu corpo como comandos de control. É dicir, os sinais producidos polo cerebro, os músculos ou os ollos, por exemplo, poden empregarse para controlar dispositivos externos. Por tanto, a combinación destas interfaces cun fogar intelixente resulta unha tecnoloxía de gran utilidade para persoas con discapacidades motrices severas ou lesións graves nas súas extremidades, xa que lles permite interactuar coa súa contorna ou controlar partes danadas do seu corpo sen necesidade de grandes movementos físicos.

Unha ampla variedade de sinais biolóxicos pode ser empregada para interactuar coas HMI. O uso de cada unha delas dependerá do obxectivo da interface e das capacidades motrices que posúa o usuario. Os tres tipos máis comúns de sinais biolóxicos son: musculares, oculares e cerebrais. A tese presentada céntrase principalmente na análise e desenvolvemento de interfaces baseadas nos sinais cerebrais, tamén coñecidas como Interfaces Cerebro-Ordenador (BCI) ou Interfaces Cerebro-Máquina (BMI). Este tipo de interfaces captura os sinais biolóxicos producidos pola actividade neuronal do usuario a través de técnicas non invasivas como a Electroencefalografía (EEG) e tradúceas en comandos de control para dispositivos externos. Por tanto, estas ofrecen unha nova canle de comunicación coa contorna que non necesita de ningún movemento muscular, simplemente utiliza os pensamentos do usuario.

Durante os últimos anos, varios traballos propuxeron diferentes interfaces BCI que ofrecen resultados precisos e de boa calidade. Con todo, a maioría deles usan dispositivos clínicos moi caros e con numerosos eléctrodos para capturar os sinais cerebrais. Isto pode resultar incómodo para os usuarios e provocar que as interfaces sexan difíciles de usar, polo que no noso traballo centrámonos en desenvolver interfaces BCI de baixo custo que empreguen dispositivos abertos cun número reducido de eléctrodos.

Como primeira proposta, presentamos unha arquitectura que integra unha aplicación BCI nunha contorna de IoT para o control dunha casa intelixente. Para este propósito, desenvolvemos un dispositivo EEG aberto e de baixo custo que captura sinais cerebrais de dúas canles de entrada. Facendo uso unicamente dunha canle, propoñemos e comparamos distintos algoritmos de extracción de características baseados en Transformadas Deslizantes (ST) para determinar o estado ocular do usuario, é dicir, ollos abertos (oE) ou ollos pechados (cE). En primeiro lugar, comparamos transformadas reais e

complexas. Posteriormente, consideramos xanelas deslizantes con solapamento en lugar de empregar o enfoque tradicional con xanelas non solapadas, reducindo así o atraso entre a adquisición do sinal e a toma de decisión. Os algoritmos inclúen diferentes configuracións orientadas a proporcionar resultados precisos con baixa carga computacional. Ademais, realizamos unha extensión da arquitectura onde os datos de ambas as canles son empregados conxuntamente para construír un conxunto de características bidimensional que proporcione resultados máis robustos e precisos. Con este propóstito, as técnicas empregadas anteriormente para extraer as características son comparadas con outras estratexias comunmente utilizadas nas aplicacións BCI, como a Transformada Discreta Wavelet (DWT). Ademais, comparamos tres algoritmos de clasificación diferentes, un baseado en limiares, e outros dous baseados na Análise Discriminante Lineal (LDA) e nas Máquinas de Vectores de Soporte (SVM).

A segunda proposta do noso traballo é unha HMI para o control dun fogar intelixente empregando un dispositivo de gravación de sinais biolóxicos dunha única canle. O potencial evocado P300 e os movementos das pálpebras son comparados como sinais de control, co obxectivo de determinar cal deles ofrece os mellores resultados en termos de precisión e tempos de resposta. Os elementos do fogar que o usuario pode controlar coa HMI son presentados nunha Interface Gráfica de Usuario (GUI). Os devanditos elementos son amosados seguindo dous paradigmas distintos de estimulación: 1) os elementos son presentados un a un ou 2) todos os elementos dunha mesma fila/columna son presentados conxuntamente. Ambas as interfaces, a baseada no potencial P300 ou a baseada en movementos das pálpebras, empregan unha única canle de entrada do mesmo dispositivo EEG para capturar a actividade cerebral/ocular do usuario. Ademais, a GUI é totalmente configurable, polo que pode adaptarse ás necesidades do usuario.

Resumen

En este trabajo analizamos y desarrollamos nuevas Interfaces Hombre-Máquina (HMI) que faciliten la comunicación y la interacción de personas que sufren problemas motrices severos con su entorno y dispositivos cotidianos a través de un hogar inteligente. Un hogar inteligente puede definirse como una residencia equipada con una red de comunicación, sensores, dispositivos y electrodomésticos que los residentes pueden controlar, acceder y monitorizar de forma remota para satisfacer sus necesidades de la vida diaria. Representa un sistema sensible al contexto que, utilizando tecnologías como Internet de las cosas (IoT) y técnicas de inteligencia artificial, puede detectar, anticipar y responder a las actividades en el hogar.

Las HMI ofrecen nuevos canales de comunicación que permiten a sus usuarios interactuar con dispositivos de su entorno empleando las señales biológicas provenientes de diferentes partes de su cuerpo como comandos de control. Es decir, las señales producidas por el cerebro, los músculos o los ojos, por ejemplo, pueden emplearse para controlar dispositivos externos. Por lo tanto, la combinación de estas interfaces con un hogar inteligente resulta una tecnología de gran utilidad para personas con discapacidades motrices severas o lesiones graves en sus extremidades, ya que les permite interactuar con su entorno o controlar partes dañadas de su cuerpo sin necesidad de grandes movimientos físicos.

Una amplia variedad de señales biológicas pueden ser empleadas para interactuar con las HMI. El uso de cada una de ellas dependerá del objetivo de la interfaz y de las capacidades motrices que posea el usuario. Los tres tipos más comunes de señales biológicas son: musculares, oculares y cerebrales. La tesis presentada se centra principalmente en el análisis y desarrollo de interfaces basadas en las señales cerebrales, también conocidas como Interfaces Cerebro-Ordenador (BCI) o Interfaces Cerebro-Máquina (BMI). Este tipo de interfaces capturan las señales biológicas producidas por la actividad neuronal del usuario a través de técnicas no invasivas como la Electroencefalografía (EEG) y las traduce en comandos de control para dispositivos externos. Por lo tanto, estas ofrecen un nuevo canal de comunicación con el entorno que no necesita de ningún movimiento muscular, simplemente utiliza los pensamientos del usuario.

Durante los últimos años, varios trabajos han propuesto diferentes interfaces BCI que ofrecen resultados precisos y de buena calidad. Sin embargo, la mayoría de ellos usan dispositivos clínicos muy caros y con numerosos electrodos para capturar las señales cerebrales. Esto puede resultar incómodo para los usuarios y provocar que las interfaces sean difíciles de usar, por lo que en nuestro trabajo nos centramos en desarrollar interfaces BCI de bajo coste que empleen dispositivos abiertos con un número reducido de electrodos.

Como primera propuesta, presentamos una arquitectura que integra una aplicación BCI en un entorno de IoT para el control de una casa inteligente. Para este propósito, hemos desarrollado un dispositivo EEG abierto y de bajo coste que captura señales cerebrales de dos canales de entrada. Haciendo uso únicamente de un canal, proponemos y comparamos distintos algoritmos de extracción

de características basados en transformadas deslizantes (ST) para determinar el estado ocular del usuario, es decir, ojos abiertos (oE) u ojos cerrados (cE). En primer lugar, comparamos transformadas reales y complejas. Posteriormente, consideramos ventanas deslizantes con solapamiento en lugar de emplear el enfoque tradicional con ventanas no solapadas, reduciendo así el retraso entre la adquisición de la señal y la toma de decisión. Los algoritmos incluyen diferentes configuraciones orientadas a proporcionar resultados precisos con baja carga computacional. Además, realizamos una extensión de la arquitectura donde los datos de ambos canales son empleados conjuntamente para construir un conjunto de características bidimensional que proporcione resultados más robustos y precisos. Con este propóstito, las técnicas empleadas anteriormente para extraer las características son comparadas con otras estrategias comúnmente utilizadas en las aplicaciones BCI, como la Transformada Discreta Wavelet (DWT). Además, comparamos tres algoritmos de clasificación diferentes, uno basado en umbrales, y otros dos basados en el Análisis Discriminante Lineal (LDA) y en las Máquinas de Vectores de Soporte (SVM).

La segunda propuesta de nuestro trabajo es una HMI para el control de un hogar inteligente empleando un dispositivo de grabación de señales biológicas de un único canal. El potencial evocado P300 y los parpadeos son comparados como señales de control, con el objetivo de determinar cuál de ellas ofrece los mejores resultados en términos de precisión y tiempos de respuesta. Los elementos del hogar que el usuario puede controlar con la HMI son presentados en una interfaz gráfica de usuario (GUI). Dichos elementos son mostrados siguiendo dos paradigmas distintos de estimulación: 1) los elementos son presentados uno a uno o 2) todos los elementos de una misma fila/columna son presentados conjuntamente. Ambas interfaces, la basada en el potencial P300 o la basada en parpadeos, emplean un único canal de entrada del mismo dispositivo EEG para capturar la actividad cerebral/ocular del usuario. Además, la GUI es totalmente configurable, por lo que puede adaptarse a las necesidades del usuario.

Abstract

In this work, we analyze and develop new Human-Machine Interfaces (HMIs) that can help the communication and interaction of people who suffer from motor or neurological damages, with their environment and daily life devices working through a smart-home system. A smart home can be defined as a residence equipped with a communication network, connected sensors, devices, and appliances that can be controlled, accessed and monitored remotely by the residents in order to satisfy their daily life needs. It represents a context-aware system that, using technologies such as Internet of Things (IoT) and artificial intelligence algorithms, can sense, anticipate and respond to activities in the home.

The HMIs offer new communication channels to interact with outer devices where the electrical signals coming from different parts of the human body, such as the brain, muscles or the eyes, can be used as control commands. Therefore, the integration of these interfaces into a smart-home system, results in an extremely useful technology for patients with severe motor disabilities or serious injuries in their limbs, since it allows them to interact with their environment or control damaged parts of their bodies without the need for large physical movements.

A wide variety of biological signals can be used to interact with HMIs. The use of each of them will depend on the objective of the interface and the motor skills that the user possesses. The three most common types of biological signals are: muscular signals, ocular signals and brain signals. The presented thesis is mainly focused on the analysis and development of interfaces based on brain signals, which are also known as Brain-Computer Interface (BCI) or Brain-Machine Interface (BMI). This kind of interfaces captures the biological signals produced by the neural activity of the user's brain, through non-invasive techniques such as Electroencephalography (EEG), and translates them into commands for external devices. Thus, they offer a new communication channel with the environment without using muscle movements, but just employing the user's thoughts.

During the last decades, several works have proposed different BCI interfaces that offer accurate and good quality results. However, most of them use expensive clinical devices and numerous electrodes to capture brain signals. This can be uncomfortable for users and make the interfaces difficult to use, so in our work we focus on developing low-cost BCI systems that employ open devices with a small number of electrodes.

As a first approach, we propose an architecture for integrating a BCI application in an IoT environment for home automation. For this purpose, we develop a low-cost open-source EEG device which acquires EEG signals from two input channels. Using the EEG data of only one channel, we propose and compare different feature extraction algorithms based on Sliding Transforms (STs) techniques for determining the user's eye states, i.e., open eyes (oE) or closed eyes (cE). Firstly, we compare real-valued and complex-valued transforms. Secondly, we consider sliding windows with overlap instead of using the traditional approach with non-overlapped windows, thus reducing the delay time between acquisition and decision. The algorithms include different configurations oriented

to provide accurate results with a low computational burden. After that, we extended the study to the situation where the data captured by both channels are jointly employed in order to build a two-dimensional feature set that may provide higher and more robust results. To this end, we compare the previously analyzed feature extraction techniques with other strategies commonly used in BCI applications, such as Discrete Wavelet Transform (DWT). We compare three classification techniques, one based on a threshold classifier and another two that implement the well known Linear Discriminant Analysis (LDA) and Support Vector Machine (SVM) algorithms.

As a second approach, we propose an HMI for environmental control using a single-channel recording system. The P300 potential and eye blinks are compared as control signals in order to determine which one offers the best performance in terms of accuracy and response time. The home elements to be controlled are displayed in a Graphical User Interface (GUI) following a matrix-form and presented to users using two different stimulation paradigms: 1) home elements are intensified one by one or 2) all the elements of the same row/column are jointly intensified at the same time. Both interfaces, P300-based or blink-based, employ only one input channel of the same EEG device to capture the brain/eye user's activity. The GUI is fully configurable, so it can be adapted to the user's needs.

Table of Contents

List of Figures

List of Tables

Chapter I

Introduction

In this first chapter of the thesis, we introduce several basic concepts that might be of interest to the reader and make the reading of the document more enjoyable. In addition, we describe and analyze the motivations that led us to develop this research work and the objectives we wanted to achieve with it. The structure of the thesis is also presented at the end of the chapter.

1.1 Motivation

A smart home can be defined as a residence equipped with a communication network, connected sensors, devices, and appliances that can be controlled, accessed and monitored remotely by the residents in order to satisfy their daily life needs [1]. It represents a context-aware system that, using technologies such as the Internet of Things (IoT) and artificial intelligence algorithms, can sense, anticipate and respond to activities in the home. Smart-home environments offer useful tools for the elderly or people suffering from motor disabilities, since these systems can be easily programmed to switch the lights on or off, control the doors or adjust the thermostat without large physical movements and efforts.

In order to improve the quality of life of people affected by motor diseases, several Human-Machine Interfaces (HMIs) based on bio-electrical signals have been proposed. These interfaces offer new communication channels to interact with outer devices, where the electrical signals coming from different parts of the human body can be used as control commands [2]. That is, the signals produced by the brain, the muscles or the eyes, for example, can be used for controlling external devices such as wheelchairs [3], virtual keyboards [4] or hand prosthesis [5], among others. Therefore, it results in an extremely useful technology for patients with severe motor disabilities or serious injuries in their limbs, since it allows them to interact with their environment or control damaged parts of their bodies without the need for large physical movements.

In this PhD thesis, we analyze and develop new HMIs that can facilitate the communication and interaction of people who suffer from motor diseases with their environment and daily life

devices working through a smart-home system.

1.2 Human-Machine Interface

A wide variety of biological signals can be used to interact with HMIs. The use of each of them will depend on the objective of the interface and the motor skills that the user possesses. Figure 1.1 shows the muscular capacities required by HMIs based on the three most common types of biological signals: muscular signals, ocular signals and brain signals [2]. For a muscular-based HMI, the user must retain some degree of muscle control, e.g., neck muscle control, eyebrow control, chewing control, etc. In the case of ocular-based interfaces, the user should have control of the eyeball and, if possible, the eyelids. In contrast, HMIs based on brain signals do not require the user to retain any muscle control, as the interaction will be through brain activity. Hence, this type of interfaces are the most powerful, since they cover all types of users. However, brain signals are difficult to process and capture due to their low amplitude level, which makes them hard to identify from external noise and artifacts. Thus, if the user is capable of generating voluntary muscular or ocular signals, these should be adopted by the HMI. The following sections describe these bio-electrical signals in more detail and introduce HMIs based on them.

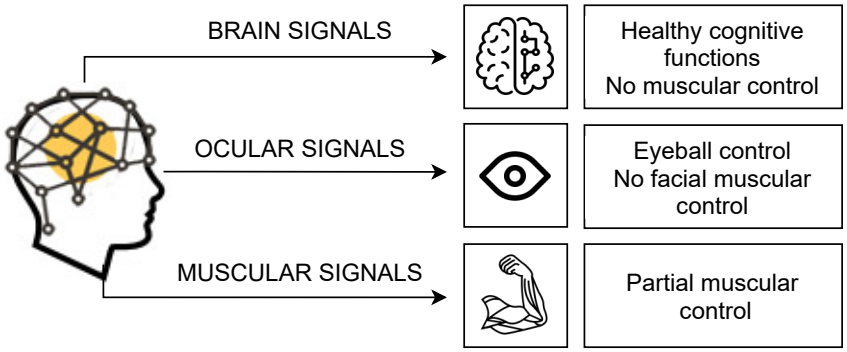

Figure 1.1: Bio-electrical signals for controlling an HMI and the corresponding levels of muscular control [2].

1.2.1 Muscular Signals

When we move any part of our body, different combinations of muscle contractions are produced. In this process, in order to achieve the intended movement, the muscle tissue conducts electrical activity, named muscle action potential, in a similar way to how nerves do. The Electromyography (EMG) technique captures this electrical activity produced by the activation of the motor units associated with the contraction of the muscles. Each of these contractions generates different patterns of shapes and firing rates in the muscle action potentials. Hence, if the appropriate signal processing techniques and pattern recognition

algorithms are applied, different muscle movements can be differentiated and, consequently, the user's intention can be recognized [6].

Analysis and detection of EMG signals is becoming a very important field in clinical diagnosis and biomedical applications. It can play a very important role in areas such as motor disabilities rehabilitation, motor function restoration using prosthesis, interaction with the environment and external devices through HMIs, etc. For this purpose, the system must recognize the user's intention by differentiating the distinct electrical patterns generated by the different muscle contractions [7]. In this sense, each detected muscle movement corresponds to an order sent by the user to the HMI. Then, the interface interprets this order and executes the corresponding action in the device.

In the last decades, several works have analyzed and processed the EMG signals for creating a new communication path that employs the electrical activity produced by the muscle contraction as control commands for external devices [8]. In this regard, Shenoy et al. [9] proposed an EMG-based system for controlling a robotic arm using the forearm muscles. This approach is a useful solution for patients that have lost part of their extremities due to amputation or those that are partially paralyzed, allowing them to recover some motor functionalities. EMG-based HMIs can be also useful for subjects that present a significant loss of motor functions. Williams et al. [10], for example, present an HMI intended for users with high levels of tetraplegia for controlling a computer mouse. In this case, the EMG signals from the user's neck and face were used for interacting with the HMI. Moreover, EMG signals have been also applied for controlling a wheelchair using, for example, the forehead muscles [11]. In a more recent study, Gomez-Gil et al. [8] proposed to use the EMG signals captured from the jaw combined with eye movements for steering a farm tractor.

1.2.2 Ocular Signals

Ocular activity can be also measured as an electrical signal using the Electrooculography (EOG) technique. The eye can be modelled as a dipole with its positive pole at the cornea and its negative pole at the retina [12]. Therefore, when moving the eyes (vertically or horizontally) it causes a change in the dipole orientation and a subsequent change in the electric potential field measured by the EOG. These changes can be detected by a classification algorithm. Thus, voluntary eye movements such as blinking, saccades or fixation can also be used as control signals in different HMIs for interacting with external devices. For this purpose, each voluntary eye movement (or combination of movements) is interpreted by the system as an order, therefore, when it occurs, the HMI executes a command action in the corresponding device.

As previously mentioned in Figure 1.1, for the proper operation of an EOG-based interface, the user must retain, at least, control of the eyeballs. In some cases, it could also be required a conscious control over blinking movements. Therefore, these types of interfaces are suitable

when the user has almost completely lost muscle control but still preserves voluntary and unrestricted control over ocular movements.

Several HMIs have been proposed during the last decades using EOG signals for its interaction. In this regard, Deng et al. [13] proposed a multi-purpose EOG-based HMI where different eye movements (horizontal and vertical) were detected by the system to control, for example, a TV view by shifting the channels or adjusting the volume. EOG signals can be also employed for communication purposes. He et al. [14] presented an EOG-based HMI that allows users to spell by only blinking. Forty characters were displayed to the subjects, which were randomly flashed. In order to select a character, the subject should blink as the target character is flashed. In this way, subjects who have suffered speech loss can communicate with the external environment through the interface. Also employing eye-movements and the generated EOG signal, Barea et al. [15] designed a system for controlling and guiding an electric wheelchair. The users of the system could adjust the direction and speed of the wheelchair only by the movement of the eyes.

1.2.3 Brain Signals

The neuronal activity of a subject and the different activation patterns of their neurons when performing different mental tasks can also be used to control an HMI. This type of interfaces captures the biological signals produced by the neural activity of the user's brain and translates them into commands for external devices [16]. Therefore, as described in Figure 1.1, these interfaces offer a new communication channel with the environment without using muscle movements but just employing the user's thoughts. Hence, it results in an extremely useful tool for people suffering from severe motor disabilities that have lost all motor functions, such as those affected by advanced stages of Amyotrophic Lateral Sclerosis (ALS) or high levels of tetraplegia, for example. The presented thesis is mainly focused on the analysis and development of this kind of interfaces, which are also known as Brain-Computer Interface (BCI) or Brain-Machine Interface (BMI).

Electroencephalography (EEG) is the most widely used technique for neuroimaging and brain signal acquisition for BCIs. This preference is mainly based on the non-invasive character of this technology, which implies a low risk for the users. Moreover, it shows several advantages such as its high portability and temporal resolution, its relatively low cost, and its ease of use [17]–[19]. This technique captures the electrical signals produced by the neural activity by placing electrodes in the user's scalp. The brain activity collected by the EEG encodes the users' intentions, which are translated into control actions for outer devices.

Several brain signal patterns have been assessed as control signals in a BCI. The most common signals are: Visual Evoked Potential (VEP), which appears as a user's response to external visual stimulation; Slow Cortical Potential (SCP), which are low frequency potentials that can be modulated by the user to control the BCI; P300 Evoked Potential (EP), which is

a positive deflection that occurs in the EEG activity 300 ms after an infrequent or surprising auditory, visual or somatosensory stimuli; and sensorimotor rhythms, which can be modulated by the user when performing Motor Imagery (MI) tasks, i.e., when the user just imagines performing a movement but no real movement is performed.

During the last decades, BCI systems have become a very active research field with significant advances and implementations in clinical and in non-clinical areas. For instance, a widely known BCI for communication purposes is the P300 speller proposed by Farwell and Donchin [4], which employs the P300 EP for controlling a virtual keyboard. Birbaumer et al. also proposed a BCI for communication, but in this case using SCPs as control signals [20]. These interfaces have been also applied for motor restoration. Pfurtscheller et al. [21] proposed to restore hand grasp function using an electrical driven hand orthosis fitting the left hand of a tetraplegic patient. For this purpose, sensorimotor rhythms produced by MI tasks were analyzed. These MI signals have also been employed for building an assisting BCI to allow disabled persons to interact with basic domestic appliances such as the TV, a door opener, etc.

The interest in the study of these interfaces is not restricted to academia, but large companies such as Neuralink [22] or Facebook [23] are also investing and supporting the development of new BCIs.

1.3 Objectives

The general objective of this thesis is to contribute to the BCI research field by proposing new developments based on open solutions including both hardware and software in order to make this technology accessible and usable by anyone who needs it for improving its quality of life. To achieve this general goal, we have accomplished more specific objectives:

- Study the physiology of the human brain and the different types of EEG signals that can be used as control signals by a BCI.
- Review the hardware devices that are currently being used in the BCI systems for capturing the cerebral activity.
- Study the signal processing techniques, feature extraction methods and classification algorithms that can be applied in the BCI field for obtaining a reliable system.
- Develop low-cost and open hardware devices for capturing the brain activity.
- Develop HMI systems that use a limited number of electrodes to ensure user comfort and system usability.
- Compare the obtained results using the proposed devices with those achieved by commercial systems.

1.4 Thesis Overview

This thesis is organized as follows:

In Chapter 2, we introduce the concept of BCI, performing an analysis of its components, studying the brain structure and neuronal activities on which it is based, and reviewing its implementation in different domains.

In Chapter 3, the EEG technique is introduced and analyzed, by going over electrode locations, EEG brain rhythms, signal artifacts and the different control signals that can be used for controlling a BCI. In addition, different low-cost devices available on the market are reviewed and compared. We analyze the advantages and drawbacks of each device and its suitability for different applications.

Once the EEG signals have been captured by the hardware devices, they need to be analyzed and processed for their posterior classification and subsequent translation into a control command for an external device. Chapter 4 describes several techniques for signal processing and classification. We study different feature extraction methods based on both frequency and time domain, and we also analyze distinct classification algorithms widely known in the BCI filed.

Based on previous techniques and devices, in Chapter 5, we present an architecture for integrating a BCI application in an IoT environment for home automation. For this purpose, we develop a low-cost open-source EEG device which acquires EEG signals from two input channels. We propose and compare different algorithms for determining the user's eye states from only one channel, i.e., open eyes (oE) or closed eyes (cE). The algorithms include different configurations oriented to provide high accurate results with a low computational burden.

After that, in Chapter 6, we extend the study to the situation where the data captured by both channels is employed together in order to build a two-dimensional feature set that may provide higher and more robust results. To this end, we compare the previously analyzed feature extraction techniques with other strategies commonly used in BCI applications, such as the Discrete Wavelet Transform (DWT). At the same time, results obtained with one and two channel data are also compared.

On the other hand, in Chapter 7, we present an HMI for environmental control using a single-channel recording system. The P300 EP and eye blinks are compared as control signals in order to determine which one offers the best performance in terms of accuracy and response time. For this purpose, we developed a Graphical User Interface (GUI) that presents the home elements the user can control. In addition, two stimulation paradigms are also compared.

Finally, the last chapter is devoted to the conclusions and future work.

Chapter II

Brain-Computer Interfaces

Brain-Computer Interface (BCI), also known as Brain-Machine Interface (BMI) [24], can be defined as the combination of hardware and software of a communication system that monitors the cerebral activity of the user and translates certain characteristics, corresponding to user's intentions, to commands for device control [16]. BCI presents a new communication channel with outer devices without involvement of peripheral nerves and muscles, where users can interact with the environment without any physical activity, just using their thoughts.

BCI technology can be implemented in a wide variety of domains, but its most relevant application is to provide useful tools and solutions to people with motor disabilities. Such disabilities include neuromuscular injuries and neurodegenerative diseases such as Amyotrophic Lateral Sclerosis (ALS) and cerebral palsy in which there is a trauma in the brain or the spinal cord, or people suffering from amputations or muscle deformations. In these cases, direct communication with external devices, e.g., a computer using keyboard and mouse, is not possible, so the BCI provides particular hardware and software for the recognition of user's thoughts and intentions that allows the communication with the device [25], [26].

The BCI history began with the German scientist Hans Berger, who discovered in the 1920s that brain activity produced electrical currents. Moreover, he proved that the fluctuation of these currents could be recorded with electrodes placed on the scalp of the subjects, leading to the first Electroencephalography (EEG) experiment [27]. This new technique proved to be a very useful tool for the study and analysis of cognitive functions and to understand or diagnose different neuropathologies. This growth of the EEG promoted the idea that brain activity could also be used as a new channel of communication [28]. In the 1960s, Kamiya carried out several studies [29] where demonstrated that some features of the brain waves (alpha waves were used in his study) could be controlled by the subjects after some training. This was the beginning of neurofeedback, where users are trained to self-regulate their brain activity through real-time feedback. Moreover, also in the 1960s, Thelma Estrin, from the Brain Research Institute at UCLA, suggested an important idea for the development of BCIs in her paper "On-line electroencephalographic digital computing system" [30]. She described that for the "electroencephalographer the input device must be able to digitize its signals continuously

and transmit them immediately to the computer", exactly formulating the requirements for an online BCI [31]. Finally, in 1973, Jacques J. Vidal, also at UCLA, coined the term "Brain-Computer Interface" in his seminal paper "Toward direct brain-computer communication" [32]. In this study, Vidal outlined the necessary elements to build a working BCI and described BCIs as "utilizing the brain signals in a man-computer dialogue" and "as a mean of control over external processes such as computers or prosthetic devices" [31]. The concepts, ideas and vision presented at that time are still followed and studied by current research works [28].

BCI research has traditionally been restricted to laboratories and clinical environments for the analysis of neurological diseases or the study of brain functions. Furthermore, BCI applications required reliable data and real-time signal processing techniques, and up until a few years, such devices and algorithms were not available or were highly expensive. Therefore, it was considered too complex and unattractive for serious scientific investigation [18]. However, during the last two decades, BCI has become an active field of research not only restricted to a clinical environment or laboratories. Several companies and research centres have shown their interest in this promising technology. Twenty years ago, BCI research was developed for six to eight research groups but, nowadays, there are more than 116 groups and 76 companies working in this field [19], [33], [34]. This has promoted important advances on neural interfaces, such as the development of low-cost and open-source hardware and software, which has facilitated its entry in a large variety of out-of-the-lab areas, from BCI-based video games [35] to robotic limbs control [36].

Despite all these advances achieved in the last years, BCI technology must face and solve several challenges to become a more usable and reliable tool for users [37]. Such challenges include aspects related to the need of reducing the training periods, to the test of applications under non-controlled environments or to the production of ready-to-use devices that can monitor the brain activity of the user during daily life activities without causing discomfort [17].

In order to better understand BCIs, in this chapter some basic neural functions and neurophysiological properties of the brain are reviewed. In addition, BCI components and their practical applications are also presented.

2.1 Brain Structure and Neural Activities

In order to have a better understanding of the BCIs, it is important to comprehend the human brain and how it works. Human brain is the main organ of the nervous system and it is responsible for controlling the hole human body and its functionalities. It receives external information through the five senses (smell, sight, touch, taste and hearing), sent by the body internal systems, and analyzes all this data to accurately control the body parts such as legs, hands, etc.

The brain can be divided into two general parts: the cerebral cortex and the subcortical regions. Each part of the brain is responsible for performing a different function. Subcortical

regions are in charge of controlling unconscious and vital tasks such as heart rate, breathing, reflexes or emotional responses. Conversely, cerebral cortex is responsible for performing higher level functions such as language processing, memory, attention or learning [19].

The cerebral cortex is also divided into two hemispheres: the right and the left one. The left hemisphere is associated to mathematical and sequential thinking, writing and speaking abilities and is responsible for motor control of the right side of the body. On the other hand, the right hemisphere is related to emotions, creativity, spatial ability and the motor control of the left side of the body. At the same time, the cerebral cortex is also portioned into four lobes, as depicted in Figure 2.1, which are symmetrically distributed in both hemispheres. Each lobe handles specific tasks:

- **Frontal lobe:** it is the biggest lobe in the human brain. It controls our behavior and personality and is responsible for thinking, language, problem solving and concentration. In the border with the parietal lobe, it houses the motor cortex, which is in charge of voluntary motor tasks.
- **Parietal lobe:** it contains the somatosensory cortex in the border with the frontal lobe, so it plays an important role in the processing of sensory information coming from different parts of the body. It processes the data from sensory skin inputs such as touch, pain or temperature.
- **Temporal lobe:** it contains the primary auditory cortex, which is responsible for hearing and language comprehension. Moreover, it contains the hippocampus, which is related to memory and the control and management of emotions.
- **Occipital lobe:** it houses the visual cortex, so it is in charge of visual perception and image interpretation.

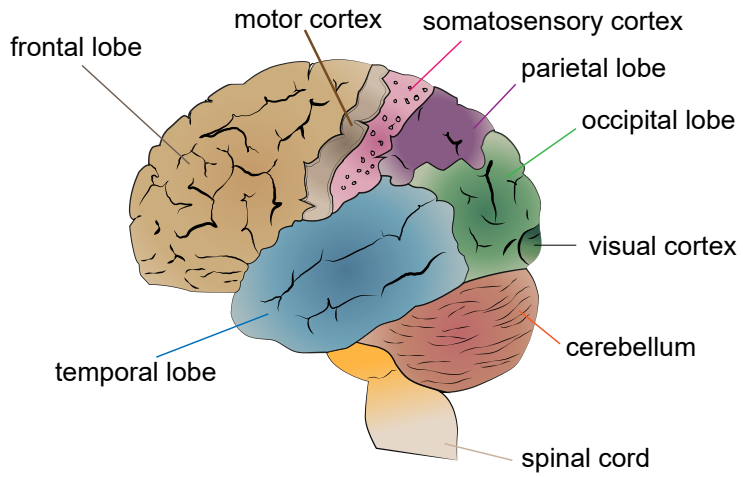

Figure 2.1: Structure of the human brain. Adapted from [38].

2.2 BCI Components

As we have already introduced, a BCI is a combination of hardware and software that translates the intentions of the user, encoded in his/her brain activity, into control commands for outer devices. Hence, as depicted in Figure 2.2, this kind of interfaces are composed by three main components: signal acquisition, signal processing and actuator/effect device. The signal acquisition component is in charge of recording the neural activity of the user, which can be done with either invasive or non-invasive techniques. Once the signal has been captured, it may be analyzed by the signal processing component in order to obtain features that allow to determine the desired intentions. Finally, the actuator device follows the orders dictated by the translated wishes of the user [17].

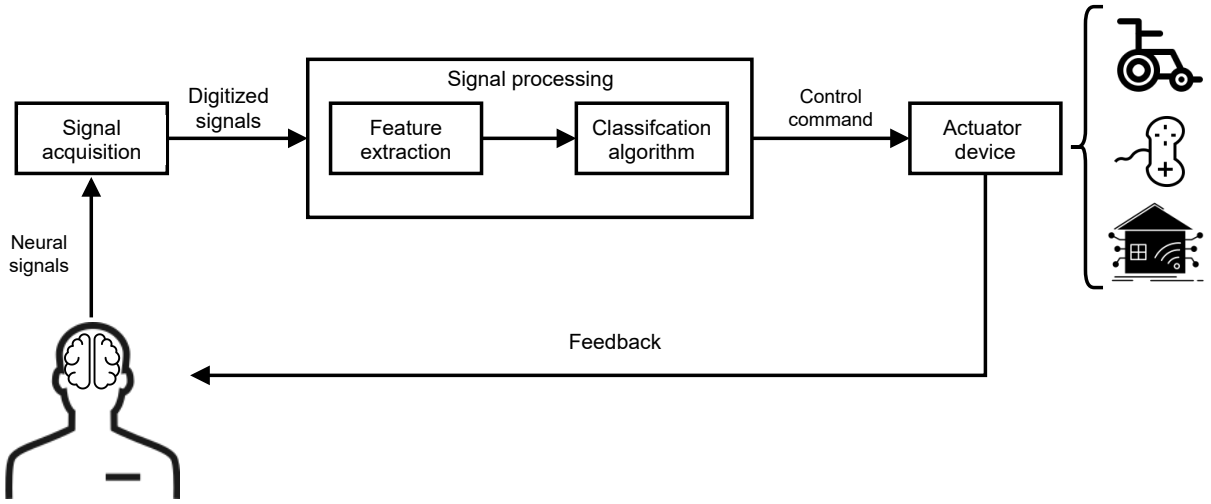

Figure 2.2: Basic components of a BCI.

2.2.1 Signal Acquisition

During the transmission of information within our brain, small ionic flows are generated due to the activation of neurons. This ionic current generates electrical activity and magnetic fields that can be measured through different techniques such as Magnetoencephalography (MEG), EEG, Electrocorticography (ECoG), among others. Signal acquisition techniques can be divided into two groups: invasive and non-invasive.

Non-invasive modalities capture the brain activity of the subject without penetrating the scalp. No surgery or any kind of implant is needed. Therefore, these modalities are preferable for the development of BCI applications. Several non-invasive techniques have been applied for brain signals acquisition, such as MEG, which registers the magnetic fields produced by the intracellular currents through magnetic induction, Functional Magnetic Resonance Imaging (fMRI), which measures changes in local areas of the cerebral blood using electromagnetic fields, or Near Infrared Spectroscopy (NIRS), that employs infrared light to detect fluctuations

in oxyhemoglobin and deoxyhemoglobin during brain activity. However, the most widely used technique, and therefore the one selected in this thesis, for neuroimaging and brain signal acquisition, is EEG [17]–[19]. This preference is caused by its relative low cost, high portability and temporal resolution, and its ease of use and low risk for the users. This method employs a set of electrodes placed over the scalp that capture electroencephalography signals from different brain areas. Details and challenges of this technology are discussed in the next chapter.

Despite the advantages and its successful implementation in a large variety of domains, some BCI modalities, such as neuroprosthesis control, require higher signal resolution than the one provided by non-invasive techniques. As a consequence, invasive methods were introduced to improve the signal quality employed by the interface and, therefore, enhance its performance.

Invasive modalities employ microelectrode arrays implanted inside the skull. This procedure involves many health risks, so these techniques have been applied mostly in animals and only to a limited extent in human cases [17], [39]. Hence, its experimental use is restricted. Two main invasive modalities have been applied in the BCI research. On the one hand, ECoG which employs electrodes located in the surface of the brain cortex, either under or outside the dura mater, has been tested in few BCI applications [18], [40]. For instance, Schalk et al. [41] implemented an ECoG-based BCI tested over 5 epileptic subjects with subdural electrode array. Their results show that the interface allowed the users to accurately control a two-dimensional joystick. On the other hand, intracortical neuron recording techniques use microelectrode arrays implanted inside the cortex of the subject to capture its brain activity. Three methods can be employed in these techniques: Single-Unit Activity (SUA), which captures the activity of a single neuron above $300\,\text{Hz}$, Multi-Unit Activity (MUA), similar to SUA but for multiple neurons, and Local Field Potentials (LFPs), which records the field potentials of a small group of neurons [17].

Based on recent literature and published applications, it seems that the most used and valid techniques for BCI implementations are EEG, ECoG and SUA, since their equipment is inexpensive and offer good communications and control channels [19].

2.2.2 Signal Processing

Once the brain activity has been captured by one of the aforementioned techniques, it has to be processed and analyzed in order to detect the user intents encoded in the signals. This task is carried out by the signal processing component.

Different mental states produce different patterns in cerebral activity. Therefore, if we detect these patterns, we can estimate the mental state of the user and its encoded intentions. It can be seen as a pattern recognition problem, where brain signals are classified into classes that represent the user's mental state and its intentions according to a set of features. Hence, the signal processing component is composed of two main steps: feature extraction and feature classification.

2.2.2.1 Feature Extraction

Feature extraction is the process where the obtained data is analyzed to build descriptors and derived values (features), usually in a lower-dimensional space, that best represents the raw data for its subsequent classification. In the case of BCI design, a feature extraction algorithm will seek for values in the raw brain signal that best reflect the subject's mental state and intents. Thus, this process is of paramount importance for the correct performance of the BCI. However, finding a suitable feature set is a complex and challenging task because of the high number of simultaneous brain signal sources and its noisy environment. Moreover, as described in Section 2.2.1, brain activity can be acquired from multiple channels, so the information of interest may be overlapped in time and space with other signals related to different brain processes. For this reason, dimensionality reduction algorithms such as Principal Component Analysis (PCA) or Independent Component Analysis (ICA) are widely used in BCI design in order to discard redundant and irrelevant data and keep the useful information [42], [43]. Moreover, we could obtain valuable information from particular areas of the brain by spatial filtering techniques. In this regard, Common Spatial Pattern (CSP) is one of these techniques widely employed, since it enhances the class separability by means of the spatial covariance of the input data [44], [45].

On the other hand, time and frequency information is also of high importance to determine the mental state of the subject. In consequence, techniques such as Discrete Fourier Transform (DFT) and Short-Time Fourier Transform (STFT) are employed to determine when a certain brain process occurs. But brain signal is inherently non-stationary, so data must be analyzed in short time segments where the information they enclose is considered to be stationary. As a consequence, Wavelet Transform (WT) and autoregressive models are preferable to Fourier transform (FT) to analyze and extract time-frequency features [18], [46]–[48].

2.2.2.2 Classification

The second step of the signal processing component is to relate the extracted features from the brain activity of the user with his/her intents. Therefore, the goal of the classification algorithms is to associate a set of features obtained in the previous step with classes that represent desired controls by the subject. Regression or classification techniques may be used to achieve this goal, but the use of classification algorithms is the most popular approach [49].

In BCI design exist three main types of sessions to build a classification algorithm: offline, online and a combination of both. Offline sessions consist of the analysis of recorded data in a controlled environment and usually collected from a closed-loop system. The calibration of the algorithm is developed with already gathered data, which does not represent real-world situations or scenarios. Conversely, online sessions are carried out in real-life environments where the user can suddenly change his/her mental state due to, for example, external stimuli. Therefore, offline sessions provide valuable data for testing new techniques, but only online

analysis can properly evaluate the performance and utility of the BCI system [18], [50]. The combination of both types of sessions is applied in order to build an efficient BCI. On the one hand, the classification algorithms are trained and tuned during offline sessions for detecting the relevant features in the data. Then, the calibrated classifier is tested during online sessions to assess its performance [18].

Traditionally, supervised learning techniques have been applied in BCI applications [49]. In this modality, a labeled data set is provided to the algorithm for its calibration. In the case of offline sessions, data is labeled according to the particular task the user is performing, while in online scenarios the label is provided by the feedback of the user. Under these scenarios, the linear classifiers, which are discriminant algorithms that employ linear functions to determine the classes, are probably the most used techniques in BCI applications, particularly two of them, known as Linear Discriminant Analysis (LDA) [50]–[52] and Support Vector Machines (SVMs) [53], [54]. On the other hand, non-linear classifiers, such as Artificial Neural Networks (ANNs), are, together with SVM and LDA, the most used algorithms in BCI research.

2.2.3 Actuator Device

The last component of the BCI architecture is the actuator device. As explained above, the main goal of these interfaces is to translate user's intentions, encoded in their brain activity, into control commands for outer devices. Hence, ideally, the actuator device will follow the orders dictated by the subject's thoughts. It will allow him/her to interact with the environment. The initial idea of BCI research was to assist people with motor disabilities, so major output devices are related to this domain. Computer spellers or cursors are, for example, active research fields [55], [56]. It has also been applied in prosthetic limbs control [5], [36], wheelchair control [3] or home automation control [57]. However, due to the advances achieved in recent years in BCI research, it has also been developed with non-rehabilitation purposes, such as leisure or entertainment [35] and educational research [58]. More details about the applications of BCIs are provided in the following section.

2.3 Applications for BCI

BCIs, as already explained, represents a new channel of communication with the user's environment without the need to use muscles or peripheral nerves. It is hoped that the recent developments of low-cost EEG-based BCI applications may help to improve the quality of life of people with severe motor disabilities, but they also represent strong support for caregivers and relatives, since they allow for a reduction in the tasks and expenses derived from care.

The target population for BCI applications can be divided into three main groups [18]. The first group is composed of patients that have lost all motor control and present a Complete Locked-In State (CLS) due to a cerebral palsy or a terminal stage of ALS. The second group

includes Locked-In State (LIS) patients, who only preserve residual motor movements such as eye blinks, eye movements or small lip movements. The final target group is composed of people with motor disabilities who preserve substantial motor functions such as speech or hand movements. Moreover, the recent developments of low-cost and easy-to-use EEG devices have promoted the use of BCI applications by healthy people in areas of neuromarketing, video games or education.

During the last decades, a vast number of BCI applications have been developed. In this section, we briefly present several BCI applications grouped into five main areas: communications, environmental control, locomotion, motor restoration and entertainment.

2.3.1 Human Communications

The main objective of this type of BCI applications is to allow patients with severe neurological damage to communicate with their environment. For this purpose, communication BCI usually displays a virtual keyboard where the user can select each of the letters which compose the final message she/he wants to transmit. According to that, the P300 speller is one of the most popular BCI for communications purposes. It takes advantage of the Event-related Potential (ERP) produced about 300 ms after oddball stimuli that appears among several frequent stimuli. For instance, Farwell and Donchin proposed a well-known P300 speller which displays a virtual keyboard organized in a 6×6 matrix whose cells contain the letters of the alphabet and also 1-word command for controlling the system [4] (see Figure 2.3). The user must focus his/her attention on the cell to be written, rows and columns of the matrix flash alternatively, so when the cell of interest flashes it should elicit a P300 ERP. Each P300 is analyzed after each flash, so the cell of interest is identified as the cell at the intersection of the row and column that elicit the largest P300s. The developed system achieved a spelling rate of 2 characters per minute.

Following this P300 speller approach, several works have been presented in order to improve the performance of the system. For example, a different organization of the characters is presented in [59] in order to avoid perceptual error in the detection of the P300 produced by adjacent rows/columns. For this purpose, a region-based paradigm is proposed, where letters are organized into different flashing regions in the computer screen instead of using rows and columns. Townsend et al. [50] also propose a change of paradigm, using a checkerboard instead of the traditional rows and columns scheme. This novel approach outperforms the row-column paradigm in terms of accuracy and transmission rates.

Other different types of brain signals have also been successfully applied for the development of BCIs with communication purposes. For example, Birbaumer et al. [20] presented a spelling device based on Slow Cortical Potentials (SCPs) that achieves a transfer rate of 2 characters per minute. Moreover, eye blinks have been also used as a control signal for character selection and the implementation of a BCI with communications purposes [60], achieving a rate of 1 character per minute.

Figure 2.3: Virtual keyboard displayed for the P300 speller developed by Farwell and Donchin [4].

2.3.2 Environmental Control

A significant aspect of the BCIs is that they can provide users with a certain level of independence. Through them, the user can independently control daily life devices, such as different types of home appliances, only making use of their mental activity. Taking this into account, home automation or smart homes are rapidly gaining interest [61], [62]. Such systems aim to make the home environment not only comfortable and accessible, but also to optimize and automate the use of appliances like TV sets, air conditioners, light bulbs, ovens or washing machines.

Cincotti et al. [57] present a pilot study where an assisting BCI is implemented to allow disabled persons to improve or recover their mobility and communication within the surrounding environment. For this purpose, they record sensorimotor rhythms at the scalp of the users. The system allows controlling basic domestic appliances such as lights, TV and stereo sets, a motorized bed, an acoustic alarm, a front door opener, and a telephone, as well as wireless cameras to monitor the surrounding environment.

The development of low-cost EEG devices together with the emerging Internet of Things (IoT) technology promoted the implementation of several BCI applications for environmental control [63]. For instance, Jagadish et al. [64] present a BCI application which detects voluntary blinks of the user and controls electrical appliances included in an IoT system. Mathe et al. [65] connect a BCI application which employs the Mindwave [66] consumer EEG device to estimate the user's depression level with an IoT ecosystem responsible for notifying the caretakers.

2.3.3 Independent Locomotion and Motor Control

BCI systems can be an important tool to help the users to move around their environment. For this purpose, brain signals are employed to control means of transportation, such as a

wheelchair. Towards this end, portable EEG-based applications should be designed to allow the user to freely move around the different spaces of the environment.

Several BCIs have been proposed during the last years for controlling a wheelchair through EEG signals. For instance, Tanaka et al. [67] employed an EEG headset of 13 channels to capture the brain activity of the subjects and control an electric wheelchair. To this end, they asked the users to think the direction (left or right) that they want to go and, according to this data, developed a recursive training algorithm to generate recognition patterns from EEG signals. The average success rate for reaching the target position was about $80\,\%$. A different approach is proposed by Rebsamen et al. [68], [69], where the wheelchair follows already defined paths by the user, so the task of the subject is only to select the path he/she wants to follow and to stop the wheelchair in the desired location. The P300 ERP is employed as control signal and a graphic user interface is used to present the possible routes. Iturrate et al. [70] also proposed a system that employs the P300 to control the wheelchair. In this case, a real-time virtual map of the environment is displayed to the user, so he/she has to focus on the location of the space to reach. A visual stimulation process elicits the P300 and the system is then able to detect the target location where the wheelchair must move around. To this end, an EEG headset of 16 channels is employed to capture the brain activity and the Stepwise Linear Discriminant Analysis (SWLDA) is used for pattern recognition.

Neurological diseases or spinal cord injury may imply a severe or total loss of motor functions. In these cases, BCIs can help to motor restoration through the control of neuroprostheses, which will significantly improve the quality of life of the patients. In this regard, Pfurtscheller et al. [71] designed an EEG-based BCI that allowed a tetraplegic patient to grasp a cylinder using its paralyzed hands. Functional Electrical Stimulation (FES), which generates electrical currents to cause an artificial muscle contraction, was employed in this application. Beta signals produced by foot imagery movement were used as control signals to activate the FES device. Also Pfurtscheller et al. [21] proposed to restore hand grasp function using an electrical driven hand orthosis fitting the left hand of a tetraplegic patient. To achieve this goal, Rolandic oscillations, which are produced by Motor Imagery (MI) tasks, were monitored and analyzed. The patient needed some months to train the system, but he achieved to open or close his hand with an accuracy close to $100\,\%$. In a more recent work [72], the same group presented a study for controlling an implanted neuroprosthesis for hand grasp functions. The user was able to control the prosthesis by generating EEG patterns associated to the imagination of movements of his paralyzed left hand. The short training times to control the BCI indicated that this method might also be an alternative approach for clinical purposes. On the other hand, ERPs have been also applied for motor restoration and neuroprosthesis control. For instance, Muller et al. [73] proposed a BCI based on Steady-State Visual Evoked Potential (SSVEP) to control a two-axes electrical hand prosthesis. In this study, four movements were allowed: to open or close the electrical hand and to turn right or left the wrist. Each of these movements corresponded to a flickering LED with a specific frequency,

which elicited the SSVEP in the patient. So the patient just needed to focus his gaze on one of the LEDs to initiate a movement.

2.3.4 Entertainment

The advances produced in the recent years in the EEG technology, together with the development of new commercial and low-cost EEG devices, have promoted the integration of BCIs into non-clinical environments. In this regard, several video games based on BCIs have been proposed [74]. BCI technology not only provides a different channel for user interaction, but it also presents a new way of accessing to user experiences and emotions while playing. BCIs allows recognizing if the user is bored or focused on the video game, thereby, future developments can be improved by taking into account this brain information [18]. On the other hand, BCI-based video games can also be applied to help motor restoration or to train specific brain functions for patients with neurological disorders [75], [76].

Several brain signals have been employed for game control [74]. For instance, Rohani et al. [76] proposed a P300-based video game for attention training for people with diagnosed attention deficit and hyperactivity disorder. For this purpose, an immersive 3D classroom environment was created. The user must perform two experiments: one using the P300 speller and the other one using a system where the user is required to search for a specific letter in a series of changing images. This study shows that low-cost and non-invasive technologies can be applied for targeting attention in a motivating and engaging environment. Finke et al. [77] propose MindGame, also a P300 video game for attention improvement. In this case, the user tries to move a character in a virtual map that follows a checkerboard scheme. Since the P300 is a marker of attention, they present MindGame as a potential neurofeedback system that allows for attention training. On the other hand, Lalor et al. [78] presented MindBalance, an EEG 3D immersive video game based on SSVEPs. The aim of the game is to control the balance of an animated character on a tightrope by means of the elicited SSVEPs. Results showed that the six test subjects demonstrated a reliable control, achieving an average of $89.50\,\%$ correct selections. Moreover, making use of different brain patterns, Bonnet et al. [79] developed BrainArena, in which two users can play a simple football game by means of two BCIs. Motor imagery movements of the right and left hand allowed the users to score goals. The players could play in a collaborative or competitive manner. Results showed that competitive and collaborative conditions may lead to similar performances and motivations, however, the multiuser condition presents significantly improvements in terms of fun and motivation when compared to the single-player condition.

Games above presented have been designed for research and academic purposes, however, commercial BCI games have also been released during the last years. In this sense, companies that develop low-cost EEG devices, such as Emotiv [80] or NeuroSky [66], have created games for their own headsets. In the case of Emotiv, for example, it has launched games such as Cortex

Arcade and Spirit Mountain Demo, among others [18].

2.4 Conclusions

In this chapter we have introduced BCI as a powerful tool to improve the life quality of patients affected by limitations in locomotion, motor function or communication with their environment. The chapter begins with a brief summary about the physical structure of our brain to follow with a deeper explanation about the components of such a BCI system and their main applications, not only medical but also social, what has contributed to independence in the daily life of these patients.

Chapter III

EEG Signal Acquisition

Electroencephalography (EEG) is a widely-known non-invasive technique for neuroimaging that captures the electric fields produced by the activity of the neurons and their synapses from outside the brain [81]. It was introduced in 1924 with the experiments of Hans Berger, the German physician who first measured traces of brain electrical activity in humans [82]. He measured the electric brain activity produced by the ionic currents within the neurons during synaptic excitations using electrodes placed over the subject's scalp. Its ease of use, low risk for users, high portability and relative low cost are the reasons why it is the preferred method for brain signal acquisition by the vast majority of Brain-Computer Interface (BCI) researchers [17], [19], [83]. However, this technique also presents some important challenges such as low spatial resolution and poor quality signals. Brain signals must cross several layers as the scalp or the skull until arriving to the electrodes, therefore the acquired signal is weak and of poor quality [18].

EEG technology has traditionally been employed for the development of medical applications [84], [85]. EEG devices developed for this purpose typically consist of a large number of sensors and are highly expensive. Nowadays, the utilization of such devices for other applications is limited, but it is a promising technology for wellness and health care. Such applications require the design and development of friendlier devices, real-time operation or greater manageability and adaptation for people with motor functional diversity. Recently, several companies have presented commercial products and open solutions oriented to open the EEG technology to applications not restricted to medical diagnosis.

In this chapter, we will detail the signal acquisition component of a BCI system using the EEG technique, going over the electrode location, signal artifacts, brain rhythms and the different control signals that can be used for interacting with the interface. Furthermore, we will review some EEG devices studied in this doctoral thesis and mostly used for research purposes, which have been selected focusing on their trade-off between low-cost and performance. We will see how some of them require the use of proprietary software against open solutions in other devices.

3.1 Devices for EEG Signal Acquisition

EEG recording devices are mainly composed of four elements: 1) electrodes, which capture electrical activity from the scalp; 2) amplifiers, which enlarge the amplitude of the signal; 3) Analog-to-Digital Converter (ADC), which digitizes the analog brain signal, and finally; 4) recording device, which stores, displays and processes the data. This EEG recording basically consists in the measurement of potential differences between pairs of electrodes: the active and the reference one [82]. Moreover, a ground electrode is included to measure the differential voltage between the active and the reference electrode. The placement of the electrodes is usually based in the 10-20 International system [86], which uses two anatomical points, nasion and inion, to situate them. Furthermore, adjacent electrodes are located using a $10\,\%$ or $20\,\%$ of the total front-back or right-left distance. Each electrode location is identified by numbers, where the even ones represent the right hemisphere and the odd ones the left hemisphere, and letters, corresponding to the lobe and area of the brain where is placed: pre-frontal (FP), frontal (F), temporal (T), central (C), parietal (P) and occipital (O). Figure 3.1 shows the electrode placement according to this system.

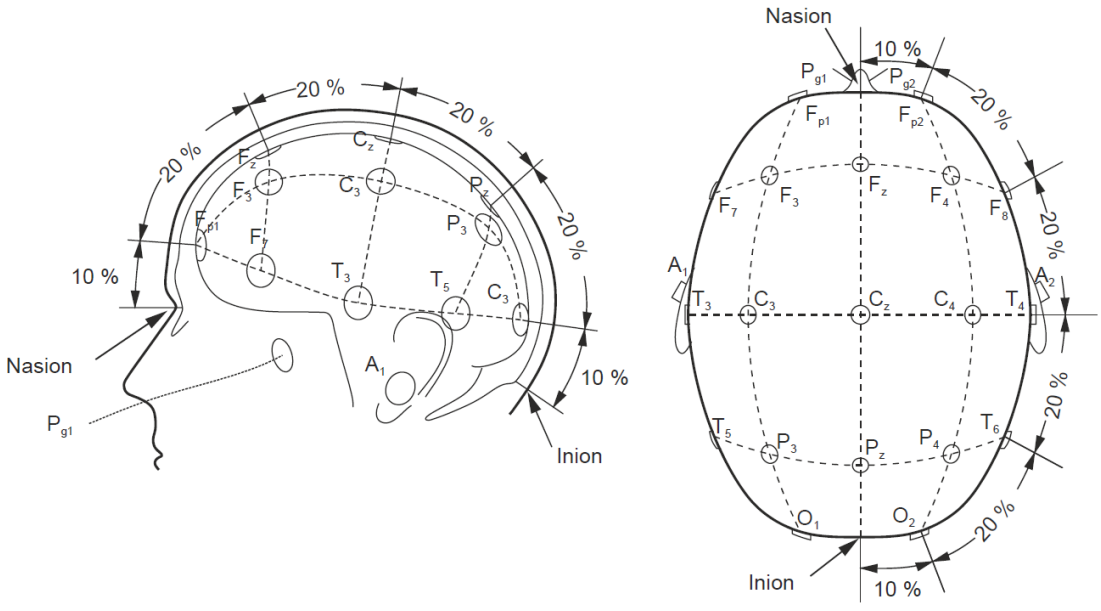

Figure 3.1: Electrode placement according to the 10-20 International System [18].

Two types of electrodes, active or passive, can be employed with the aim of reducing the external noise and cable movements during EEG recordings. Passive electrodes require an external amplifier, while active ones usually include embedded amplifiers [19], [87]. Additionally, gel or saline liquid is used in some electrodes (wet electrodes) to create a conductive path that improves signal quality and reduces skin impedance. However, this gel will eventually dry out, resulting in a poor quality signal and the need for electrode replacement. Moreover, this procedure may result cumbersome for the user in the recording

Table 3.1: Basic comparison of EEG devices.

	Device			
Parameters	MindWave	Epoc+	Cyton	Ganglion
Available channels	1	14	8	4
Sampling rate (Hz)	128	128 or 256	250	200
Wet/dry electrodes	Dry	Wet	Wet/Dry	Wet/Dry
ADC resolution	12 bits	16 bits	24 bits	24 bits
Data transmission	Bluetooth	BLE	BLE	BLE
Captured bio-signal	EEG	EEG	EEG, EMG & ECG	EEG, EMG & ECG
Fixed electrodes	✓	✓	×	×
Open hardware	×	×	✓	✓
Price (€)	$100 - 150$	$680 - 730$	$400 - 450$	$200 - 250$

sessions. Therefore, dry electrodes that do not need gels have been implemented to offer a faster setup time and greater user comfort but with, usually, a higher skin impedance than the wet ones [88].

Recent advances in biomedical technologies, integrating circuits, sensors, and data analysis techniques, have led to the development of new wearable EEG devices that can be applied in both clinical and non-clinical applications [87]. The reduction in the cost, their greater ease of use, the lower need for human expert intervention and their lower maintenance have promoted these new devices to be employed outside the laboratory and use this technology in daily life and real-world environments, such as homes and schools [58], [89].

While multi-electrode devices, such as those used in clinical applications, gather more and better quality signals than consumer-grade devices, the latter are preferable in the development of domestic BCI applications because of their lightweight, comfort and a small number of electrodes, which make them suitable for continuous monitoring during daily life activities [58].

Several consumer-grade EEG devices have been presented in recent years [19]. Two of the most popular low-cost headsets are Epoc+ and MindWave [66], [80] which, although they require the use of proprietary software, have been assessed in numerous research works and BCI applications [90]–[95]. On the other hand, open-software and open-hardware devices have also been proposed for capturing brain signals. In this case, the boards presented by OpenBCI [96] (Cyton and Ganglion boards) are well-known open solutions. In this section, we analyze the main characteristics of these four popular devices. Table 3.1 summarizes some of their basic specifications.

3.1.1 NeuroSky MindWave

NeuroSky company has presented a single–sensor EEG device, known as the NeuroSky Mindwave [66], of low cost and oriented to the consumer market. It has only one input electrode, placed at Fp1, and an ear-clip electrode acting as reference in the A1 position according to the 10-20 International System [97]. The signal is sampled at 128 Hz and sent to the computer via Bluetooth. Neurosky claims that the MindWave headset can detect blinks and two mental states (attention and relaxed) besides acquiring the raw EEG data. Figure 3.2 shows the Mindwave headset and its electrode placement.

From a point of view of applications using Neurosky MindWave, several studies are focused on educational research [58], [98]. For instance, Chen et al. [90] gather EEG signals from students in order to identify high- and low-attention levels in an autonomous e-learning environment. The prediction accuracies achieved by their proposed algorithm on high- and low-attention levels were of $91.60\,\%$ and $87.44\,\%$, respectively. Patsis et al. evaluated the attention levels of the users while they played Tetris as a function of game difficulty [91]. The results obtained for both intra- and inter-player analysis show how an increase in game difficulty was followed by the corresponding increase in attention. These findings can provide useful tools for future developments of educational games that adapt to the mental state of player/learner. On the other hand, Vourvopoulos et al. [92] presented a study which identified user's adaptation on brain-controlled systems and evaluated how to control a robot in both real and virtual worlds via brainwaves. The study employed both Emotiv Epoc and Neurosky MindWave to acquire brain signals. The obtained results indicated that robot navigation through commercial EEG devices can be effective and natural in both the real and the virtual environments. Röesler et al. presented also a comparison of both devices for the detection of the eye state of the user [93]. The results showed that MindWave equipped with only one sensor cannot be used for eye state prediction, since the highest accuracy it achieves is of $43.52\,\%$. They conclude that MindWave does not seem to be useful for serious EEG experiments or to control an application. However, Epoc achieves a high performance with a minimum error rate of $1.38\,\%$ for the K-star classifier and an average error rate over all tested classifiers of $16.50\,\%$. Moreover, other portable and single–sensor EEG devices presented by Neurosky such as MindWave Mobile, MindSet or MindBand have been also applied for the development of out-of-the-lab applications [58], [89], [99].

3.1.2 Emotiv Epoc+

Emotiv Epoc+ is a lightweight consumer-grade EEG device which announces that thoughts, feelings and emotions can be used for computer control. It claims that five different types of mental states and eight facial expressions can be detected using the software they provide. The headset has 14 sensors which acquire the EEG signals, located following the 10-20 International System [97]. Brain signals are internally sampled at 2048 Hz and downsampled to 128 Hz or

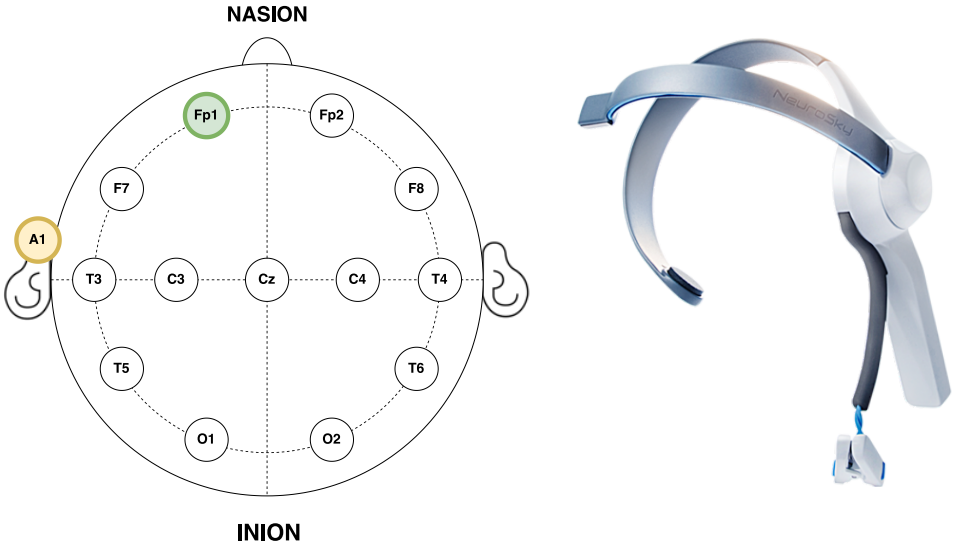

(a) (b)

Figure 3.2: (a) Anatomical electrode distribution in accordance with the 10-20 International System used by the Neurosky Mindwave headset. Green circle represents the input electrode, while the yellow one represents reference and ground electrode. (b) Neurosky Mindwave headset.

256 Hz before becoming available to the system. It employs Bluetooth Low Energy (BLE) as the communication protocol to transmit the data to computers or mobile phones. Its bandwidth ranges from 0.16–43 Hz and digital notch filters at 50 Hz and 60 Hz are implemented. Both hardware and software are proprietary, and no open–source code or hardware circuit schematic is provided. Figure 3.3 shows the anatomical distribution of the electrodes and the Epoc+ headset.

Emotiv Epoc and its latest version, Epoc+, have been employed in several BCI applications during the last years [89]. In educational research, for example, the Emotiv headset is used to measure students' engagement in game-based lessons [94], [95]. Duvinage et al. [100] compare the performance of the Epoc headset and a medical EEG device based on a standard P300 BCI. They conclude that the Emotiv device is an interesting option whose performance is far above the chance level. However, results show that it clearly underperforms the medical device. Therefore, authors claim that Emotiv Epoc should only be chosen for non-critical applications such as games, communication systems, etc. and not be used in clinical applications, since its lack of reliability may lead to serious consequences. Chumerin et al. [101] developed a BCI maze game based on Steady-State Visual Evoked Potential (SSVEP) response in which the brain signals of the player are captured by the Epoc headset. Their system achieved a mean accuracy of 80.37 % and a standard deviation of 11.85 % for game control over 20 test subjects. In a more recent study, Lin et al. [102] developed a SSVEP to control a treadmill for human walking.

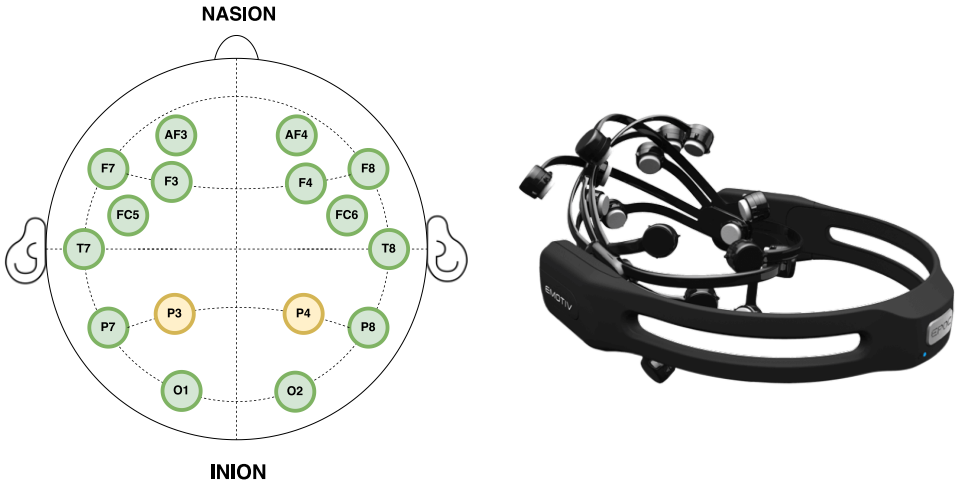

(a) (b)

Figure 3.3: (a) Anatomical electrode distribution in accordance with the 10-20 International System used by the Emotiv Epoc+ headset. Green circles represent input electrodes, while the yellow ones represent Common Mode Sense (CMS) active electrode and Driven Right Leg (DRL) passive electrode employed as references. (b) Emotiv Epoc+ headset.

3.1.3 OpenBCI Devices

OpenBCI [96] presents open hardware and software solutions for Human-Machine Interface (HMI) implementation. Circuit schematic, source code and plans of the headsets for its 3D impression are provided on their website. Recent studies have been presented analyzing and employing the OpenBCI devices for capturing the brain activity of the subjects, as we will see in the following.

The most popular and complete device is the Cyton board, that is built around an ADS1299, developed by Texas Instruments for biopotential measurements. The ADS1299 is an 8-channel, low-noise, 24-bit ADC specifically designed for measuring EEG signals. The board uses an Arduino-compatible ATmega328P and a SD card for local storage. EEG signals are sampled at $250\,\text{Hz}$. An adjustable $50\,\text{Hz}$ or $60\,\text{Hz}$ notch filter can be applied to the acquired data. The number of available channels can be extended to 16 with the incorporation of an external module. Figure 3.4(a) shows the Cyton board.

Different works used Cyton technology for Motor Imagery (MI) classification [103]. For instance, Yohanandan et al. [104] employ the Cyton board to gather the EEG signals of 7 subjects for MI classification using Deep Neural Networks (DNN). They found that the classification accuracies increased with imagery duration, achieving the best results with data segments of $7\,\text{s}$. However, authors claim that the there is no statistical improvement beyond segments of $5\,\text{s}$, so it is the optimal trade-off between imagery duration and accuracy ($\sim 83\,\%$).

Also for MI classification, Belwafi et al. [105] employ adaptive filter and Common Spatial Pattern (CSP) for feature extraction and Linear Discriminant Analysis (LDA) for the

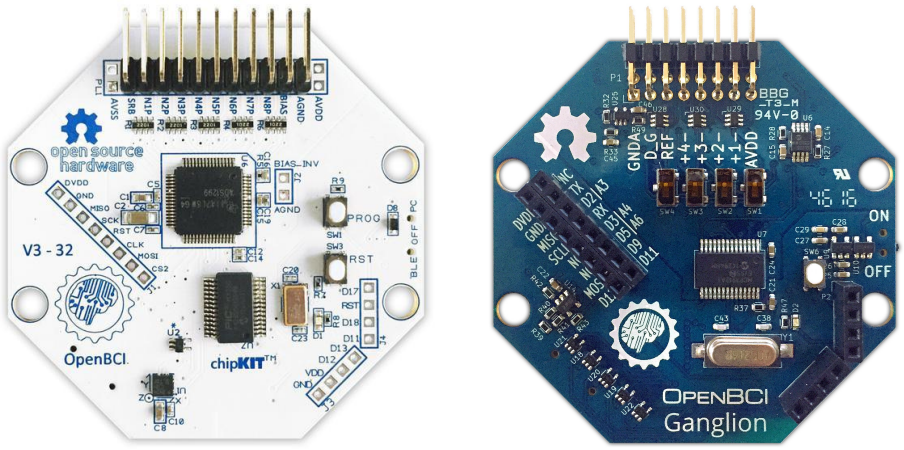

(a) (b)

Figure 3.4: OpenBCI EEG boards: (a) Cyton board; (b) Ganglion board.

classification of EEG data collected with the Cyton board. The results achieved by the proposed system showed an accuracy of $80.50\,\%$. On the other hand, Frey presents a comparison of the Cyton board extended with 16 channels and a medical device [106]. Both devices were compared in the P300 speller and in an EEG-based workload monitoring using the n-back task. The obtained results showed that the OpenBCI board is an effective alternative to traditional EEG devices. Although medical grade device still outperforms the Cyton board in terms of classification, the latter gives very close EEG readings, and may be suitable for building reliable BCIs.

On the other hand, OpenBCI offers also the Ganglion board, a more affordable bio-sensing device with only four channels. It is built around the microchip MCP3912 which presents a 24-bit ADC and BLE is employed for the communication of the raw data. The signal is sampled at $200\,\text{Hz}$ on each of the 4 channels (see Figure 3.4(b)). This board was released later than the Cyton board, therefore, we can not find many research papers based on it yet. However, some works have started to prove its feasibility for recording EEG activity [107] and to implement Electromyography (EMG)-based HMIs [108].

In addition, open source software is also provided. OpenBCI Graphical User Interface (GUI) is a powerful software tool for visualizing, recording, and streaming data from the hardware devices. Moreover, complete software libraries such as BrainFlow are also available, which offer solutions for obtaining, parsing and analyzing data from EEG, EMG and Electrocardiogram (ECG) in several programming languages and from a wide variety of devices, including those of OpenBCI [109].

3.2 EEG Brain Rhythms

EEG activity is composed of a set of signals that can be divided according to their frequency and amplitude. Well-known EEG rhythms have been defined according to specific mental states and their distribution in the scalp. Figure 3.5(a) shows the EEG rhythms. These frequency bands and their relevant features are detailed below:

- *Delta (δ):* It lies below 4 Hz and is typically encountered during deep sleep states. It is usually not observed in awake states, in such case, it could indicate cerebral damage or brain disease.
- *Theta (θ):* It ranges between 4 and 7 Hz. Theta rhythm occurs during certain stages of sleep, meditative and drowsiness state, either in adults or children.
- *Alpha (α):* It lies between 8 and 12 Hz. Alpha rhythm is related to a relaxed and a closed eye state, and its activity is attenuated when the eyes open and mental effort increases [110]. It is mainly located in the occipital area and primarily reflects visual processing tasks. The mu (μ) rhythm also occurs in this frequency band, but it is strongly related to motor activities in the motor cortex and is attenuated when voluntary movement is produced [111].
- *Beta (β):* It is mainly observed in frontal and central regions of the scalp and it is associated to motor activities. It ranges between 12 and 30 Hz and is symmetrically distributed when there is no motor activity and desynchronized when real movements or motor imagery occur [16].
- *Gamma (γ):* Gamma rhythm ranges from 30 to 100 Hz. It is related to a state of active information and focus. It is not commonly used in EEG-based BCI because muscle artifacts are likely to affect them [18].

3.3 EEG Artifacts

The amplitude of the recorded signals by the electrodes is in the order of microvolts, ranging from a few microvolts to approximately $100\,\mu V$. Therefore, the acquired EEG signal is very sensitive to either internal or external noises, such as electromagnetic interference produced by surrounding devices or different biological signals produced by the subject from other sources different from the brain (e.g., eyes, jaw, etc.). Thus, a common categorization of the artifacts that can be found in the EEG is based on its origin, i.e., physiological or non-physiological [113]. The following sections detail the common types of artifacts according to such origins.

3.3.1 Physiological Artifacts

Physiological artifacts are those produced by biological signals generated by the subject that contaminate the EEG signal. The most common types of non-cerebral artifacts present in the

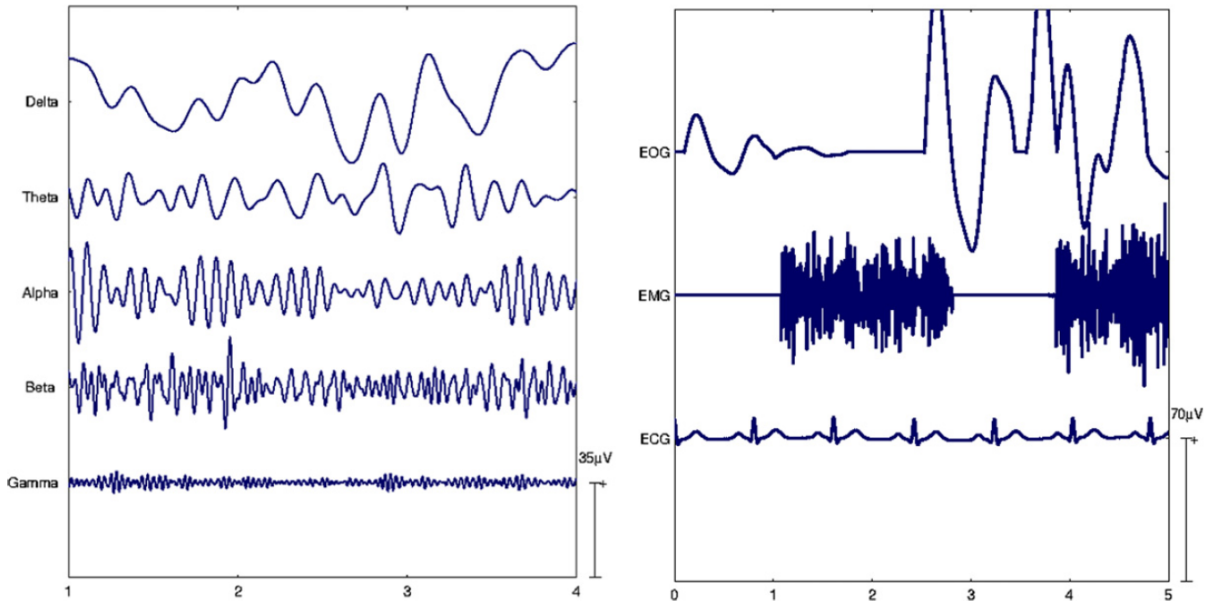

(a) (b)

Figure 3.5: (a) EEG rhythms from low to high frequency; (b) most common physiological artifacts in the EEG signals [112].

EEG signals are described below. Figure 3.5(b) shows the most common physiological artifacts.

3.3.1.1 Ocular Artifacts: Eye Movements and Blinks

Eye movements (saccades), either vertical or horizontal movements, produce electrical activity, known as Electrooculography (EOG), which is generally visible in the EEG. The EOG reflects the potential difference between the cornea and the retina, which changes during eye movement [113]. These artifacts are mainly present in frontal and lateral frontal electrodes, and its strength depends on the proximity of the electrodes to the eyes and the direction of the saccades. Blinking also causes artifacts in the EEG signals due to the corneal-retinal potential difference. It produces more abruptly changes than the eye movements, which are related to higher frequency interference.

In order to attenuate or cancel ocular artifacts, a pure EOG signal can be captured simultaneously to EEG by positioning reference electrodes near the eye. EOG and EEG recordings will be correlated, so artifact cancellation can be developed [113].

3.3.1.2 Muscle Artifacts: Myogenic Activity

Muscle contraction produces electrical activity that can interfere in EEG signals. The technique that measures this electrical activity in the surface of the body is known as EMG. These artifacts are present in an awake state when the subject swallows, chews, talks, etc. The shape and strength of the interference depends on the degree of muscle contraction and the type of muscle contracted, so it is difficult to stereotype [112].

EMG artifacts are more difficult to correct than EOG artifacts. They mainly affect the beta activity ($12 - 30$ Hz) but it can also be found below 2 Hz. Moreover, due to volume conduction, EMG activity can be distributed in the entire scalp, which makes it complex to characterize for artifact removal [114].

3.3.1.3 Cardiac Artifacts

The electrical activity produced by the heart when pumping blood can also interfere with the EEG. ECG is the employed method to measure the cardiac activity. Although the amplitude of the cardiac signals is usually low in the scalp, it can distort the EEG for certain electrode positions and body shapes. Fortunately, heartbeats have a repetitive pattern that can be easily identified. Nevertheless, in some cases, the spike-shaped ECG waveform can be confused with epileptic activity when the ECG is barely visible in the EEG.

ECG activity, similar to EOG, can be captured using independent electrodes, which facilitates artifact cancellation [113].

3.3.2 Non-physiological Artifacts

We refer to as non-physiological artifacts to those produced by technical problems encountered in the EEG recordings or by electromagnetic interference from surrounding devices. The most common types of non-physiological artifacts are described below.

3.3.2.1 Electrode Artifacts

Electrode movements or improper contact with the scalp can produce a technical artifact known as 'electrode-pop'. This artifact usually presents an abrupt change in the baseline level, followed by a gradual return to the original baseline. Moreover, an insufficient shielding in the electrode wires can lead to electromagnetic interference caused by currents flowing nearby the EEG acquisition device [113].

3.3.2.2 Power Line Interference

Power line introduces electromagnetic interference with 50 or 60 Hz signals that disrupt the EEG data. The amplitude of the Alternating Current (AC) signals ranges between 10 mV to 1 V, so the brain signals are completely hidden behind this artifact [115].

Several techniques have been applied for artifact rejection or attenuation. Linear filtering has been considered for the reduction of EMG or power line artifacts. However, it must be applied with caution, since EEG data of interest and artifact spectra overlap each other considerably [113]. Therefore, more advanced techniques such as Independent Component Analysis (ICA) or Principal Component Analysis (PCA) have been proposed to remove the sources of artifacts and keep the valuable EEG data [116]–[118].

3.4 Control Signals

BCIs are intended to control external devices by interpreting the subject's intentions in her/his brain activity. This brain activity is made up of a large number of brain signals related to different cognitive tasks. Some of these brain patterns and signals can be modulated or controlled by the subjects in order to communicate their intentions to the BCI. Therefore, this kind of signals are considered as possible control signals in BCIs [18].

There is a vast number of studies analyzing different types of control signals. In this work the four main groups are described: Visual Evoked Potentials (VEPs), Slow Cortical Potentials (SCPs), P300 Evoked Potential (EP) and sensorimotor rhythms.

3.4.1 Visual Evoked Potentials

VEPs are electrical potentials registered in the visual cortex produced when the subject receives a visual stimuli [119], [120]. It reflects the mechanism by which the brain processes visual information. A VEP-based BCI can identify the target the user is staring at by analyzing the recorded EEG. Each target is represented by a unique stimulus sequence which evokes a unique VEP pattern. The target can then be identified by analyzing the characteristics of the VEP and translated to its corresponding control command [121]. According to the frequency used to present the stimuli to the subject, two kinds of VEPs can be differentiated. When the visual stimulation is presented at a frequency lower than $6\,\text{Hz}$, Transient Visual Evoked Potentials (TVEPs) are elicited. Conversely, when the frequency of visual stimulation is higher than $6\,\text{Hz}$, SSVEPs occur [18], [120]. The latter potentials are widely used for the implementation of BCIs. In this approach, one or more stimuli are presented to the subject in different and constant frequencies. When the subject focus his/her attention on one of the stimulus, EEG activity may be detected over occipital areas at corresponding frequencies [122]. Therefore, a BCI based on SSVEP consists of presenting different visual stimuli to the user at different frequencies and then he/she chooses the one that corresponds to the desired control command. The SSVEPs have been applied in a wide range of BCI domains such as video games control [78], virtual navigation and environmental control [123], [124] or control of electrical orthosis [5] and prosthesis [73].

3.4.2 Slow Cortical Potentials

SCPs are low frequency potentials detected in the central and frontal part of the cortex [19]. They belong to the EEG signals present below $1\,\text{Hz}$ and they can last from a second to several seconds [18], [125]. Negative SCPs are related to movement and other cortical activation functions, while positive SCPs coincide with reduced cortical activation [126]. Several studies have proved that people can learn to self-modulate these signals in order to control external devices using a BCI [20], [127]. For instance, Birbaumer et al. [127] developed a Thought

Translation Device (TTD) which trains locked-in patients to control their SCPs for selecting letters, words or pictograms in a computerized language support program, allowing them to communicate using an alternative channel. The SCPs have been also successfully tested in a patient with late stage Amyotrophic Lateral Sclerosis (ALS) [128]–[130], who managed to communicate through the BCI with an accuracy between $70\,\%$ and $80\,\%$. However, SCP BCI systems offer low information rates, need long training periods, professional attention and continuous technical support, and not all patients are able to fully control their SCPs [18], [126], [131].

3.4.3 P300 Evoked Potential

The P300 EP is a positive deflection located in the parietal area of the cortex that occurs in the EEG brain activity $300\,\text{ms}$ after an infrequent or surprising auditory, visual or somatosensory stimuli [4], [126], [132]. The potential is usually evoked by the "oddball" paradigm, where several stimuli are presented to the subject and one of them is less frequent than the others. When these rare stimuli appear, they elicit a positive peak about $300\,\text{ms}$ later, i.e., a P300 EP. Based on this brain response, a specific action can be associated to the rare stimulus, so it will be executed when the P300 is detected. The most common way to employ the P300 in the BCIs is through visual stimulation, where the different elements which the user can interact with are, usually, randomly presented on a screen. The user must focus its attention in one of these infrequent elements, so that when it appears it will elicit the P300 potential that the BCI can detect and execute the associated action.

A large number of works can be found in the literature of recent years proposing the use of the P300 for building assistive systems in order to facilitate communication and environmental control for patients with severe motor and neurological damages [18]. For instance, the P300 speller proposed by Donchin and Farwell [4] is a well-known BCI for communications purposes which served as the basis for more recent works applying different paradigms [50], [59]. It has also been implemented in other domains such as home automation [133]–[135].

3.4.4 Sensorimotor Rhythms

Sensorimotor rhythms are the oscillations recorded from the brain activity in the sensorimotor area, i.e., the area that comprises the somatosensory and motor cortex [136]. These rhythms are concentrated in the frequency bands of mu ($8 - 12\,\text{Hz}$) and beta ($12 - 30\,\text{Hz}$) [18]. When a person performs a motor movement or just imagines that it is performed, the amplitude of the sensorimotor rhythms exhibits different modulation patterns. Two main patterns can be found: Event-related Desynchronization (ERD), when the amplitude of the rhythms in the area involved in the movement becomes weaker and could even be suppressed, or Event-related Synchronization (ERS), the opposite phenomenon, i.e., the power of the rhythms in the sensorimotor area increases [137].

Sensorimotor rhythms have been widely applied in BCIs because the users can learn and train to generate these modulations [18], [138]. Therefore, MI tasks, i.e., the mental rehearsal of a movement without any motor output, have been selected as the approach for implementing several BCI systems, such as the Wadsworth BCI for communication purposes [138], the Graz BCI for virtual keyboard interaction or hand orthosis control [16], [139] or the Berlin BCI [140].

3.5 Conclusions

In this chapter, we have introduced EEG as the most used and appropriate technique for neuroimaging and brain signal acquisition for BCIs. This preference is mainly based on the non-invasive character of this technology, which implies a low risk for the users. Moreover, it shows several advantages such as its high portability and temporal resolution, its relatively low cost, and its ease of use [17]–[19]. We have also reviewed several commercial devices presented during the last years oriented to open the EEG technology to applications not restricted to medical diagnosis. Each of these devices offers different benefits, such as the number of available channels, the ADC resolution, the electrode types, etc., so depending on the application area some will be more appropriate than the others.

The brain activity collected by these EEG devices encodes the users' intentions, which can be translated into control commands for interacting with their surroundings. For this purpose, several brain signal patterns can be applied, where VEPs, SCPs, the P300 EP and MI synchronization/desynchronization are the most common approaches [18].

Chapter IV

EEG Signal Processing

Brain signals captured by Electroencephalography (EEG) devices need to be analyzed and processed for their posterior classification and subsequent translation into a control command for an external device. In a Brain-Computer Interface (BCI) application, this task is developed by a signal processing unit, whose two main components are the feature extraction and the feature classification. The feature extraction process aims to find the most relevant values, called 'features', that best describe the original raw EEG data [141]. These features are sent to a classification algorithm, which is responsible for estimating the mental state of the user that usually corresponds with a control command.

In this chapter, we will present the feature extraction techniques to be used in our experiments and the classification algorithms implemented throughout this work using those features.

4.1 Feature Extraction

Feature extraction is one of the most important and challenging steps in the design of a BCI application due to the complex processes involved in the brain [17]. Its correct performance is critical for the proper representation of user's mental states and their posterior classification. Therefore, the feature extraction method chosen for the development of a BCI must be carefully selected. In this section, we will show the techniques used in our further experiments.

4.1.1 Time Methods

These methods directly extract the features from the EEG signals in the time domain using arithmetic or statistical operators.

4.1.1.1 Peak-picking

Peak-picking is one of the most basic and simple feature extraction technique employed in the BCI systems [81]. A peak is defined as the maximum or minimum voltage amplitude value of the recorded signal in a time interval. This time interval is usually determined by the presentation of an external stimulus (e.g., visual or auditory stimuli). The peak-picking algorithm computes the largest and smallest values inside this time interval and employs them, and possibly the time instant when they occur, as features for their classification.

Let $x(n)$ be the sample at the discrete time n of the signal x of length N. The method computes the following features

$$x_{max} = \max(x(n)),\ n = 0, \ldots, N-1, \tag{4.1}$$

$$x_{min} = \min(x(n)),\ n = 0, \ldots, N-1, \tag{4.2}$$

where x_{max} and x_{min} represent the maximum and minimum signal values, respectively. Taking into account these two features, the latency, i.e., the time instant when those peaks occur, can be also obtained as a new feature

$$t_{x_{max}} = \{n \mid x(n) = x_{max}\},\ n = 0, \ldots, N-1, \tag{4.3}$$

$$t_{x_{min}} = \{n \mid x(n) = x_{min}\},\ n = 0, \ldots, N-1, \tag{4.4}$$

where $t_{x_{max}}$ and $t_{x_{min}}$ represent the instant times where the maximum and minimum occur, respectively.

As a result, a set of four features is extracted for the signal x, which will be used to feed a classification algorithm to predict the mental state of the user. Moreover, new features can be obtained as linear combinations of the already calculated peaks and latencies. For example, latency/amplitude ratio, $t_{x_{max}}/x_{max}$, peak-to-peak value, $x_{max} - x_{min}$, peak-to-peak time window, $t_{x_{max}} - t_{x_{min}}$, among others, can be computed as new features for the classification process [142], [143].

Several works have applied peak-picking as feature extraction method for the analysis of EEG signals and the implementation of BCIs based on Event-related Potentials (ERPs). For instance, Farwell and Donchin used this basic technique in the widely-known P300-based speller [4]. In a more recent study, the combination of peaks, latencies, latency/amplitude ratio, among other features, was employed for the detection of depressive patients using the P600 potential of ERP signals [143]. In this regard, a similar feature set is employed in a P300-based lie detection study [142]. It is important to note that, most of the studies combine the features extracted by this straightforward technique with other kind of features [4], [142], [143].

4.1.1.2 Sum of values

The measurement of the area under the EEG or ERP curve for a specific time interval is another basic and straightforward feature extraction technique employed in BCI systems [81]. Areas

are obtained by integrating the amplitude voltage values of the continuous signal that belong to the defined time interval. In a discrete time signal, this integration becomes the summation of its values. Let $x(n)$ be the sample at the discrete time n of the signal x of length N. The summation is computed as follows [4]

$$A = \sum_{n=0}^{N-1} x(n). \tag{4.5}$$

The sum of discrete values within a time interval of interest has been employed in several studies for the analysis and classification of ERP signals and for the implementation of BCIs based on them. For example, Farwell and Donchin combine these features with those obtained by the peak-picking in the P300-speller [4]. Xu et al. [144] also apply this technique after an Independent Component Analysis (ICA) decomposition of the data for P300 detection. Moreover, summation of signal values is employed together with peak-picking features for a P300-based lie detection study [142] and for the detection of depressive patients using the P600 potential of ERP signals [143].

4.1.2 Frequency Methods

These methods directly extract the features from the EEG signals in the frequency domain.

4.1.2.1 Digital Transforms

Digital transforms are used to represent digital signals in other domain, termed transformed-domain. The Discrete Fourier Transform (DFT) is the most used one and allows to obtain a signal in the frequency-domain. Let $x(n)$ be the sample at the discrete instant n of the signal x of length N. Then its DFT is given by

$$X(\omega_k) = \sum_{n=0}^{N-1} x(n) \cdot \phi(\omega_k, n), \ k = 0, \ldots, N-1, \tag{4.6}$$

where $X(\omega_k)$ is the complex Fourier coefficient at the frequency $\omega_k = 2\pi k/N$, with k being the frequency bin, and

$$\phi(\omega_k, n) = e^{-j\omega_k n}. \tag{4.7}$$

In this work we also consider a complex-valued function expressed as

$$\phi(\omega_k, n) = \text{sign}(\cos(\omega_k n)) - j\,\text{sign}(\sin(\omega_k n)) \tag{4.8}$$

and two real-valued functions, given as

$$\phi(\omega_k, n) = \cos(\omega_k n), \tag{4.9}$$

$$\phi(\omega_k, n) = \text{sign}(\cos(\omega_k n)), \tag{4.10}$$

where sign$(\cdot)$ represents the sign function that returns the sign of the input number.

EEG signals are non-stationary, so their frequency components change over time. DFT is not suitable for non-stationary signals, since it fails to provide the exact location of an event occurred in the time domain [145]. Thus, Short-Time Fourier Transform (STFT) was proposed to overcome this shortcoming of the Fourier analysis. The STFT divides the signal into successive time windows and applies the Fourier transform (FT) in each epoch of the signal. It provides time-localized frequency information, whereas DFT provides the frequency information averaged over the entire signal time interval [146]. Let $w(n)$ be a sampled window function of length L. Then the STFT of a discrete time signal x of length N can be expressed as

$$X(\omega_k, m) = \sum_{n=0}^{L-1} x(n) \cdot w(n-m) \cdot \phi\left(\omega_k, n\right),\ k = 0, \ldots, L-1, \tag{4.11}$$

with $m \in [0, M]$, $\omega_k = 2\pi k/L$ and ϕ as expressed in Eq. (4.7). The number $M = N - L$ represents the maximal instant of the signal where the window's time range is fully contained in the signal's time range. The complex number $X(k, m)$ represents the k^{th} Fourier coefficient for the m^{th} time instant.

A trade-off between time and frequency resolution exists in the STFT. The design of the window function is a critical step, since narrow-width windows lead to higher temporal resolution but it also generates a poor resolution in the frequency domain, and vice versa [18], [146]. This is an important issue to take into account for the design of BCI applications, since rapid feedback to the user must be given in response to its brain activity.

4.1.2.2 Sliding Methods

Let $x(n)$ be the sample at the discrete instant n of the zero-mean signal x. The Sliding Transform (ST) is obtained by applying an N-point discrete transform to moving windows starting at instant n, i.e., $[x(n), x(n+1), \ldots x(n+N-1)]$. The signal in the transform-domain is given by the following expression

$$X(\omega_k, m) = \sum_{n=0}^{N-1} x(n) \cdot \phi(\omega_k, n-m),\ k = 0, \ldots, N-1, \tag{4.12}$$

where $m \in [0, M]$, ϕ can be any of the previously defined functions in Eq. (4.7) – Eq. (4.10) and ω_k denotes the frequency bin.

This expression corresponds to the DFT (see Eq. (4.6)) when ϕ is

$$\phi(\omega_k, n-m) = e^{-j\omega_k(n-m)} = \cos\left(\omega_k(m-n)\right) + j\sin\left(\omega_k(m-n)\right), \tag{4.13}$$

where the Euler's formula is applied and $\omega_k = 2\pi k/N$. The sliding Discrete Fourier Transform (SDFT) is an efficient algorithm for performing the DFT on sliding windows updated sample by sample. It exploits the information similarity between two consecutive windows for improving

computational efficiency. The DFT of a new window is calculated directly on the result of the DFT of the previous window. The circular shift property is the main concept used for developing the SDFT [147], [148]. It claims that if the DFT of a discrete time window is $X(\omega_k)$ then the DFT of that window circularly shifted by one sample to the left is $X(\omega_k)e^{j\omega_k}$, where ω_k represents the k^{th} DFT bin. Therefore, we can relate the DFTs of two consecutive windows as [148]

$$X(\omega_k, n) = X(\omega_k, n-1)e^{-j\omega_k} - x(n-N) + x(n), \tag{4.14}$$

where $X(\omega_k, n)$ is the spectral component of the new window and $X(\omega_k, n-1)$ is the spectral component of the previous window.

4.1.3 Time-Frequency Methods

In this section, we explain the methods known as *time-frequency techniques* since they use transformations between the time and the frequency domains of the EEG signals. The Wavelet Transform (WT) is the most employed algorithm for this purpose in the BCI domain.

WT is a mathematical technique particularly suitable for non-stationary signals due to its capability of localizing a function or a set of data in both time and frequency. It is an effective tool in the signal processing domain due to its properties of time-frequency localization, i.e., a signal can be extracted at a particular time and frequency, and multi-rate filtering, i.e., a signal can be differentiated at various frequencies [149]. For this purpose, WT replaces sines and cosines of Fourier analysis by smooth and quickly vanishing oscillating mathematical functions, called 'wavelets', with good localization in frequency and time. Wavelets can be defined as small 'waves' limited in time, with zero-mean, finite energy over their time course and band-limited, i.e., they are composed of a relatively limited range of frequencies [150], [151].

Wavelet functions can be scaled in time and translated to any time point without changing their original shape. WT breaks down the input signal into a set of time-scaled and time-translated versions of the same basic wavelet. The set of scaled and translated wavelets of a unique mother wavelet $\psi(t)$ is called wavelet family, denoted as $\psi_{a,b}(t)$, and obtained as follows

$$\psi_{a,b}(t) = \frac{1}{\sqrt{a}}\psi\left(\frac{t-b}{a}\right), \tag{4.15}$$

where t denotes time, $a, b \in \mathbb{R}$ and $a \neq 0$, $\mathbb{R}$ is the set of real numbers. The wavelet function in Eq. (4.15) becomes wider when a decreases and is shifted in time when b varies. Therefore, a is called the scaling parameter which determines the oscillatory frequency and length of the wavelet, while b is called the translation parameter, which localizes its shifting position at time $t = b$. There are several shapes for wavelet functions, such as Haar, Daubechies, Coiflets or Symlets (see Figure 4.1), however, depending on the application or analysis where they are involved, a particular wavelet family will result in a more efficient performance than the others. For instance, Al-Qazzaz et al. [152] compared 45 mother wavelets to select the one that optimally represented the EEG signal during a working memory task. They concluded that the

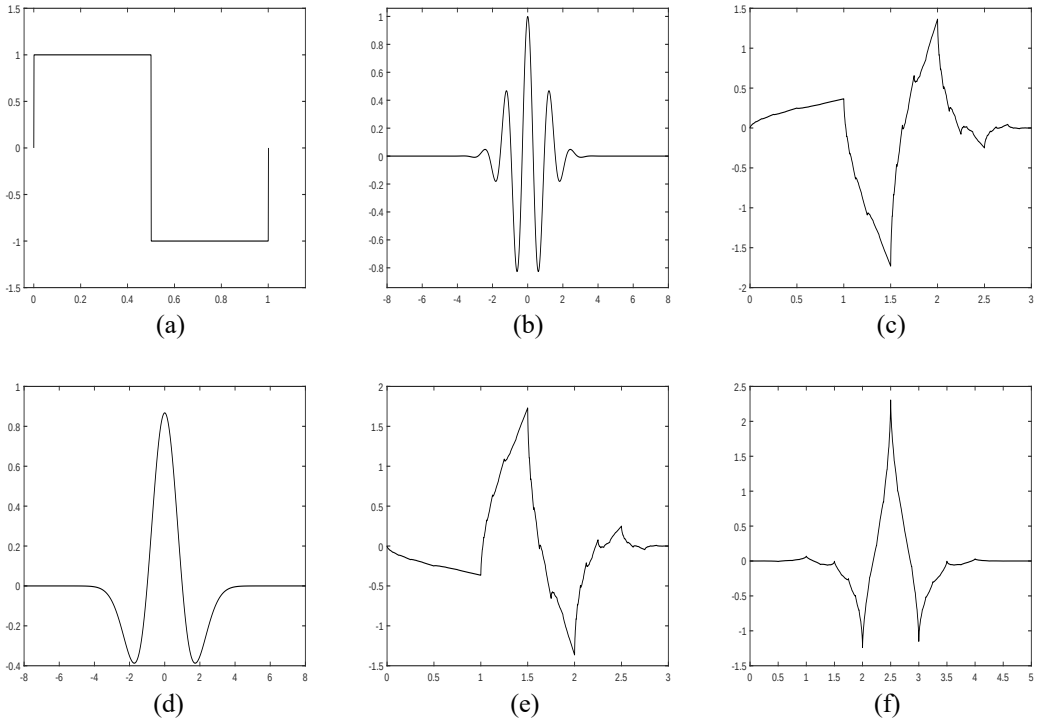

Figure 4.1: Wavelet families: (a) Haar; (b) Morlet; (c) Symlet2; (d) Mexican Hat; (e) Daubechies2; (f) Coiflet1.

Symlet wavelet of ninth order (sym9) exhibited the highest similarities and compatibilities with the recorded data. On the other hand, Adeli et al. [149] studied the Daubechies family with different orders for the analysis of epileptic EEG records. Their results showed that Daubechies of fourth order (db4) presented the highest representation of the data. Moreover, Gandhi et al. [151] concluded in their study that Coiflets 1 (coif1) was the most suitable candidate among the wavelet families for accurate classification of both normal and abnormal signals like epileptic EEG.

There are two types of WT: Continuous Wavelet Transform (CWT) and Discrete Wavelet Transform (DWT). The idea behind CWT is to scale and translate the basic wavelet shape and convolve it with the signal to be analyzed at continuous time and frequency increments. If $f(t)$ is a function of time t (e.g. a neuroelectric signal), the CWT of $f(t)$ is defined as [149], [153]

$$W_{a,b} = \int_{-\infty}^{+\infty} f(t)\psi^*_{a,b}(t)dt, \tag{4.16}$$

where * represents the complex conjugation. By applying CWT we produce a set of wavelets coefficients $W_{a,b}$ at every possible scale a and translation b. In practice, a finite set of coefficients is obtained, which is calculated over a digitally sampled signal, a few dozen scales where useful frequencies of the signal can be found and finite translations, b, which ranges over the entire sampled signal in increments of one sample point. Therefore, $W_{a,b}$ represents the wavelet coefficient of a signal for a specific scale a and time point b.

Analyzing the signal at every time point and scale is time-consuming. Moreover, the information achieved by the CWT at closely time points and scales is highly correlated and redundant [150]. DWT is a more efficient and computationally simpler algorithm for the wavelet analysis [154]. In this case, discrete a and b parameters based on powers of both dyadic scales and translations are usually employed, i.e.,

$$a_j = 2^j, b_{j,k} = k2^j, \ \forall \ k, j \in \mathbb{Z}, \tag{4.17}$$

where $\mathbb{Z}$ is the set of integer numbers.

Substituting in Eq. (4.15) we obtain dyadic wavelets as given

$$\psi_{j,k}(t) = \frac{1}{\sqrt{2^j}} \psi \left(\frac{t - k2^j}{2^j} \right), \ \forall \ k, j \in \mathbb{Z}. \tag{4.18}$$

If ψ is chosen to be orthogonal, the DWT will discard all the redundant information produced by the CWT. In this case, the number of coefficients will be the same as the number of time points in the sampled signal. Moreover, applying these orthogonal wavelets the original signal can be efficiently reconstructed without any loss of information. DWT based on multi-resolution can be implemented as a simple recursive filter scheme composed by a pair of digital filters, high- and low-pass filters, whose filter coefficients are determined by the employed wavelet shape in the analysis. The output of the filters is a series of wavelet coefficients downsampled by a factor of 2. In particular, the output of the high-pass filter is associated with the wavelet function, since it contains the details and all the high frequency energy of the signal. On the other hand, the output of the low-pass filter is associated with the scaling function, since it contains a coarser information of the approximation to the signal and its low frequency energy. The signal is convolved with the high-pass filter to produce detailed wavelet coefficients (D) and with the low-pass filter to produce the shape approximating scale coefficients (A) [149]. This latter output usually feeds another pair of digital filters. This procedure can be recursively repeated, and the result is a set of signals whose spectrum is divided into octave bands with a successively lower resolution in time and narrower bands in frequency. Figure 4.2 shows the multi-resolution DWT for an EEG signal sampled at 128 Hz.

The WT has been widely applied in EEG signal processing, particularly as a feature extraction method that feeds a classification algorithm for mental state recognition. For instance, it has been applied for the classification and analysis of ERP signals [51], [155]–[157], such as the P300 potential, self-regulated Slow Cortical Potentials (SCPs) [158], single-sweep ERPs [159], among others. It has also been applied for Motor Imagery (MI) data classification [160], [161]; seizure detection [162]; epileptic characterization through EEG recordings [149], [163] and mental workload analysis [164]. Moreover, WT has also been employed for the detection of ocular artifacts in EEG recordings [165], [166].

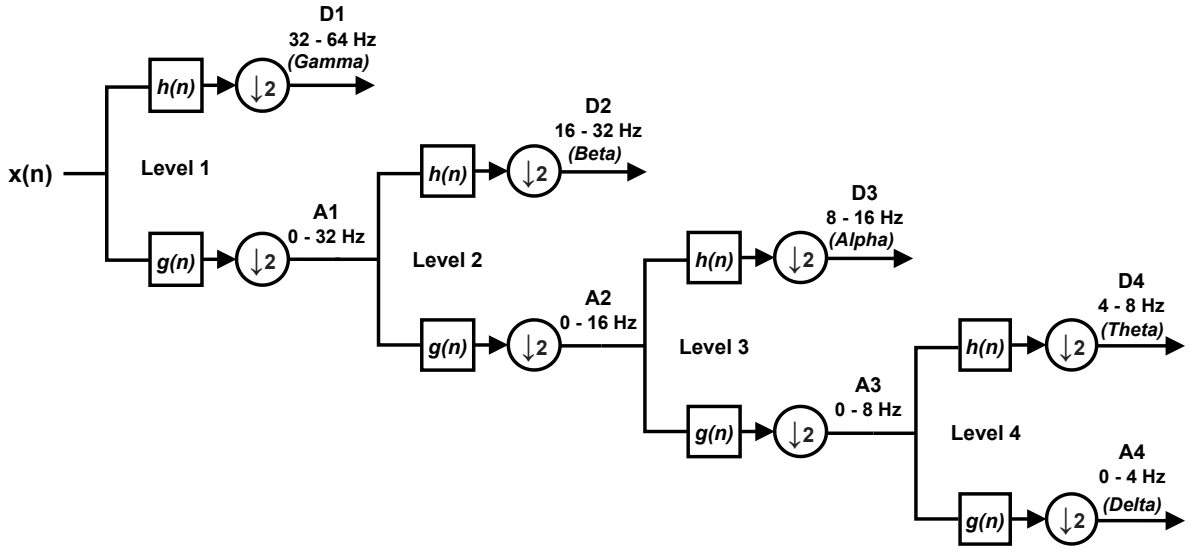

Figure 4.2: Filter scheme for a multi-resolution DWT of an EEG signal sampled at 128 Hz, where $g(n)$ and $h(n)$ represent the impulse response of the high- and low-pass filters, respectively, and $\downarrow 2$ represents downsampling by a factor of 2.

4.2 Feature Classification

The last step to transform the brain activity of the user into control commands for external devices is the feature classification step. Its main objective is to detect the user intentions making use of the previously extracted features. For this purpose, regression and classification algorithms can be employed, although the classification approach is the most popular in the BCI field [49]. These classification algorithms learn how to identify the class (or mental state) of a new feature vector by means of the training feature sets, which are already labeled as feature vectors extracted from training EEG samples [141]. In order to translate the extracted features into control commands, supervised machine learning algorithms are employed in this work.

4.2.1 Linear Discriminant Analysis

The main goal of Linear Discriminant Analysis (LDA) is to project the original multidimensional data into a lower dimensional subspace with higher class separability [167], [168]. For this reason, it is also widely used as a dimensionality reduction algorithm as well as a classifier. LDA assumes that all the classes are separable and that they follow a Gaussian distribution. Let us consider a binary classification problem with training samples $D = \{(\mathbf{x}(n), y(n)), (\mathbf{x}(n+1), y(n+1)), \ldots, (\mathbf{x}(n+N-1), y(n+N-1))\}$, where $\mathbf{x} \in \mathbb{R}^d$ is the input feature vector and $y \in \{-1, 1\}$ is the class label. LDA seeks for a hyperplane in the feature space that separates both classes. In the case of a multi-class problem with more than two classes, several hyperplanes are used [18]. The optimal separating hyperplane can be

expressed as

$$f(\mathbf{x}) = \mathbf{w} \cdot \mathbf{x} + b, \tag{4.19}$$

where $\mathbf{w}$ is the projection vector and b is a bias term. The projection vector $\mathbf{w}$ is defined as [169]

$$\mathbf{w} = \boldsymbol{\Sigma}_c^{-1} \left(\boldsymbol{\mu}_1 - \boldsymbol{\mu}_2 \right), \tag{4.20}$$

where $\boldsymbol{\mu}_i$ is the estimated mean of the i–th class and $\boldsymbol{\Sigma}_c = \frac{1}{2} \left(\boldsymbol{\Sigma}_1 + \boldsymbol{\Sigma}_2 \right)$ is the estimated common covariance matrix, i.e., the average of the class-wise empirical covariance matrices [169]. The corresponding estimators of the covariance matrix and the mean are calculated as follows

$$\boldsymbol{\Sigma} = \frac{1}{N-1} \sum_{i=1}^{N} \left(\mathbf{x}(i) - \boldsymbol{\mu} \right) \left(\mathbf{x}(i) - \boldsymbol{\mu} \right)^T, \tag{4.21}$$

$$\boldsymbol{\mu} = \frac{1}{N} \sum_{i=1}^{N} \mathbf{x}(i). \tag{4.22}$$

The predicted class for an unseen feature vector $\mathbf{x}$ is determined by sign $\left(f\left(\mathbf{x} \right) \right)$. Thus, the assigned class to $\mathbf{x}$ will be 1 if $f\left(\mathbf{x} \right) > 0$ and -1 otherwise.

LDA is probably the most used classifier for BCI design [141]. It has been successfully applied in different BCI systems, such as P300 spellers [51], motor imagery–based applications for prostheses and orthosis control [170], [171], among others [17], [18], [49]. Notice that LDA has lower computational requirements and faster rates than other popular classifiers such as Support Vector Machines (SVMs) or Artificial Neural Network (ANN), which makes it suitable for the development of online BCI systems [18], [172].

4.2.2 Support Vector Machine

The concept of SVM was first introduced by Vapnik in 1979 [173]. It is a supervised learning algorithm widely used for classification and regression problems. SVM, in a similar way to LDA, seeks for a hyperplane or a set of hyperplanes that efficiently separate the features vector into several classes. But, in contrast to LDA, these hyperplanes must maximize their distance to the closest training samples (Support Vectors (SVs)), i.e., the margin [18], [174].

Let us consider a binary classification problem of a two-dimensional feature space and non-separable training samples $D = \{(\mathbf{x}(n), y(n)), (\mathbf{x}(n+1), y(n+1)), \ldots, (\mathbf{x}(n+N-1), y(n+N-1))\}$, where $\mathbf{x} \in \mathbb{R}^d$ is the input vector and $y \in \{-1, 1\}$ is the class label. The objective of SVM is to find an optimal hyperplane that separates both classes with the largest margin, as depicted in Figure 4.3. This optimal hyperplane defined as $\mathbf{w} \cdot \mathbf{x} + b = 0$, where $\mathbf{w}$ is normal to the hyperplane, can be obtained solving the convex

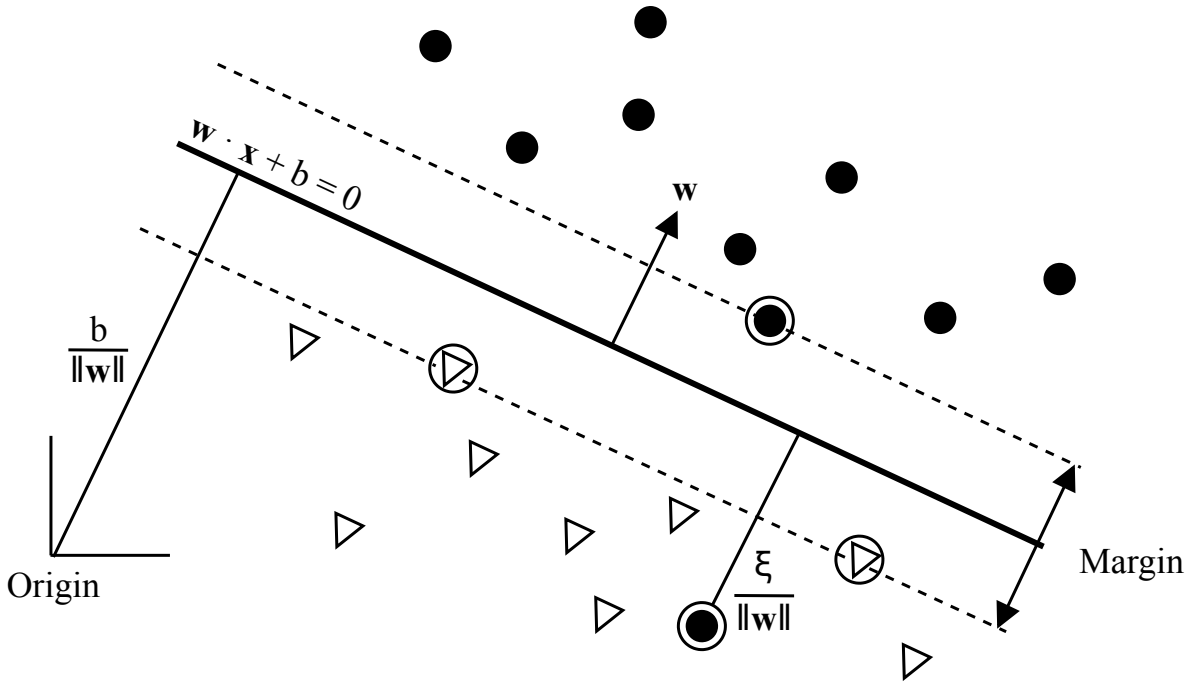

Figure 4.3: Linear separating hyperplane for the non-separable case. SVs are circled. The slack variable ξ stores the deviation of the features that fall in the wrong side of the hyperplane.

optimization problem

$$\begin{aligned} &\min_{\mathbf{w},b,\xi} \frac{1}{2}\|\mathbf{w}\|^2 + C\sum_{i=1}^{N}\xi_i, \\ &\text{s.t. } y(i)\left(\mathbf{x}(i)\cdot\mathbf{w}+b\right) \geq 1-\xi_i \ , \text{ and } \xi_i \geq 0 \ , i=1,\ldots,N, \end{aligned} \tag{4.23}$$

where $\|\mathbf{w}\|$ is the Euclidean norm of $\mathbf{w}$, $b \in \mathbb{R}$ and $\xi \in \mathbb{R}^N$ is the slack variable which stores the deviation of the features that fall in the wrong side of the hyperplane (see Figure 4.3). The parameter C is chosen by the user, so a larger C corresponds to higher penalty to errors. It is well known that the numerical computation of Eq. (4.23) can be achieved though its dual formulation [54], [174]. Consider α_i the Lagrange multiplier corresponding to the *ith* inequality. Then the dual of Eq. (4.23) is obtained as in [175]:

$$\begin{aligned} &\min_{\alpha} \frac{1}{2}\sum_{i,j=1}^{N} y(i)y(j)\alpha_i\alpha_j\mathbf{x}(i)\cdot\mathbf{x}(j) - \sum_{i=1}^{N}\alpha_i \ , \\ &\text{s.t.} \sum_{i=1}^{N} y(i)\alpha_i = 0 \text{ and } 0 \leq \alpha_i \leq C, \text{for } i=1,\ldots,N. \end{aligned} \tag{4.24}$$

The solution is given by

$$\mathbf{w} = \sum_{i=1}^{N} y(i)\alpha_i\mathbf{x}(i), \tag{4.25}$$

and the class of a new unseen feature is determined by the side of the decision hyperplane it falls, i.e., the class of $\mathbf{x}$ is given by $\text{sign}(\mathbf{w}\cdot\mathbf{x}+b)$. In multidimensional problems the hyperplane dimension changes in accordance to the number of feature types, but there will be no changes in the formulation of the SVM [175].

In most of the real-world problems, data is not linearly separable in the input space $\mathbb{R}^d$. In these cases, nonlinear SVM is employed by mapping the feature vector $\mathbf{x} \in \mathbb{R}$ into a high dimensional Euclidean space, $\mathcal{H}$, using a nonlinear mapping function $\Phi : \mathbb{R}^d \rightarrow \mathcal{H}$. Thus, a kernel function K can be defined such that

$$K\left(\mathbf{x}(i), \mathbf{x}(j)\right) = \Phi\left(\mathbf{x}(i)\right) \cdot \Phi\left(\mathbf{x}(j)\right), \tag{4.26}$$

where the mapping function need not be known, since the dot product is sufficient for the mapping. This simplifies the computational burden and largely mitigates the dimensionality problem. If we substitute the input feature dot product in Eq. (4.24) by the appropriate kernel function K, the algorithm will produce a SVM which lives in an infinite dimensional space. Hence, the relevant classifier function becomes

$$f\left(\mathbf{x}\right) = \text{sign}\left[\sum_{i=1}^{nSVs} y(i)\alpha_i K\left(\mathbf{s}(i), \mathbf{x}\right) + b\right], \tag{4.27}$$

where $\mathbf{s}(i)$ are the SVs and sign represents the sign function. The predicted class for unseen samples will be 1 if $f(\mathbf{x}) > 0$ and -1 otherwise.

Several nonlinear classification functions such as polynomial or sigmoidal neural network have been applied in classification problems for EEG [175]. However, the most common kernel for BCIs is the Gaussian or Radial Basis Function (RBF) given as

$$K\left(\mathbf{u}, \mathbf{v}\right) = \exp\left(-\frac{\left\|\mathbf{u}-\mathbf{v}\right\|^2}{2\sigma^2}\right). \tag{4.28}$$

SVM is a very popular classifier for BCI applications [141]. It has been successfully applied to classify different control signals such as P300 potential [135], [176]–[178], MI signals [179], [180] or Steady-State Visual Evoked Potential (SSVEP) [181], among others. It has also been applied in a wide variety of domains such as home automation [135], locomotion [182], communication [176], [183] or gaming [181].

4.2.3 Threshold-based Classifier

A threshold-based classifier is one of the simplest techniques that can be used for allocating a new set of features into their corresponding class group. Let us consider a binary classification problem of a one-dimensional feature space and training samples $D = \{(\mathbf{x}(n), y(n)), (\mathbf{x}(n+1), y(n+1)), \ldots, (\mathbf{x}(n+N-1), y(n+N-1))\}$, where $x \in \mathbb{R}$ is the input feature and $y \in \{-1, 1\}$ is the class label. The objective of the classifier is to find a threshold value T

that separates the instances of each class, so that those features below T will be assigned to the class -1 and those which exceeds T to class 1. Therefore, the predicted class of the classifier for an unseen feature x is determined by the decision function

$$Y = f(x) = \begin{cases} -1, & x \leq T, \\ 1, & x > T. \end{cases} \tag{4.29}$$

The threshold values depend on the problem that the classifier has to face, so they must be correctly calibrated for each particular case. Several strategies have been proposed for threshold tuning, such as using Receiver Operating Characteristic (ROC) or Precision-Recall curves and grid search [184]–[186].

An example of threshold classification in BCIs and EEG signals is presented in the Thought Translation Device (TTD) proposed by Birbaumer et al. [20], [127], [129]. It is a communication BCI based on SCPs that allows patients to communicate by selecting letters from a screen. Selection of the letters occurred when the SCP signals exceeded a predefined amplitude threshold. The system was successfully applied in locked-in patients who gained the ability to communicate by using the BCI. In a more recent study, the same group of researchers presented a comparison of different EEG classifications for the TTD [158]. They concluded that the threshold technique is an easy and often sufficient method for online classification of EEG time series, but when no continuous feedback is required in the BCI, other methods should be considered to improve the accuracy of the system, such as WT or LDA, among others. In this regard, Kirkup et al. [187] also presented a BCI where a threshold-based classifier was applied to detect when the user closed his/her eyes. In this case, the amplitude EEG signal was analyzed at $10\,\text{Hz}$ and when it exceeded the predetermined threshold level, a control command was sent to an electrical appliance. The system was successfully tested on two subjects without prior learning. Moreover, threshold classifiers have been also applied in other EEG studies. For instance, Wan et al. [188] calculated the optimal threshold for determining driving anger intensity using EEG signals, the ROC curve and the WT. EEG data was collected from 30 subjects during real driving experiments. Four types of anger were defined: none, low, moderate and high anger. The relative energy spectrum of the beta and delta bands were extracted as features, and the optimal threshold for its classification in one of the four anger levels was determined by the ROC curve analysis. Their results showed an $80.21\,\%$ overall accuracy for beta feature and a $75.20\,\%$ for delta feature.

4.3 Conclusions

In this chapter we have introduced two key elements in a BCI: feature extraction and classification. These two tasks are in charge of interpreting the brain signals obtained by the EEG and detecting the mental state and the intentions of the user. For this purpose, in the feature extraction process several techniques in different domains are applied to find the most relevant

values that best describe the brain activity. Some techniques in time, frequency and time-frequency domain are briefly presented in this chapter. Once these features have been extracted, they are sent to a classification algorithm that estimates the mental state and intentions of the user. Two widely known classifiers in the field of the BCIs, such as LDA and SVM, are also shortly described. Finally, a straightforward algorithm such as the threshold-based classifier is also presented.

Chapter V

EEG Eye State Detection Using One Sensor

In this chapter, we present a prototype of an Electroencephalography (EEG) device designed to acquire signals using a reduced number of sensors. The hardware is composed of low-cost components, including a dual core microcontroller that allows us to perform all operations associated to signal classification simultaneously to the transmission of data to an Internet of Things (IoT) environment. We propose and compare different algorithms for determining the user's eye states, i.e., open eyes (oE) or closed eyes (cE). The algorithms include different configurations oriented to provide high and accurate results with a low computational burden. First, we compare real-valued and complex-valued transforms. Secondly, we consider sliding windows with overlap instead of using the traditional approach with non-overlapped windows, thus reducing the delay time between acquisition and decision. Finally, we compare three classification approaches, one based on a threshold classifier and the other two that implement the well known Linear Discriminant Analysis (LDA) and Support Vector Machine (SVM) algorithms. We also show the integration of this system with IoT protocols in order to obtain a realizable prototype for controlling different IoT devices by means of on/off operations.

During the last years, both the eye state identification and the eye-gaze analysis have become an active research field due to their implication in Human-Machine Interfaces (HMIs) [189], [190]. In particular, EEG eye state detection has been successfully applied in a wide variety of domains [191], such as driving drowsiness detection [54], infant sleep-waking state classification [192] and stress features identification [193], among others. Several previous papers have associated cE and oE with particular frequency and amplitude ranges of the brain waves [110], [194]–[196]. For instance, Kirkup et al. [187] presented a home automation control system for a rapid on/off switch appliance which bandpass filters the signal between $8\,\text{Hz}$ and $12\,\text{Hz}$. It calculates a threshold employing these alpha values to determine the user's eye state and control external devices.

In a more recent study, Naderi et al. [197] have proposed a technique based on Welch's method for estimating the Power Spectral Density (PSD) and on Recurrent Neural Networks

(RNNs) to distinguish a relaxed and open eye state from an epileptic seizure. Features from EEG time series and PSD levels were extracted to train and test the classifier which, at the end, exhibited an accuracy of $100\,\%$. In another study on the same data set, Acharya et al. [198] propose the employment of Convolutional Neural Networks (CNNs) for the development of a Computer-Aided-Diagnosis (CAD) system that automatically detects seizure using EEG signals. For this purpose, they implement an algorithm based on a 13-layer deep convolutional neural network for the detection of normal, preictal, and seizure classes, where the normal state corresponds to a relaxed and closed eyes situation. Their proposed technique achieves an accuracy, specificity, and sensitivity of 88.67%, 90.00%, and 95.00%, respectively. Moreover, EEG-based eye state detection has been successfully applied for automatic driver drowsiness detection. Yeo et al. [54] proposed to use SVM as classification algorithm to identify and differentiate EEG changes that occur between alert and drowsy states. Four main EEG rhythms (delta, theta, alpha and beta) were employed for extracting different frequency features, such as dominant frequency, frequency variability, center of gravity frequency and the average power of dominant peak. Their method reached a classification accuracy of $99.30\,\%$ and was also able to predict the transition from alertness to drowsiness with an accuracy over $90\,\%$.

Due to the wide variety of areas where the EEG eye state detection can be applied, several methods have been presented to achieve higher classification accuracies. In this sense, Rösler and Sunderman [199] tested 42 classification algorithms on their performance to predict the eye state. For this purpose, a dataset containing the two possible ocular states was recorded using the 14 channels of the Emotiv EPOC headset. The reported results showed that standard classifiers such as naïve Bayes, Artificial Neural Networks (ANNs) or Logistic Regression (LR) offered poor classification accuracies, while instance-based algorithms such as IB1 or KStar offered significantly higher results. The latter classifier achieved the best performance with a classification accuracy of $97.30\,\%$. However, it took at least 20 minutes to classify the state of new instances. Moreover, the dataset included the data of only one subject, so the authors cannot assure that the obtained results can be generalized. Several works have presented new classification methods based on this dataset. For example, Wang et al. [191] proposed to extract channel standard deviations and averages as features for an Incremental Attribute Learning (IAL) algorithm and achieve an error rate of $27.45\,\%$ for eye state classification. In a more recent study, Saghafi et al. [200] propose to study the maximum and minimum values in the EEG signals in order to detect any eye state change. Once this change has been detected, the last two seconds of the signal are low-pass filtered below $8\,$Hz and passed through Multivariate Empirical Mode Decomposition (MEMD) for feature extraction. These features are fed into a classification algorithm to confirm the eye state change. For this purpose, they tested ANNs, LR and SVM. Their proposed algorithm using LR as classifier detected the eye state with an accuracy of $88.2\,\%$ in less than $2\,$s. Hamilton et al. [201] proposed a new system based on eager learners (e.g. decision trees) in order to improve the classification time achieved by Rösler and Sunderman [199]. For this purpose, three ensemble learners were evaluated: a rotational forest

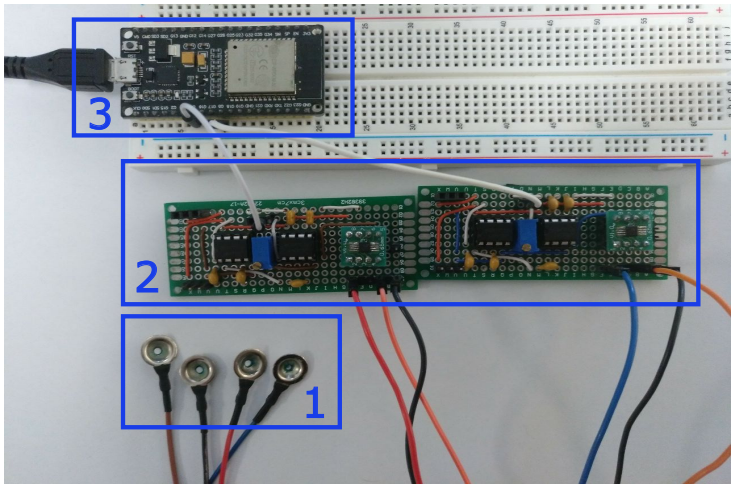

Figure 5.1: Proposed device details. (**1**) Sensors; (**2**) Amplifiers; (**3**) ESP32 module.

that implements random forests as its base classifiers, a rotational forest that implements J48 trees as its base classifiers and is boosted by adaptive boosting, and an ensemble of the rotational random forest model with the KStar classifier. Results achieved in the study showed that the approach using J48 trees and adaptive boosting offered accurate classification rates within the time constraints of real-time classification.

Although the aforementioned papers show methods to detect eye states with high accuracy, they gather the brain activity using at least 14 electrodes and large EEG devices. The main drawback of these devices is that they are uncomfortable for the user and cumbersome to use for long periods of time and during daily life activities. Moreover, they use large training sequences. In order to avoid these limitations, in this chapter we propose a simple threshold-based algorithm that uses both powers of alpha and beta bands with short training periods. The proposed system has been presented in [202]–[208].

5.1 Proposed Low-cost EEG Device

Figure 5.1 shows the elements of the device. This prototype has a total of four sensors: two inputs, the reference and the ground sensors. The signal is amplified and bandpass filtered between $4.7 - 29.2\,\text{Hz}$. Towards this end, we use the AD8221 instrumentation amplifier followed by a $50\,\text{Hz}$ notch filter to avoid the interference of electric devices in the vicinity of the sensor wires, a second order low pass filter, a second order high pass filter and a final bandpass filter with adjustable gain. The different filter stages that follow the instrumentation amplifier are shown in Figure 5.2. Both the low and high pass filters use a Sallen-Key architecture [209]. The low-pass filter has a cut-off frequency of

$$f_{c1} = \frac{1}{2\pi \cdot 300 \times 10^3 \cdot 10 \times 10^{-9} \cdot \sqrt{3.3}} = 29.204\,\text{Hz},$$

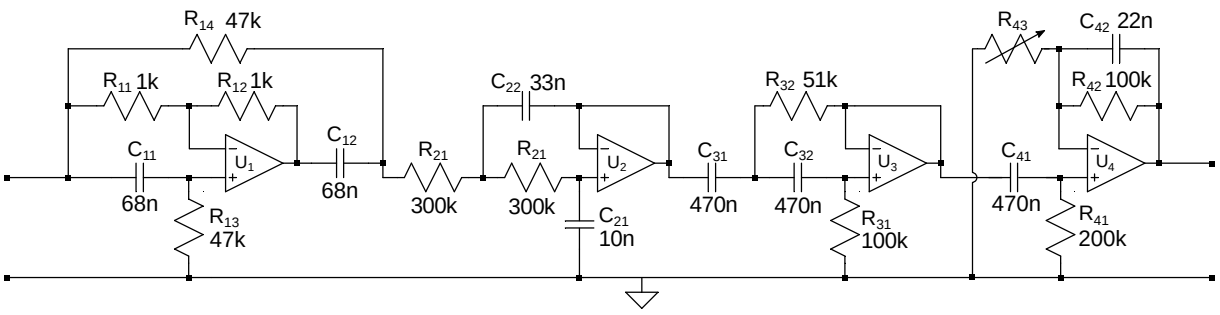

Figure 5.2: EEG sensor filters.

and a Q-factor of

$$Q = \frac{\sqrt{3.3}}{2} = 0.908,$$

whereas the high pass filter has a cut-off frequency of

$$f_{c2} = \frac{1}{2\pi \cdot 470 \times 10^{-9} \cdot 100 \times 10^{3} \cdot \sqrt{1.961}} = 4.742\,\text{Hz},$$

and a Q-factor of

$$Q = \frac{\sqrt{1.961}}{2} = 0.7.$$

The Q-factor of the high pass filter is higher in order to compensate the response of the notch filter near the $30\,$Hz cut-off frequency. The final bandpass filter has cut-off frequencies of

$$f_{c3l} = \frac{1}{2\pi \cdot 470 \times 10^{-9} \cdot 200 \times 10^{3}} = 1.693\,\text{Hz},$$

and

$$f_{c3h} = \frac{1}{2\pi \cdot 22 \times 10^{-9} \cdot 100 \times 10^{3}.} = 72.343\,\text{Hz},$$

and a gain of

$$G = 1 + \frac{100 \times 10^{3}}{R_{43}}.$$

The R_{43} rheostat, with values up to $1\,\text{k}\Omega$, allows us to adjust the gain to better utilize the whole range of the ADC.

Figure 5.3 shows the response of the filter stages for $R_{43} = 220\,\Omega$, which results in a gain of $53.171\,$dB.

Once the brain signal has been captured, amplified and filtered, the ESP32 microcontroller [210] is responsible for its sampling. Moreover, thanks to its dual core nature, complex processing tasks such as Fast Fourier Transform (FFT) or Wavelet Transform (WT) and its subsequent classification can be performed while the signal is sampled.

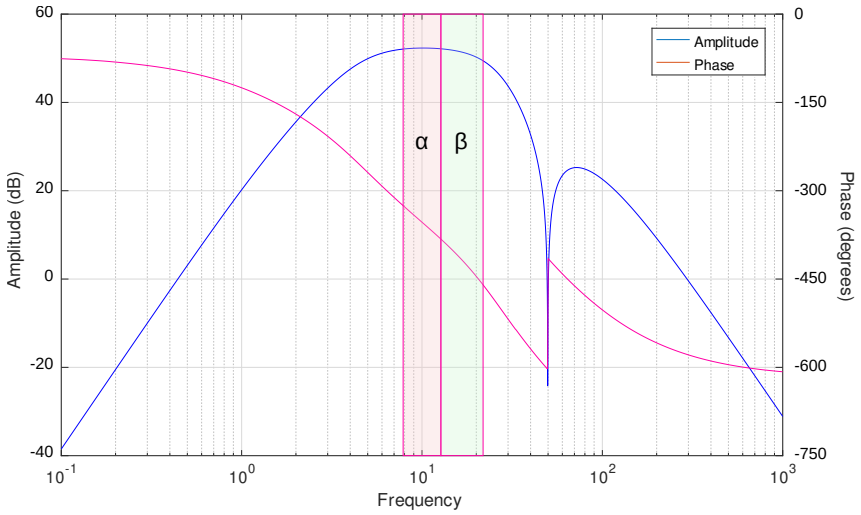

Figure 5.3: EEG filter response.

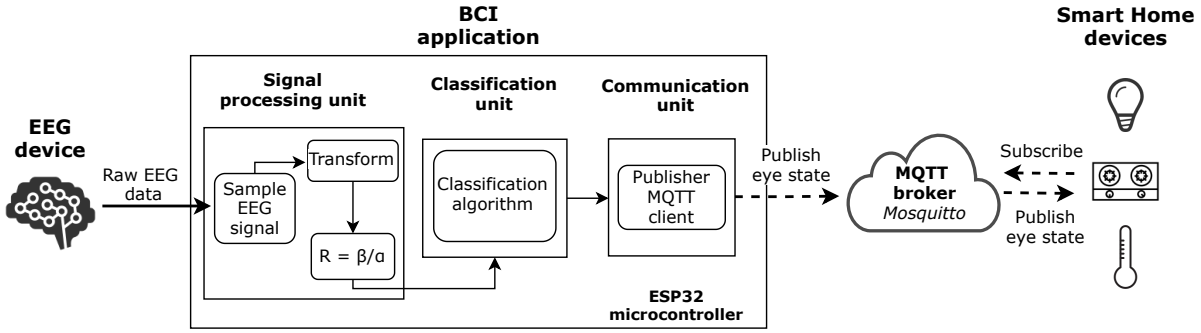

Figure 5.4: Proposed system architecture.

5.2 Proposed Architecture

Figure 5.4 shows the architecture of the proposed system. The first component of the system is the EEG device, which is responsible for capturing the brain activity of the user. The employed EEG device is the one presented in Section 5.1. The raw EEG data captured is then sent to the Brain-Computer Interface (BCI) application for its digitization and interpretation.

The BCI application is in charge of sampling the raw brain signal and detecting the user's ocular state based on that signal. Two main steps are required for detecting the eye state of the user. First, the brain signals must be processed and the features that best describe both ocular states must be extracted. Then, these features are fed into a classification algorithm that estimates the eye state of the user.

Power Spectral Density Analysis (PSDA), which is based on frequency analysis of the EEG signal, is one of the most widely used feature extraction methods for EEG classification. The PSD represents the distribution of signal power in different bands. Several studies have proved that the alpha power increases during closed eyes state, while significant reductions are produced when subjects open their eyes. On the other hand, beta power does not show

relevant differences between both eye states [110], [196]. Therefore, we use the power ratio between alpha and beta frequency bands for the determination of the user's eye state. Different transforms have been applied in order to determine which of them offered the best performance.

According to the general expression of the Sliding Transform (ST) described in Eq. (4.12) as

$$X(\omega_k, m) = \sum_{n=0}^{N-1} x(n) \cdot \phi(\omega_k, n-m),\ k = 0, ...N-1, \tag{5.1}$$

where $m \in [0, M]$ and ω_k denoted the frequency bin, we consider the following complex- and real-valued functions (ϕ) to be applied in those transformations, denoted as $\phi_1, \phi_2, \phi_3, \phi_4$, and given as

$$\phi_1(\omega_k, n) = e^{-j\omega_k n} = \cos(\omega_k n) + j\sin(\omega_k n), \tag{5.2}$$

$$\phi_2(\omega_k, n) = \text{sign}(\cos(\omega_k n)) - j\text{sign}(\sin(\omega_k n)), \tag{5.3}$$

$$\phi_3(\omega_k, n) = \cos(\omega_k n), \tag{5.4}$$

$$\phi_4(\omega_k, n) = \text{sign}(\cos(\omega_k n)). \tag{5.5}$$

The ϕ_2 transform only takes $\pm 1 \pm j$ values and therefore, the products in Eq. (5.1) can be easily implemented by only two sign changes per $x(n)$ sample. Contrary to the ϕ_1 and ϕ_2 transforms, both ϕ_3 and ϕ_4 only use the real values and, as a consequence, the number of operations is also reduced in half with respect to the two first transforms. Moreover, since the ϕ_4 transform only takes values $+1$ and -1, only one sign change per $x(n)$ sample is computed in Eq. (5.1).

In general, ST is computed over the input windows beginning at the instant n, without taking into account the result obtained for previous windows. However, for some transforms, the computational overhead can be considerably reduced by using recursive algorithms [148], [211]. In Chapter 4, we have shown that the sliding Discrete Fourier Transform (SDFT) can be computed as follows [148]

$$X(\omega_k, n) = X(\omega_k, n-1)e^{-j\omega_k} - x(n-N) + x(n), \tag{5.6}$$

where $X(\omega_k, n)$ is the spectral component of the new window and $X(\omega_k, n-1)$ is the spectral component of the previous one.

The transforms previously described are used to compute the alpha and beta bands using Eq. (5.1) taking into account that the alpha band ranges from 8 Hz to 13 Hz, while the beta band ranges from 14 Hz to 19 Hz. From each band, we obtain the mean power of alpha and beta, respectively denoted by α and β, and calculate their ratio, i.e., $R = \beta/\alpha$. Note that R is a real number for all real- or complex-valued transforms. This ratio R is extracted for each channel of the EEG devices and this set of features is then sent to a classification algorithm for estimating the ocular state of the user.

We compare the performance offered by three classification algorithms: threshold-based, LDA and SVM classifiers. The threshold-based classifier is one of the simplest techniques

that can be used for allocating a new set of features into their corresponding class group. As explained in Section 4.2.3, the objective of the classifier is to find a threshold value T that separates the instances of each class, so that those features below T will be assigned, for example, to the first class and those which exceed T to the second class. The threshold values depend on the problem that the classifier has to face, so they must be correctly calibrated for each particular case. Therefore, taking advantage of the ratio fluctuation according to the eye state, we propose a threshold-based classifier for the detection of cE or oE user states. Those values that fall below that threshold, T, will be classified as cE, while those above will be associated to oE. Thus, the criteria for our classifier is defined by the following decision rule

$$\begin{aligned} &\text{cE}, \qquad R \leq T, \\ &\text{oE}, \qquad R > T. \end{aligned} \tag{5.7}$$

The threshold value is determined in a training step by computing the power of alpha and beta bands and then the ratio R for cE and oE sates, respectively denoted by R_{cE} and R_{oE}. Subsequently, we have obtained that threshold applying the following expression

$$T = \frac{\max(R_{\text{cE}}) + \min(R_{\text{oE}})}{2}. \tag{5.8}$$

To improve the robustness of the threshold calibration, we compute the ratio R for each window of the training set. Then, all the values that lie more than three standard deviations away from the mean are treated as outliers and are not taken into account for the calculation of T in Eq. (5.8).

Two additional classifiers are considered in this work: LDA and SVM. As mentioned in Sections 4.2.1 and 4.2.2, the basis of both classifiers are the hyperplanes for separating feature vectors of the different classes. The location and orientation of these hyperplanes is determined from training data. These two algorithms are probably the most used classifiers for BCI designs [141].

Once the eye state of the user has been detected, it is transmitted to the IoT environment, so the connected devices can react to this information. The communication between the different IoT agents is based on the Message Queue Telemetry Transport (MQTT) protocol. It is a publish/subscribe, extremely simple and lightweight messaging protocol, designed for constrained devices and low-bandwidth networks. The publish/subscribe model is built around a central broker and a number of clients which connect to the broker. The broker acts like an intermediary agent, responsible for relating the information that the publishers provide with the subscribers clients [212].

Publishers send messages to the broker on a specific topic and subscribers register their interest about some of them with the broker, which acts as a matchmaker, dealing with authentication and controlling who is allowed to publish or subscribe to which topics. Those topics can be combined and created in a simple way, so the system ca be easily expanded by the inclusion of new devices or applications into the new topics.

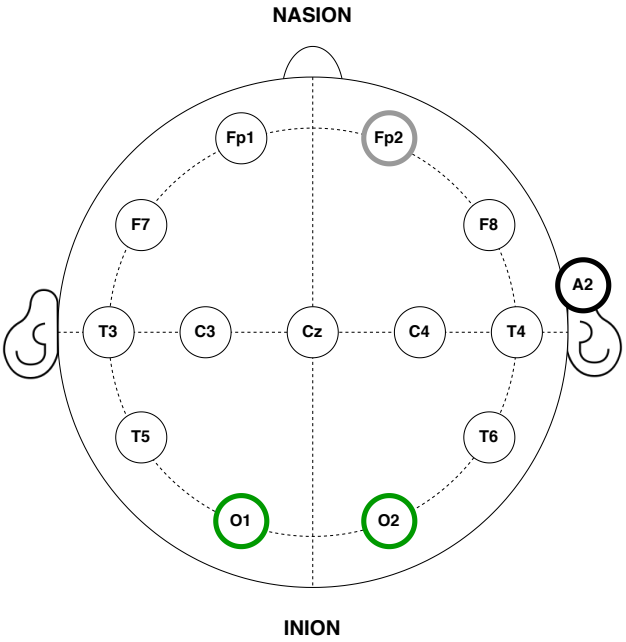

Figure 5.5: Anatomical electrode distribution in accordance with the standard 10–20 placement system used during the electroencephalography measurements. The green circle represents the input channels, while gray and black bordered circles represent reference and ground, respectively.

A wide variety of household devices can be included in the system as subscriber clients (e.g., light bulbs, kitchen burners, heating system). These devices receive the information from the broker and react accordingly to it, e.g., if the kitchen burners client observes that the user has had their eyes closed for a long time, which likely means that he or she has fallen asleep, then the subscriber client should turn the burners off in order to avoid any risk.

5.3 Experimental Results

This section presents the methodology employed during the EEG recordings as well as the group of subjects that participated in the study. Feature extraction and classification algorithms used in the experiments are also explained. Moreover, we show the comparative results obtained from experiments performed when applying the STs, described in Section 5.2, for feature extraction and threshold-based, LDA and SVM algorithms for feature classification. For this purpose, the performance of each classifier is evaluated when data from only one channel is used to estimate the ocular state of the subject. Additionally, for comparison purposes, results obtained for the Cyton board are included.

The participant group included a total of 7 volunteers who agreed to participate in the research. Their mean age was 29.67 (range $24 - 56$). The participants indicated that they did not have hearing or visual impairments. Participation was voluntary and informed consent was obtained for each participant in order to employ their EEG data in our study.

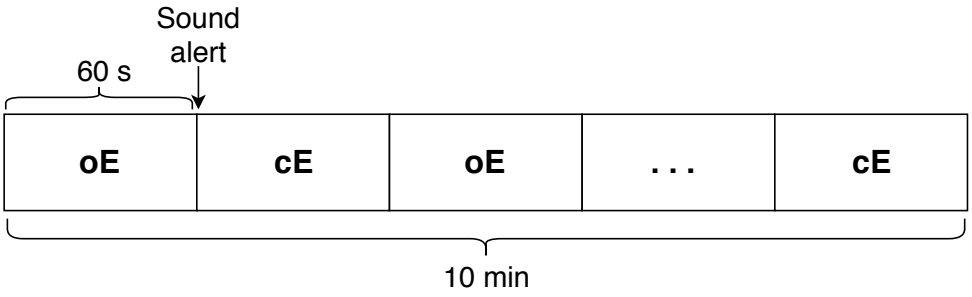

Figure 5.6: User's experiment flowchart.

The Cyton board and the proposed EEG prototype (see Sections 3.1.3 and 5.1, respectively) were used to capture the brain activity of the subjects. Gold cup electrodes were placed in accordance with the 10-20 international system for electrode placement [86] and attached to the subjects scalp using a conductive paste. Electrode-skin impedances were checked to be below $15\,\mathrm{k}\Omega$ at all electrodes. Several studies have proved that the alpha rhythm predominates in the occipital area of the brain when subjects remain with their eyes closed, and it is reduced when visual stimulation takes place [110], [213], [214]. In accordance with these works, the input channels of the EEG devices were located in the O1 and O2 positions. Moreover, for optimizing the setup time and EEG signal quality, the reference and ground electrodes were placed in the FP2 and A2 positions, respectively, where the absence of hair facilitates its placement [215] (see Figure 5.5).

All the experiments were conducted in a sound-attenuated and controlled environment. Participants were seated in a comfortable chair and asked to be relaxed and focused on the task, trying to avoid any distraction or external stimulus. Experiments were composed of 2 tasks: the first one, $60\,\mathrm{s}$ of oE, and the second, $60\,\mathrm{s}$ of cE. In order to simulate a real-life situation, the subject could freely move his gaze during the eye-open tasks, without the need to keep it at a fixed point. The procedure was conveniently explained in advance, allowing the participants to feel comfortable and familiar with the test environment. Moreover, possible artifacts were minimized by asking them not to speak, move or blink (or at least as little as possible) throughout the oE task.

A total of 10 tasks (i.e., 10 minutes) were continuously recorded for each participant, which corresponds to 5 tasks of oE and 5 tasks of cE. Each task was separated by a sound alert, which indicated the user to change the state. All the experiments started with oE as the initial state (see Figure 5.6). Recordings were monitored and analyzed in order to detect artifacts or external noise introduced into the signal.

Taking advantage of the fluctuation of the alpha power between both eye states, we implement the sliding transforms presented in Section 5.2 to compute its mean power and its relative ratio R with beta band. This ratio R represents the extracted feature of the data that is used for training and testing the classification algorithms.

Since an essential feature of our proposed architecture is its ease of use and the users' comfort, a main objective of this system is to guarantee that good performances can be achieved using short training periods. In the developed experiments, the system was trained using 4 minutes of recorded data, where 2 minutes correspond to the oE state, and the remaining 2 minutes to the cE one. From these data, the R ratio is calculated for each window considering each type of transform. These ratios are then used to calibrate the threshold level using Eq. (5.8) or to train the LDA or SVM classifiers.

To compare the accuracies obtained using overlapped and non-overlapped windows, several independent experiments were performed in which only the recordings not considered for the training step were used as test data, i.e., 3 minutes of data corresponding to each eye state. We have considered time windows of D seconds and an overlapped time slot of d seconds. Two important parameters must be taken into account when designing these experiments:

- Computational overhead, which is given by the window size D that determines the number of samples used to compute transforms, denoted by N. Additionally, the number of windows grows with the size of the overlapped time slot, i.e., d.
- Decision delay, which is the waiting time for a new classifier decision, given by $D - d$ seconds.

The performance of each transform has been measured considering only the non-overlapping samples, i.e., only the new instances, corresponding to the $D-d$ part of the window, are classified and taken into account for the calculation of the accuracy.

With the goal of avoiding classification bias, each experiment has been repeated ten times, each time implementing a cross-validation process, i.e., a different combination of training and test recordings is implemented in each of them. For example, the first execution uses recordings 1 and 2 of each eye state to train the classifier, and recordings 3, 4 and 5 for the test; the second execution uses recordings 1 and 3 to train and 2, 4 and 5 for testing and so on until all training combinations are reached. Therefore, the results shown throughout this work correspond to an average of all the executions.

For the LDA and SVM classifiers, in addition to perform a cross-validation process to separate independent training and test data, an inner 5-fold cross-validation is performed in the training step for tuning the hyperparameters of the classifier. This process is carried out by the Bayesian Optimization algorithm [216].

5.3.1 Results from the Threshold-based Classifier

Figures 5.7 and 5.8 show the mean threshold obtained for each subject using the proposed EEG device, non-overlapped windows and different window sizes for the four transforms explained in Section 5.2. Although our system works with only one sensor, we show the results considering the data collected from O1 and O2. In these figures, we observe that the obtained threshold values are highly user-dependent, and it is not possible to find a common pattern

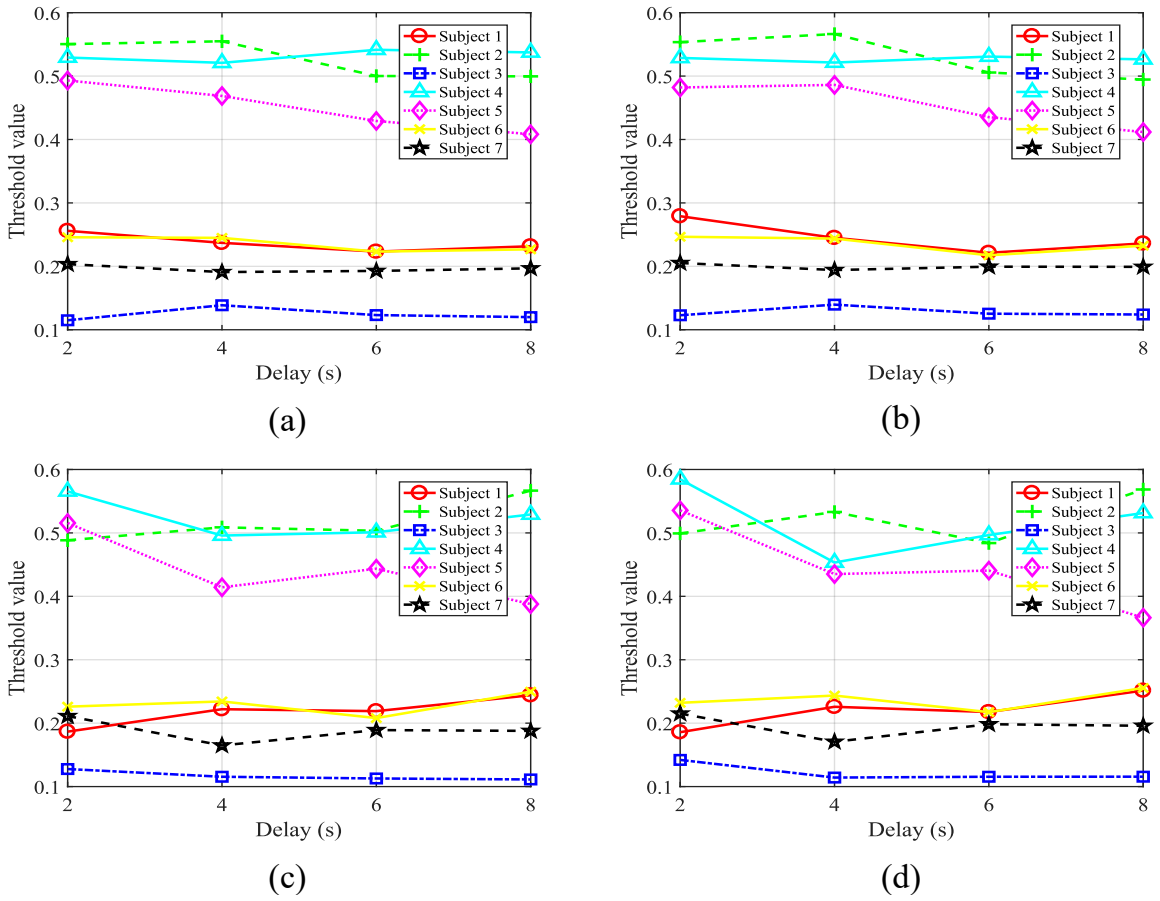

Figure 5.7: Obtained users' threshold from O1 channel data of the EEG prototype for the proposed transforms: (a) ϕ_1; (b) ϕ_2; (c) ϕ_3 and (d) ϕ_4.

among them. As a consequence, the classifier accuracy and the performance of the system will also depend on the brain characteristics of each subject. The same phenomenon occurs with the data captured with the Cyton board, which achieved similar threshold values to those presented in Figures 5.7 and 5.8.

First, we present results corresponding to experiments performed using non-overlapped windows. In this case, the decision delay is the same as the window size, i.e., $D - d = D\,\mathrm{s}$. Table 5.1 shows the results obtained for recordings of both oE and cE states from O1 and O2 channels. We can observe that, although oE achieves, in general, slightly higher results than cE, both eye states offer similar performances, where ϕ_1 and ϕ_2 are the transforms that work best, with accuracies above $90\,\%$ for a $6\,\mathrm{s}$ delay in both channels. It can also be seen that the performance of both channels is comparable, where the maximum difference between the obtained accuracies by each of them is $3.25\,\%$ for the ϕ_2 transform and the oE state.

On the other hand, Table 5.2 shows the accuracies obtained with non-overlapped windows for the OpenBCI Cyton recordings. It can be observed that the achieved results are similar to those acquired by the proposed EEG device, where the oE recordings offer a success rate lightly greater than cE, the ϕ_1 and ϕ_2 transforms obtain the best results and an $8\,\mathrm{s}$ delay is

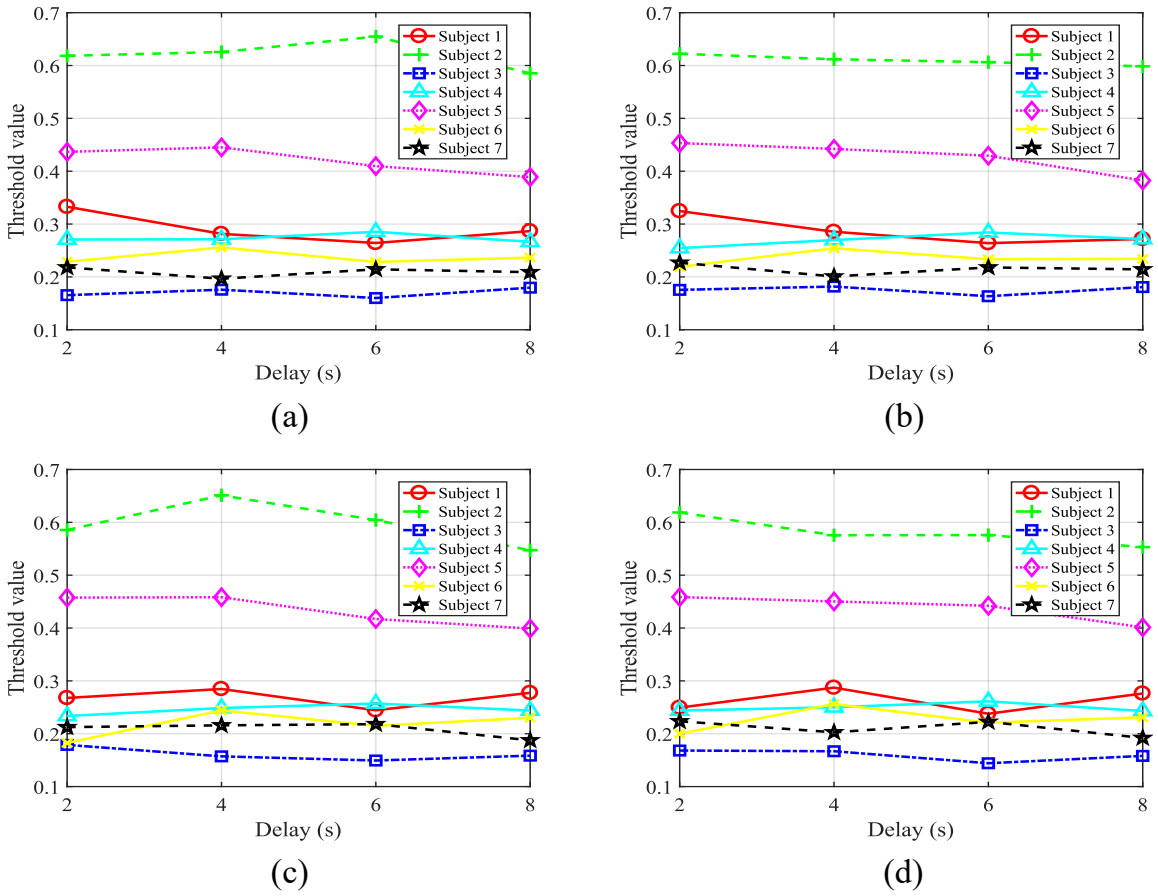

Figure 5.8: Obtained users' threshold from O2 channel data of the EEG prototype for the proposed transforms: (a) ϕ_1; (b) ϕ_2; (c) ϕ_3 and (d) ϕ_4.

needed to obtain the best performance. Moreover, it is also important to highlight that, in both EEG devices, as the window size increases, the obtained accuracy improves, and vice versa. Therefore, there is an important trade-off between system response time and classifier accuracy.

For the second experiment, we consider overlapped windows of size $D = 10\,\mathrm{s}$ and different overlapped sizes, i.e., d is variable. Table 5.3 shows the results obtained for oE and cE recordings from channels O1 and O2. We can observe that all the accuracies, independently of the channel used, have considerably improved for short delays compared to non-overlapped windows (see Table 5.1). In both states, all the transforms and delays exceed $90\,\%$ accuracy, except just in one case, the corresponding to ϕ_4 transform, O1 channel, cE state and $6\,\mathrm{s}$ delay. Table 5.4 presents the classification rates obtained for the OpenBCI Cyton recordings. It can be observed, again, that the performance of both devices is similar, although the results of the proposed device are, in general, slightly higher.

Table 5.1: Performances (in %) for non-overlapped windows with the threshold-based classifier and recordings acquired with the proposed EEG device.

(a) Accuracy for oE

Transform	Delay $D-d$ (s)							
	2		4		6		8	
	O1	O2	O1	O2	O1	O2	O1	O2
ϕ_1	82.55	85.60	88.77	90.70	90.74	92.76	92.18	94.01
ϕ_2	82.45	85.70	89.04	91.13	90.49	92.76	92.59	94.22
ϕ_3	77.55	77.83	86.25	87.64	88.72	90.34	90.00	91.29
ϕ_4	77.31	78.65	85.61	86.64	88.18	89.95	89.86	91.09

(b) Accuracy for cE

Transform	Delay $D-d$ (s)							
	2		4		6		8	
	O1	O2	O1	O2	O1	O2	O1	O2
ϕ_1	83.12	81.95	87.77	88.77	91.53	91.18	92.45	93.95
ϕ_2	82.50	82.04	88.31	88.84	91.67	91.23	92.65	93.88
ϕ_3	75.29	74.52	82.49	83.19	87.49	87.98	89.80	90.82
ϕ_4	74.96	73.96	82.39	84.32	87.59	87.04	89.39	90.61

Table 5.2: Performances (in %) for non-overlapped windows with the threshold-based classifier and OpenBCI Cyton recordings.

(a) Accuracy for oE

Transform	Delay $D-d$ (s)							
	2		4		6		8	
	O1	O2	O1	O2	O1	O2	O1	O2
ϕ_1	81.13	80.79	87.67	86.58	91.03	91.63	92.38	93.54
ϕ_2	80.30	79.90	87.11	86.48	90.25	91.03	91.97	92.52
ϕ_3	73.55	73.94	82.13	81.93	86.16	86.65	88.78	87.89
ϕ_4	72.86	73.71	81.46	82.72	86.11	87.00	88.50	87.76

(b) Accuracy for cE

Transform	Delay $D-d$ (s)							
	2		4		6		8	
	O1	O2	O1	O2	O1	O2	O1	O2
ϕ_1	80.03	80.07	86.51	87.38	89.56	89.56	91.77	90.61
ϕ_2	81.18	80.28	86.81	87.31	89.90	89.85	91.63	90.00
ϕ_3	74.04	73.65	80.80	79.34	85.32	85.57	86.53	86.39
ϕ_4	74.07	73.91	80.50	78.44	84.53	85.37	85.99	85.58

Table 5.3: Performances (in %) for overlapped windows with the threshold-based classifier and proposed EEG device recordings.

(a) Accuracy for oE

Transform	Delay $D-d$ (s)							
	2		4		6		8	
	O1	O2	O1	O2	O1	O2	O1	O2
ϕ_1	93.08	95.63	92.69	95.44	92.65	95.15	94.15	94.01
ϕ_2	93.12	95.92	92.48	95.82	92.65	95.51	93.20	94.90
ϕ_3	91.19	93.70	90.58	93.84	90.66	92.96	90.14	92.59
ϕ_4	91.10	93.73	90.75	93.64	90.71	93.67	90.00	92.04

(b) Accuracy for cE

Transform	Delay $D-d$ (s)							
	2		4		6		8	
	O1	O2	O1	O2	O1	O2	O1	O2
ϕ_1	93.32	94.39	93.27	94.59	93.11	93.72	94.08	94.42
ϕ_2	92.87	94.08	92.89	94.08	92.55	93.93	94.90	94.22
ϕ_3	91.24	92.55	91.05	92.93	91.33	91.63	92.04	92.31
ϕ_4	90.34	92.62	90.10	92.65	89.95	91.48	91.29	92.72

Table 5.4: Performances (in %) for overlapped windows with the threshold-based classifier and OpenBCI Cyton recordings.

(a) Accuracy for oE

Transform	Delay $D-d$ (s)							
	2		4		6		8	
	O1	O2	O1	O2	O1	O2	O1	O2
ϕ_1	92.72	93.20	92.04	93.10	91.94	93.37	93.20	93.95
ϕ_2	92.53	93.27	92.11	93.06	91.43	93.47	92.99	93.27
ϕ_3	90.02	89.40	89.93	89.56	90.71	90.26	90.82	89.66
ϕ_4	89.14	89.43	88.44	89.12	89.74	90.05	88.84	89.46

(b) Accuracy for cE

Transform	Delay $D-d$ (s)							
	2		4		6		8	
	O1	O2	O1	O2	O1	O2	O1	O2
ϕ_1	93.94	93.01	93.88	92.86	94.80	92.14	93.06	92.45
ϕ_2	93.91	93.08	93.84	93.10	94.49	92.30	92.93	92.86
ϕ_3	91.67	90.50	90.82	90.71	91.53	91.02	89.12	88.98
ϕ_4	91.43	90.07	91.67	90.75	90.92	91.07	90.14	89.66

For robustness analysis and user's verification purposes, we evaluate in detail our system for oE and cE detection on each subject. We use window sizes of $D = 10\,\mathrm{s}$ and overlapped windows. Figures 5.9 (a) and (b) show the accuracies and standard deviations obtained for the O1 channel considering $2\,\mathrm{s}$ as decision delay and oE and cE recordings, respectively. The equivalent results for a higher delay of $4\,\mathrm{s}$ are depicted in Figures 5.9 (c) and (d). Figure 5.10 presents the same results for channel O2. It can be seen that both channels offer better performance in open eyes, where there are more subjects that exceed a $90\,\%$ of mean accuracy. It can also be appreciated that, although there is no big difference in the mean accuracy achieved by each channel, the standard deviation is smaller for most of the subjects in the O2 channel, which will imply more robust results. Moreover, it can also be seen that ϕ_1 and ϕ_2 offer the best and similar results for all the subjects and channels (see Table 5.3).

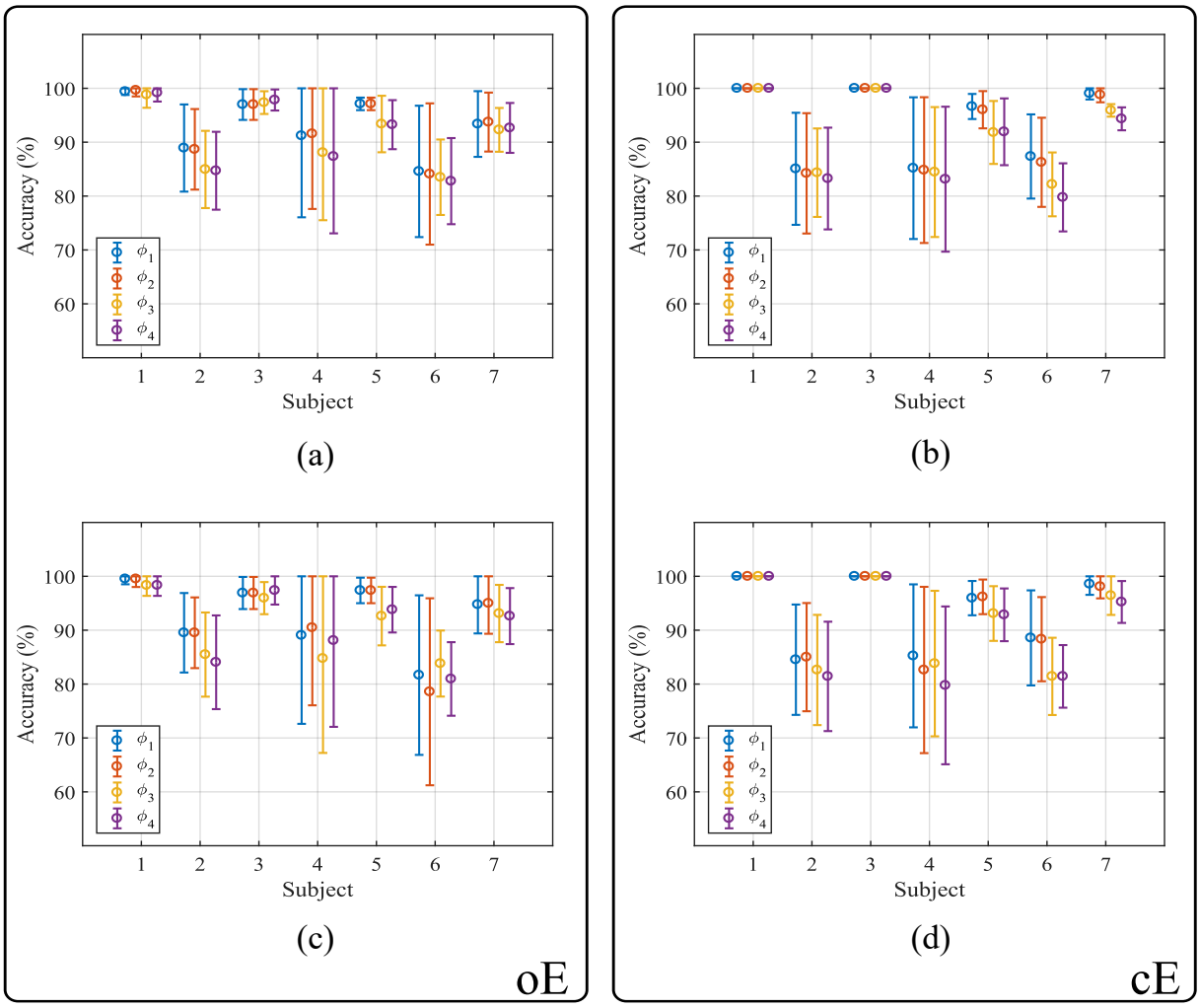

Figure 5.9: Classification accuracies and standard deviation with the threshold-based method and data from the O1 channel and the proposed EEG device: (a) oE with decision delay of 2 s; (b) cE with decision delay of 2 s; (c) oE with decision delay of 4 s and (d) cE with decision delay of 4 s.

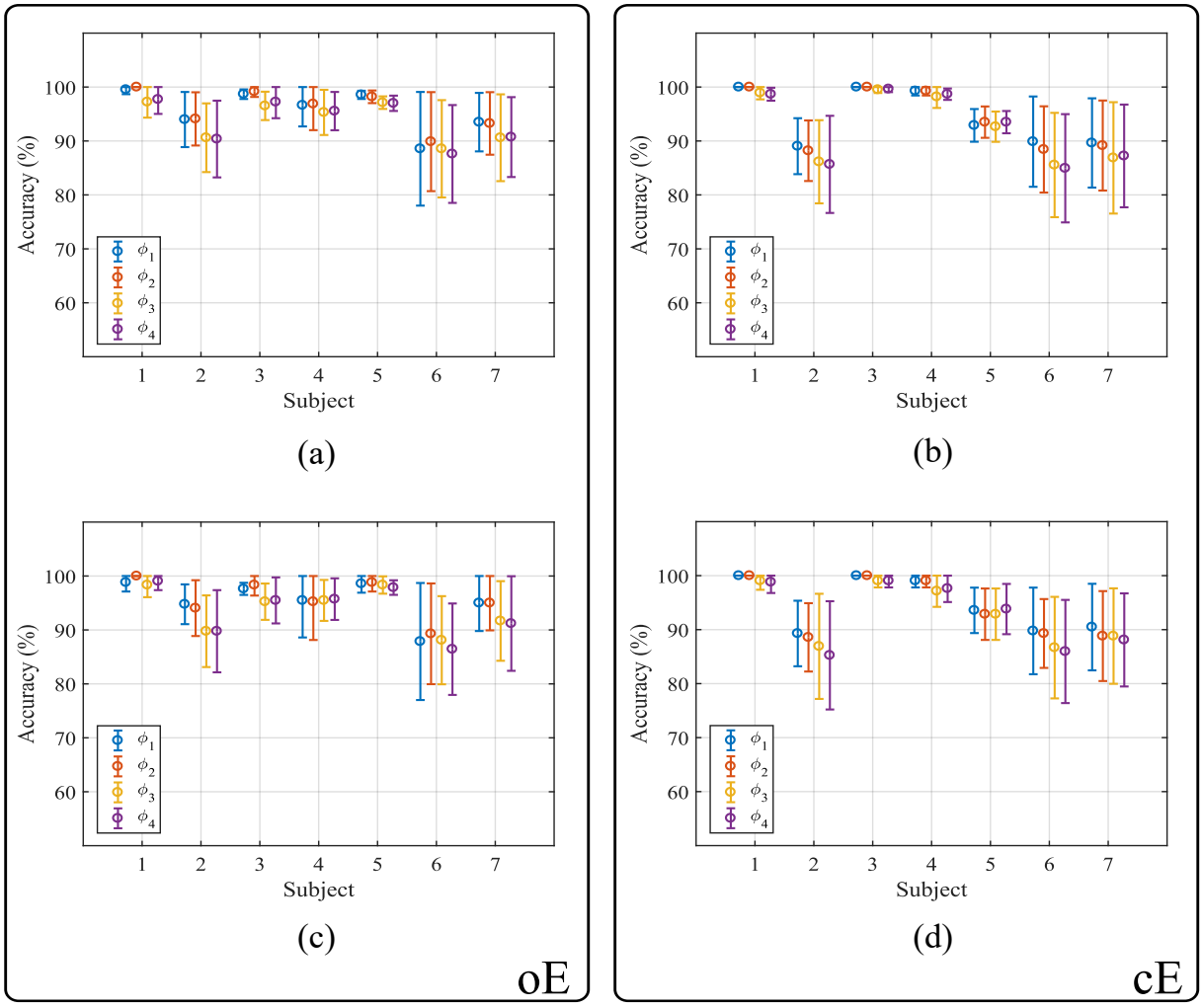

Figure 5.10: Classification accuracies and standard deviation with the threshold-based method and data from the O2 channel and the proposed EEG device: (a) oE with decision delay of 2 s; (b) cE with decision delay of 2 s; (c) oE with decision delay of 4 s and (d) cE with decision delay of 4 s.

5.3.2 Results from the LDA-based Classifier

The same experiments as before have been developed to test the performance of the LDA classifier. Tables 5.5 and 5.6 show the results obtained for cE and oE applying the four proposed transforms of Section 5.2 when the R ratio is extracted considering non-overlapped or overlapped windows, respectively. It can be observed that, for both cases, the oE performance is lower than that achieved by the threshold-based method. For the ϕ_1 transform, the maximum accuracy for non-overlapped windows is $84.42\,\%$ with a delay of 8 s, while the maximum for overlapped windows is $88.32\,\%$ with a delay of 6 s. Tables 5.7 and 5.8 show the same experiments for the Cyton board recordings. It can be appreciated that the performance is comparable to that achieved by the proposed EEG device, although the latter offers, again, slightly better results.

Table 5.5: Performances (in %) for non-overlapped windows with the LDA classifier and recordings of the proposed EEG device.

(a) Accuracy for oE

Transform	Delay $D-d$ (s)							
	2		4		6		8	
	O1	O2	O1	O2	O1	O2	O1	O2
ϕ_1	68.06	69.36	77.61	76.71	81.82	81.23	84.01	84.42
ϕ_2	67.67	68.90	78.11	76.71	81.92	82.17	84.83	85.31
ϕ_3	55.91	56.16	68.70	69.53	75.12	74.53	78.44	78.50
ϕ_4	56.04	56.21	68.41	69.63	75.62	75.52	78.23	79.32

(b) Accuracy for cE

Transform	Delay $D-d$ (s)							
	2		4		6		8	
	O1	O2	O1	O2	O1	O2	O1	O2
ϕ_1	90.84	92.66	93.89	94.52	95.22	95.47	96.26	97.55
ϕ_2	90.82	92.97	93.55	94.45	94.83	95.42	96.33	97.41
ϕ_3	88.95	88.75	92.03	93.65	92.96	94.04	94.01	96.87
ϕ_4	88.59	88.74	92.62	93.09	92.81	93.69	93.95	96.19

Table 5.6: Performances (in %) for overlapped windows with the LDA classifier and recordings of the proposed EEG device.

(a) Accuracy for oE

Transform	Delay $D-d$ (s)							
	2		4		6		8	
	O1	O2	O1	O2	O1	O2	O1	O2
ϕ_1	86.40	87.97	86.39	87.89	85.61	88.32	86.80	87.82
ϕ_2	86.39	88.07	86.53	88.16	85.51	88.16	87.41	87.62
ϕ_3	80.77	82.79	81.50	83.30	79.69	81.28	80.95	83.95
ϕ_4	81.05	82.32	81.84	83.33	80.05	81.48	81.63	83.88

(b) Accuracy for cE

Transform	Delay $D-d$ (s)							
	2		4		6		8	
	O1	O2	O1	O2	O1	O2	O1	O2
ϕ_1	96.78	97.87	96.87	97.76	96.89	97.45	97.21	97.62
ϕ_2	96.73	97.68	96.63	97.69	96.58	97.19	97.07	97.55
ϕ_3	95.82	97.21	95.58	97.41	95.51	96.58	95.92	97.55
ϕ_4	95.54	97.13	95.41	97.18	95.51	96.38	95.71	97.62

Table 5.7: Performances (in %) for non-overlapped windows with the LDA classifier and OpenBCI Cyton recordings.

(a) Accuracy for oE

Transform	Delay $D-d$ (s)							
	2		4		6		8	
	O1	O2	O1	O2	O1	O2	O1	O2
ϕ_1	64.89	64.52	75.25	77.21	80.05	82.76	84.42	86.94
ϕ_2	63.78	64.93	76.15	77.31	80.20	83.35	84.01	87.07
ϕ_3	52.87	54.60	65.55	66.25	72.61	75.67	75.99	79.25
ϕ_4	54.06	54.98	64.55	65.65	71.67	75.42	77.89	81.56

(b) Accuracy for cE

Transform	Delay $D-d$ (s)							
	2		4		6		8	
	O1	O2	O1	O2	O1	O2	O1	O2
ϕ_1	89.15	89.05	92.29	91.86	93.65	92.51	95.92	92.99
ϕ_2	89.03	88.57	91.99	91.63	93.55	92.61	95.24	92.59
ϕ_3	87.77	87.54	91.46	89.93	93.50	91.43	93.47	91.90
ϕ_4	87.36	87.01	90.96	89.10	92.56	91.53	92.65	91.22

Table 5.8: Performances (in %) for overlapped windows with the LDA classifier and OpenBCI Cyton recordings.

(a) Accuracy for oE

Transform	Delay $D-d$ (s)							
	2		4		6		8	
	O1	O2	O1	O2	O1	O2	O1	O2
ϕ_1	84.99	88.26	84.86	88.03	85.36	88.42	86.05	88.44
ϕ_2	85.44	88.47	85.51	88.10	85.77	88.47	85.71	88.30
ϕ_3	78.78	82.58	79.63	83.10	79.08	82.96	81.02	82.65
ϕ_4	78.62	82.27	78.74	82.11	78.93	81.89	80.27	81.56

(b) Accuracy for cE

Transform	Delay $D-d$ (s)							
	2		4		6		8	
	O1	O2	O1	O2	O1	O2	O1	O2
ϕ_1	96.21	95.32	96.36	95.44	97.35	95.20	96.33	95.24
ϕ_2	95.92	95.27	95.95	95.34	96.63	95.20	95.51	95.31
ϕ_3	95.89	94.66	96.53	95.17	96.28	95.56	95.92	95.10
ϕ_4	95.11	94.35	96.16	94.97	95.82	95.31	95.71	94.56

Figures 5.11 and 5.12 show the accuracy and standard deviation obtained for each subject employing $2\,\mathrm{s}$ and $4\,\mathrm{s}$ as decision delays and data recorded from channels O1 and O2, respectively, from the proposed EEG device. A window size of $D = 10\,\mathrm{s}$ and overlapped windows were used. It can be seen that the results of cE are significantly better than those obtained for oE, specially for ϕ_1 and ϕ_2, where only one subject does not exceed an accuracy of $90\,\%$. On the contrary, in the open eyes state, only three subjects are above $90\,\%$.

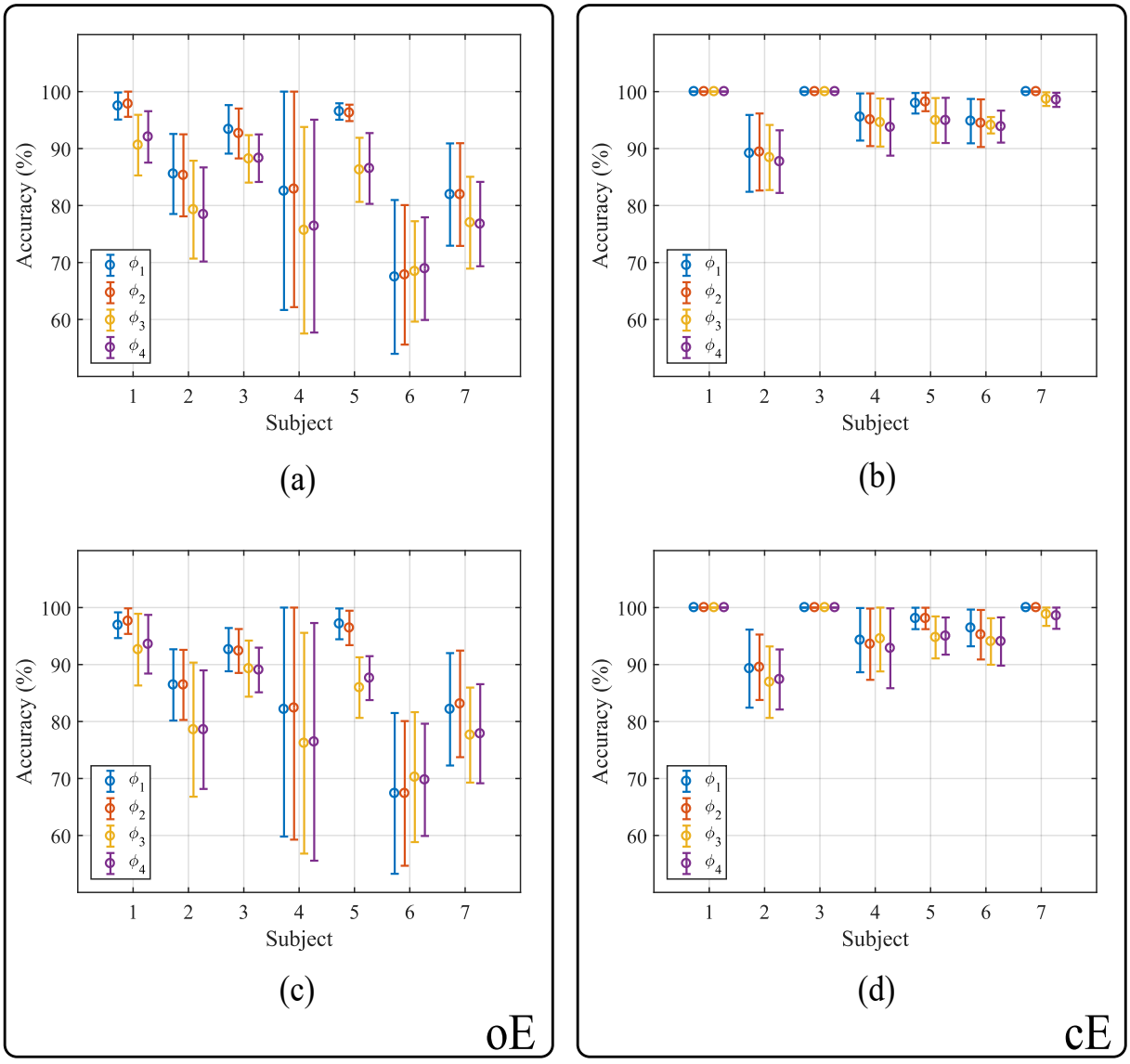

Figure 5.11: Classification accuracies and standard deviation with the LDA classifier and data from the O1 channel and the proposed EEG device: (a) oE with decision delay of $2\,\mathrm{s}$; (b) cE with decision delay of $2\,\mathrm{s}$; (c) oE with decision delay of $4\,\mathrm{s}$ and (d) cE with decision delay of $4\,\mathrm{s}$.

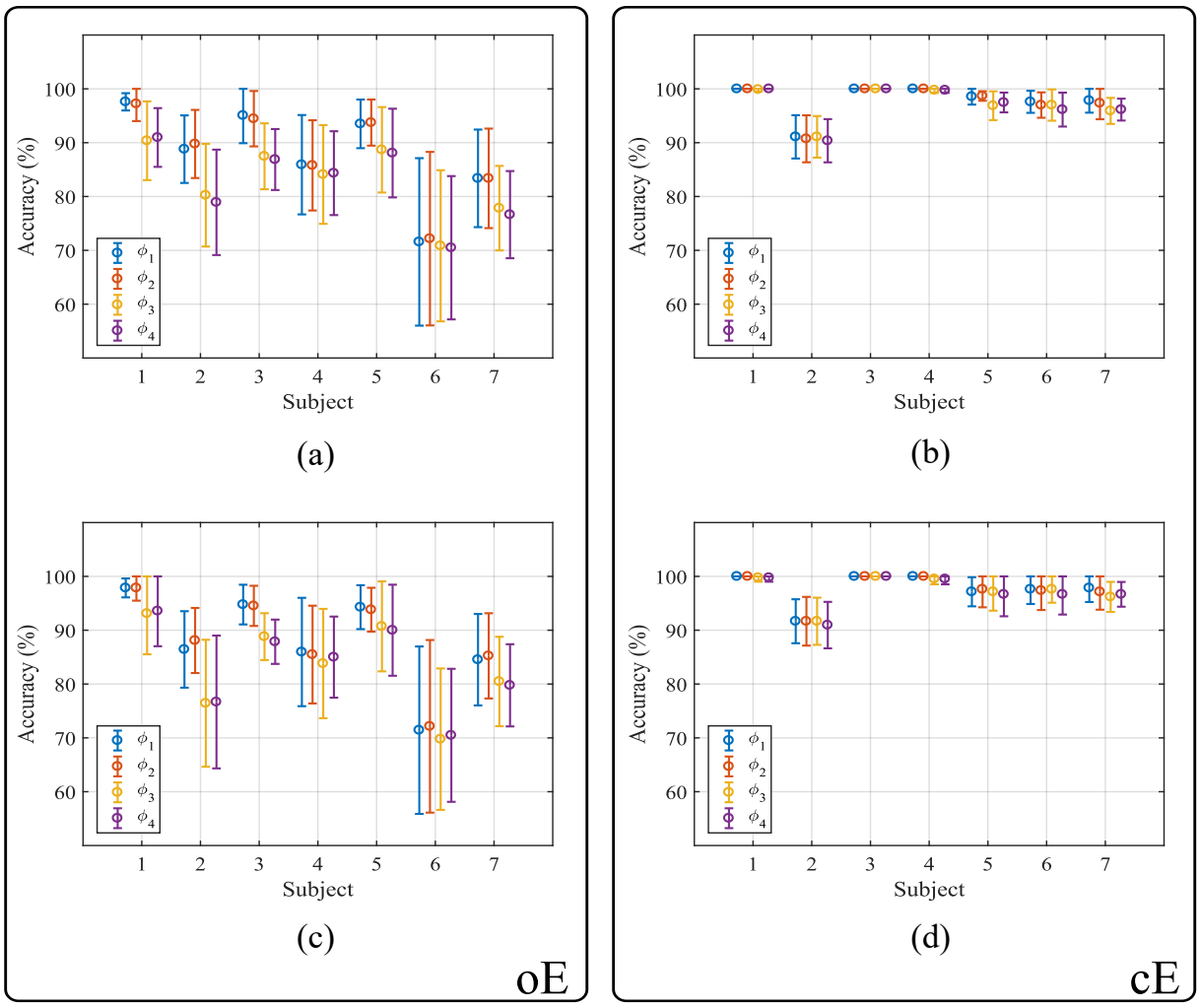

Figure 5.12: Classification accuracies and standard deviation with the LDA classifier and data from the O2 channel and the proposed EEG device: (a) oE with decision delay of 2 s; (b) cE with decision delay of 2 s; (c) oE with decision delay of 4 s and (d) cE with decision delay of 4 s.

5.3.3 Results from the SVM-based Classifier

The same experiments as before have been developed in order to test the performance of the SVM classifier. Tables 5.9 and 5.10 show the obtained results for cE and oE applying the four proposed transforms of Section 5.2 when the R ratio is extracted considering non-overlapped or overlapped windows, respectively. We can appreciate that, for short delays and non-overlapped windows, the threshold-based classifier offers significantly higher results for oE. However, SVM outperforms it in the cE case. Conversely, for overlapped windows, both classifiers offer similar accuracies for both eye states and all the delays. From Tables 5.11 and 5.12, we can also appreciate that the results achieved by the Cyton board are comparable to those achieved by the proposed EEG device.

Table 5.9: Performances (in %) for non-overlapped windows with the SVM classifier and recordings of the proposed EEG device.

(a) Accuracy for oE

Transform	Delay $D-d$ (s)							
	2		4		6		8	
	O1	O2	O1	O2	O1	O2	O1	O2
ϕ_1	79.10	79.93	86.64	89.20	89.66	92.12	91.22	93.61
ϕ_2	77.82	79.74	88.07	89.34	89.36	91.03	91.16	92.59
ϕ_3	67.49	65.81	79.17	83.26	84.98	86.35	85.92	88.50
ϕ_4	66.86	67.31	80.37	81.73	83.25	85.22	86.26	88.37

(b) Accuracy for cE

Transform	Delay $D-d$ (s)							
	2		4		6		8	
	O1	O2	O1	O2	O1	O2	O1	O2
ϕ_1	85.44	87.77	89.53	90.17	92.12	92.32	93.33	94.15
ϕ_2	86.91	87.60	88.11	88.74	92.17	92.56	94.35	94.35
ϕ_3	83.05	82.63	88.41	87.38	89.56	89.21	90.95	91.56
ϕ_4	84.27	82.69	88.01	87.74	90.15	89.80	91.43	91.43

Table 5.10: Performances (in %) for overlapped windows with the SVM classifier and recordings of the proposed EEG device.

(a) Accuracy for oE

Transform	Delay $D-d$ (s)							
	2		4		6		8	
	O1	O2	O1	O2	O1	O2	O1	O2
ϕ_1	93.84	95.78	92.89	95.17	92.55	95.10	93.13	94.15
ϕ_2	93.24	95.71	92.04	95.20	92.14	95.77	92.31	93.13
ϕ_3	90.65	92.86	90.54	93.10	90.36	93.01	88.98	92.31
ϕ_4	90.59	92.75	90.20	93.44	88.78	92.86	88.16	91.36

(b) Accuracy for cE

Transform	Delay $D-d$ (s)							
	2		4		6		8	
	O1	O2	O1	O2	O1	O2	O1	O2
ϕ_1	93.67	94.54	93.81	94.80	93.93	94.64	95.51	94.90
ϕ_2	93.58	94.30	93.37	94.39	93.32	94.23	95.37	95.51
ϕ_3	90.57	92.99	91.60	93.23	90.46	93.42	92.52	92.99
ϕ_4	91.36	92.99	91.22	93.57	91.58	93.37	92.72	94.22

Table 5.11: Performances (in %) for non-overlapped windows with the SVM classifier and recordings of the OpenBCI Cyton board.

(a) Accuracy for oE

Transform	Delay $D-d$ (s)							
	2		4		6		8	
	O1	O2	O1	O2	O1	O2	O1	O2
ϕ_1	77.47	74.24	86.81	85.71	89.80	90.69	91.29	91.50
ϕ_2	75.78	73.92	85.98	84.55	90.05	90.39	90.14	91.63
ϕ_3	60.85	61.79	77.38	73.39	81.82	84.04	86.53	82.52
ϕ_4	61.90	62.27	75.78	76.08	80.79	84.53	85.65	84.69

(b) Accuracy for cE

Transform	Delay $D-d$ (s)							
	2		4		6		8	
	O1	O2	O1	O2	O1	O2	O1	O2
ϕ_1	82.20	84.07	86.54	87.57	90.49	89.56	93.13	90.82
ϕ_2	83.42	83.99	88.04	87.84	89.80	89.85	91.22	90.95
ϕ_3	84.12	83.56	84.45	85.61	86.26	86.31	87.82	88.71
ϕ_4	82.50	82.78	85.85	82.69	87.39	87.39	88.71	84.63

Table 5.12: Performances (in %) for overlapped windows with the SVM classifier and recordings of the OpenBCI Cyton board.

(a) Accuracy for oE

Transform	Delay $D-d$ (s)							
	2		4		6		8	
	O1	O2	O1	O2	O1	O2	O1	O2
ϕ_1	92.94	92.91	92.72	92.86	91.99	92.35	91.77	92.24
ϕ_2	92.72	93.10	92.41	91.60	91.17	92.14	91.63	91.56
ϕ_3	88.93	88.35	87.41	88.06	89.44	87.81	87.41	87.62
ϕ_4	87.83	88.80	86.60	87.93	87.40	87.30	86.53	85.78

(b) Accuracy for cE

Transform	Delay $D-d$ (s)							
	2		4		6		8	
	O1	O2	O1	O2	O1	O2	O1	O2
ϕ_1	94.04	91.55	94.39	92.79	95.10	91.33	93.88	92.79
ϕ_2	94.04	92.58	93.88	93.06	95.36	93.47	93.27	93.27
ϕ_3	92.22	91.39	92.86	91.56	92.81	93.37	92.31	89.59
ϕ_4	92.27	91.38	92.96	91.73	92.50	92.50	92.38	90.95

Figures 5.13 and 5.14 show the accuracy and standard deviation obtained for each subject employing $2\,\mathrm{s}$ and $4\,\mathrm{s}$ as decision delays and data recorded from channels O1 and O2, respectively, from the proposed EEG device. A window size of $D = 10\,\mathrm{s}$ and overlapped windows were used. We can appreciate that similar results are achieved for both eye states, where 4 of the 7 subjects present a mean accuracy above $90\,\%$ for most of the transforms. However, significant differences can be seen among subjects. For example, subjects 1 and 3 achieve high classification accuracies close to $100\,\%$ and short deviations. Conversely, subjects 2, 4 and 6 show lower results (below $90\,\%$ for most of the cases) and larger deviations. Furthermore, we can observe that the ϕ_1 and ϕ_2 transforms offer, for most subjects, the highest results.

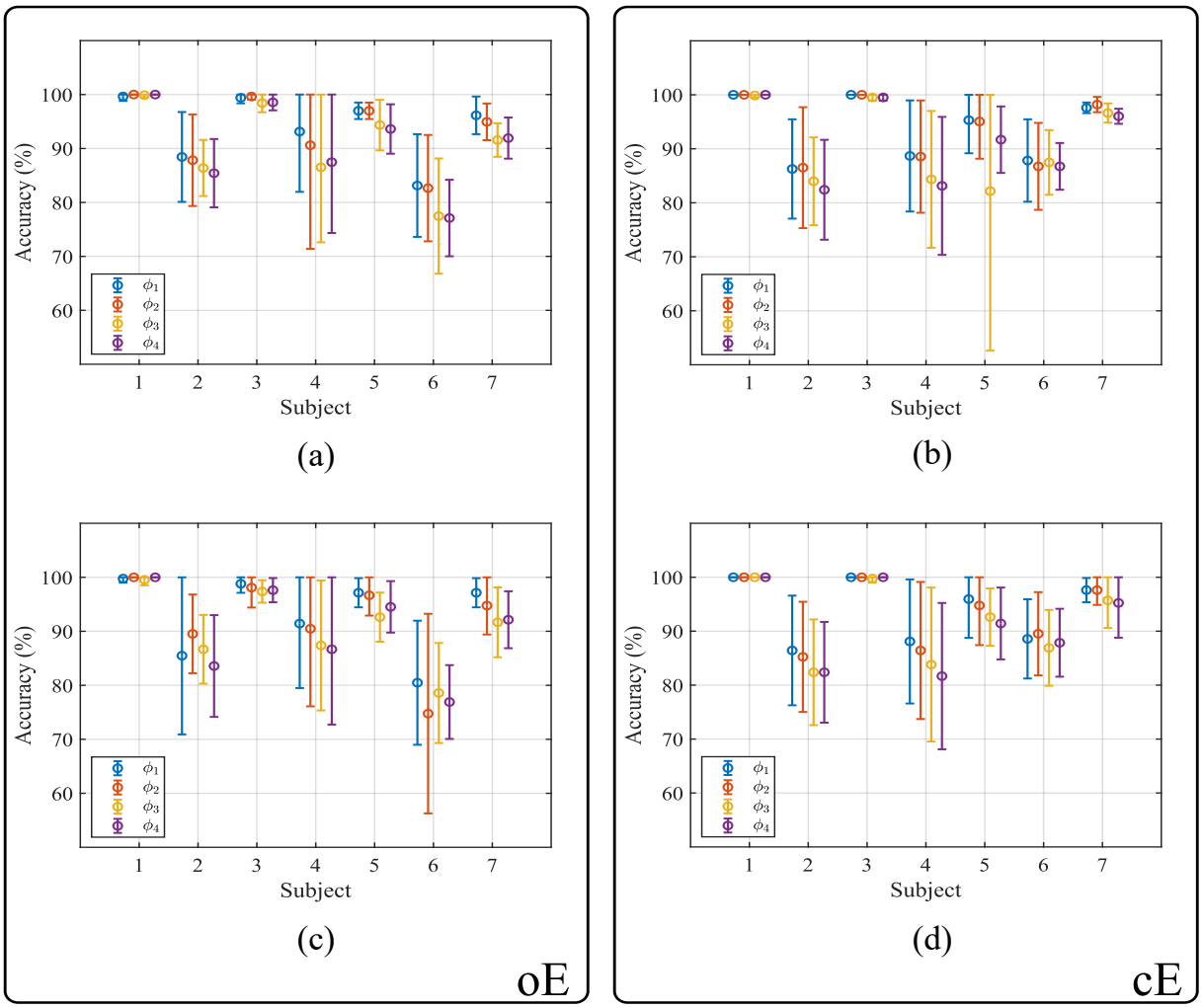

Figure 5.13: Classification accuracies and standard deviation with the SVM classifier and data from the O1 channel and the proposed EEG device: (a) oE with decision delay of $2\,\mathrm{s}$; (b) cE with decision delay of $2\,\mathrm{s}$; (c) oE with decision delay of $4\,\mathrm{s}$ and (d) cE with decision delay of $4\,\mathrm{s}$.

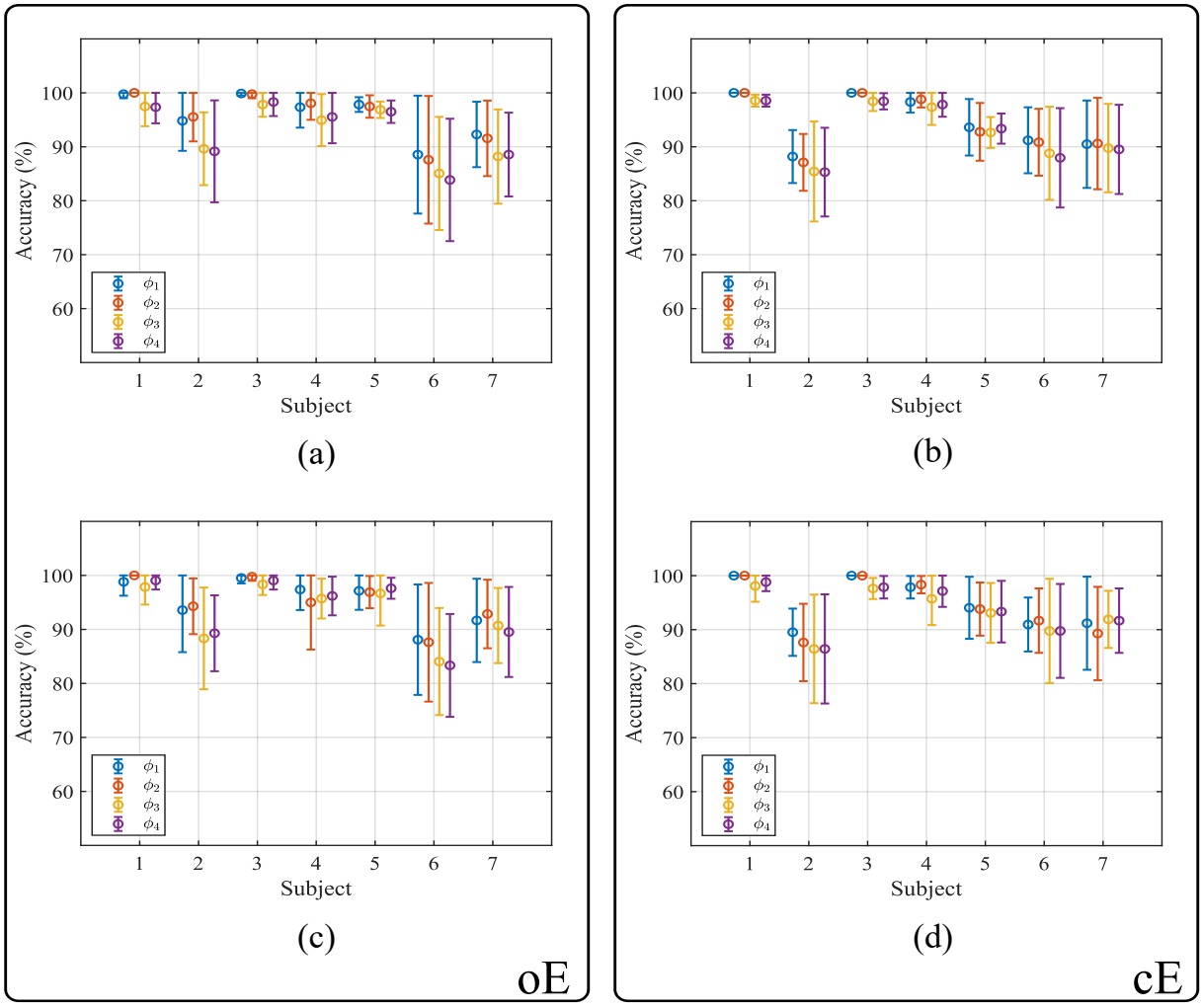

Figure 5.14: Classification accuracies and standard deviation with the SVM classifier and data from the O2 channel and the proposed EEG device: (a) oE with decision delay of 2 s; (b) cE with decision delay of 2 s; (c) oE with decision delay of 4 s and (d) cE with decision delay of 4 s.

5.3.4 Results from the Application in an IoT Environment

This section presents the integration of the previously explained classification system with an IoT environment, where the classifier estimation will be translated into control commands for external devices located in a smart home.

For the proposed architecture presented in Figure 5.4, referred to as *Architecture 1*, the BCI application running on an ESP32 is the first publisher client of the IoT ecosystem. It is in charge of sampling the signal, detecting the eye state of the user and, making use of the built-in Wi-Fi module, publishing the extracted information to the broker. The MQTT broker deals with the messages received from the BCI application and forwards it to interested subscribers. The transmitted data correspond with one byte of information, which represents the ocular state of the user. The broker is deployed in a Raspberry Pi 2 model B and implemented using Eclipse Mosquitto [217], an open source and lightweight MQTT broker.

The data transmission in the MQTT protocol is performed through the exchange of a series of MQTT Control Packets (CPs). These CPs consist of up to three parts: 1) a fixed header, which is always present in all CPs; 2) a variable header and 3) a payload, both existing in some CPs. This final part of the packets is employed by the application to publish the information extracted by the system. Moreover, the protocol allows CPs sizes up to 256 MB [218].

Therefore, once the signal has been captured, the features have been extracted and the eye state of the user has been detected, it is sent to the IoT environment, so the connected devices can react to this information. For this purpose, the BCI application will publish this eye state in a general topic (e.g. "home") where the interested devices are subscribed and listening. The payload of this published message will be only one number which represents the ocular state, i.e., the number "0" represents cE while the number "1" represents oE.

An alternative architecture, termed as *Architecture 2*, consists of running the BCI application in a control unit, like a Raspberry Pi or a PC. In this case, the ESP32 transmits the captured samples directly to that control unit, which is in charge of processing and classifying the signal.

For applications oriented to control IoT devices, it is important to consider and assess the response delay. We have shown in previous sections the results obtained for delays of 2 and 4 s. Table 5.13 shows the payload size of each packet and the number of packets sent during one minute for different architecture configurations. The first two rows show the data transmitted using the *Architecture 1* with delays of 2 and 4 s in that minute. In this case, the payload of each packet will only contain one byte, which represents the user's eye state. Hence, the method with a response delay of 2 s sends the double of packets than the method with 4 s, since it publishes the double of messages. On the other hand, the other three rows show the amount of data transmitted using the *Architecture 2*, so each packet would contain the users' raw brain activity. For this purpose, two scenarios have been assessed. The first one is the transmission of each sample captured by the EEG device, so the external devices can monitor in real-time the user's EEG data. Each sample is encoded in three bytes, so the system sends 36 000 bytes/minute for a sampling rate of 200 Hz. The second scenario corresponds to the transmission of chunks of recorded data related to the non-overlapped slots (for delays of 2 s or 4 s).

Table 5.13: Payload size of each packet and number of packets sent during one minute for different architecture configurations.

Architecture	Method	Payload (bytes)	Packets
1	Eye state (2 s)	1	30
1	Eye state (4 s)	1	15
2	Samples	3	12000
2	Samples (2 s)	1200	30
2	Samples (4 s)	2400	15

5.3.5 Discussion

In this chapter, we have proposed an open EEG device that captures the brain activity of the subjects using a reduced number of sensors. Several algorithms have also been proposed and compared in order to analyze the captured data and determine the ocular state, i.e., cE or oE. In addition, this system has been integrated into an IoT environment for smart home control. We have defined several requirements for the final system:

- The oE detection is usually more important to guarantee comfort.
- The accuracy must be high to avoid undesired situations in which devices turn on/off needlessly.
- Robustness against environment changes and the user's brain activity.
- Ready-to-use application, with short training times that facilitate its usability and integration in our daily life.

The system is trained using two minutes for each eye state and tested with three minutes per state. Tables 5.1 to 5.12 show the results obtained with both overlapped and non-overlapped windows for the calculation of the R ratio. According to those results, it can be observed that the utilization of overlapped windows significantly improves the system accuracy, especially for short delay times. Moreover, from those transform comparisons, we can conclude that ϕ_1 and ϕ_2 are the most suitable transforms for eye state identification. However, for the case of overlapped windows or large delays with non-overlapped ones, all the transforms offer similar results, so any of them may be adequate for the classification. The performances achieved by the ϕ_2 transform are very similar to those obtained by the ϕ_1 transform, although with a lower computational cost (see Section 5.2). Moreover, the success rates provided by the ϕ_3 and ϕ_4 transforms are not as high as for the first two transforms, but they reduce the computational needs even more.

From Figures 5.9 to 5.12 we can observe that the threshold-based classifier performs notably better for the oE state than LDA, in which with the ϕ_1 transform only 3 of 7 subjects achieve an accuracy above $90\,\%$. Conversely, the results obtained by LDA for cE show higher accuracies and shorter deviations than the threshold-based method, but these differences are smaller than those of the oE experiments. Therefore, we can say that our proposed threshold-based classifier provides greater robustness for decision making, so it will be preferable for the system implementation.

On the other hand, Figures 5.13 and 5.14 show that the SVM classifier achieves similar results to those with the threshold-based classifier for both eye states, channels and delays. However, the implementation of this algorithm and its training for a correct classification require a higher computational cost than the threshold-based classifier, since the decision hyperplane is obtained after solving a complex optimization problem (see Section 4.2.2).

Moreover, Tables 5.1 to 5.12 show that the device proposed in this work achieves performances that are, at least, similar to those of a widely-known commercial device such as the Cyton board, offering in the majority of the cases slightly higher results.

Furthermore, the proposed BCI application has been integrated in an IoT environment for smart home control. The detected eye state is translated into a control command and, through the MQTT protocol, transmitted to the interested devices. Table 5.13 shows the packets sent by two different architectures. We can see that *Architecture 1*, which only sends the detected ocular state, uses few packets per second with a minimum payload, so it does not imply a high load on the network or the devices. Conversely, *Architecture 2*, which sends the captured raw samples, will imply a higher load, since it employs a higher number of packets or a larger payload. Therefore, the election between both architectures will depend on the purpose of the final system. *Architecture 2* will be more appropriate if we want to monitor the ocular activity of the user, while *Architecture 1* will be better if we only want to control home devices and not analyzing or transmitting the raw data.

We can appreciate that, for a delay of $2\,\mathrm{s}$ with overlapped windows, the threshold-based method obtains an accuracy greater than 90% for the majority of the subjects in both eye states. This means that the system could correctly perform in non-critical applications which does not require short response times. However, for certain environments, this delay could produce user disagreements or artifacts, and therefore it should be mitigated in future developments. In addition, better success rates must be achieved for those subjects with lower accuracies, since the wrong estimation of the eye state can lead to incorrect performance of the system and turn on/off external devices needlessly.

Besides, taking into account the results presented above, it can be seen that the performance of the system is highly dependent on the subject. That is, for each subject, there is an optimal configuration of channel, transforms and delays that achieves the best results, but it is not shared by other users. For example, from Figures 5.9 and 5.10 it can be seen that subject 7 achieves better results with data of O1 channel, while subject 4 clearly improves his/her accuracy and standard deviation for O2 channel. This indicates that it is not possible to take a general criterion that correctly works for all the subjects, but for each of them it would be necessary to find the optimal parameters for the proper classification of the eye state. This makes difficult the implementation of a BCI based on this system, so the next chapter tries to mitigate this issue, combining the data of both channels to extract the features and train the classification algorithm.

5.4 Conclusions

In this chapter, we have presented an architecture for integrating a BCI application in an IoT environment for home automation. For this purpose, we have developed a low-cost open-source EEG device which acquires EEG signals from two input channels. We employed this prototype to determine the state of open and closed eyes. To this end, we proposed a threshold-based algorithm that uses the ratio between powers of both alpha and beta bands for feature extraction. We compare the performance obtained for different transforms and classifiers applied on overlapped and non-overlapped windows. The obtained results show the advantages

of using the proposed threshold-based classifier and overlapped windows to reduce decision delays and increase robustness. In this sense, we have reached high accuracies for both cE and oE detection independently of the used transform, although for some subjects the Discrete Fourier Transform (DFT) and its binary representation exhibit better results.

Chapter VI

EEG Eye State Detection Using Two Sensors

As presented in Chapter 5, detection of a subject's ocular state can be performed with Electroencephalography (EEG) recordings from a single channel placed over the occipital area of the scalp. However, each subject requires a particular configuration of delays and channels to achieve his/her optimal classification rates. Therefore, in this chapter, in order to mitigate this issue, the data of both channels, i.e., channel O1 and O2, are employed to build a two-dimensional feature set that may provide higher and more robust results. For this purpose, the methods for feature extraction already applied in Chapter 5 are compared with other strategies commonly used in Brain-Computer Interface (BCI) applications, such as Discrete Wavelet Transform (DWT). This study is an extension of the system presented in [202], [203].

6.1 Feature Extraction with Two-Sensor Data

As presented in Section 5.2, the alpha band plays an important role in detecting the user's eye state, while beta shows no significant difference between both states. Therefore, the value determined from the ratio between the mean powers of each band is used as a feature to train and test the classifiers.

In this section, we will briefly introduce the methods for extracting the features from the data captured from two channels.

6.1.1 Sliding Transforms for Two-Sensor Data

Remember the transforms introduced in Chapter 5 as follows,

$$\phi_1(\omega_k, n) = e^{-j\omega_k n} = \cos(\omega_k n) + j\sin(\omega_k n), \tag{6.1}$$

$$\phi_2(\omega_k, n) = \text{sign}(\cos(\omega_k n)) - j\,\text{sign}(\sin(\omega_k n)) \;\; k = 0, ...N-1, \tag{6.2}$$

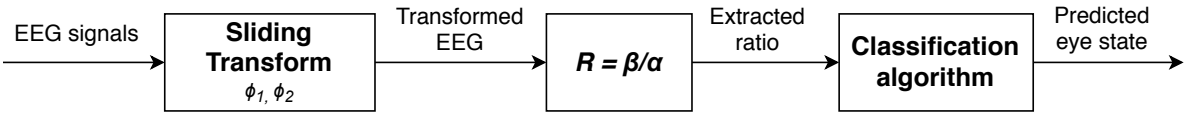

Figure 6.1: Flow chart for experiments based on feature extraction from STs.

referred to as ϕ_1 and ϕ_2, respectively. As was explained, these transforms exhibited the most efficient results. Therefore, for the experiments performed in this chapter, Sliding Transforms (STs) ϕ_1 and ϕ_2 will be the transforms to be applied on the recorded EEG data for the extraction of the features for each channel. They are applied to compute the alpha and beta bands and, according to the mean power of each band, the R ratio is obtained. Then, in accordance to this information, the user's eye state is predicted by a previously trained classifier. Figure 6.1 shows the flow chart of this process when these STs are applied for the feature extraction.

6.1.2 Discrete Wavelet Transform

Wavelet Transform (WT) is a popular technique for the analysis of non-stationary signals, particularly it has been widely applied for denoising EEG signals, stroke detection and feature extraction in BCI applications [219]–[221]. As explained in Section 4.1.3, wavelets are quickly vanishing oscillating mathematical functions with good localization both in time and frequency [151].

The DWT algorithm based on multi-resolution analysis can be implemented as a simple recursive filter scheme composed by a pair of digital filters, high- and low-pass filters, whose their coefficients are determined by the wavelet shape used in the analysis. Therefore, as depicted in Figure 4.2, it decomposes the input signal into a set of Approximation (A) coefficients, which represent the output of the low-pass filter, and Detail (D) coefficients, which are the output of the high-pass filter. The features extracted from these wavelet coefficients at different levels can reveal the inner characteristics of the signal. Hence, both the selection of a proper mother wavelet and the number of decomposition levels are of critical importance for the analysis of signals using DWT [222]. For this purpose, in this experiment, different types of wavelets, already used in previous works for EEG analysis and BCI applications, are evaluated and compared [149], [151], [219], [221], [223]–[225]. In particular, nine types of wavelets are tested: db2, db4, db8, coif1, coif4, haar, sym2, sym4, and sym10. The number of decomposition levels is based on the dominant frequency component of the signal. Therefore, the levels are chosen such that those parts of the signal that correlate well with the frequencies needed for signal classification are retained in the wavelet coefficients [222]. In this experiment, the number of levels of decomposition is selected to be 4. Hence, the signal is decomposed into four detail levels D1-D4 and one final approximation level, A4. Table 6.1 shows the wavelet coefficients and their EEG rhythms equivalence.

According to the decomposition levels presented in Table 6.1 and their equivalent EEG

Table 6.1: Wavelet coefficients and EEG rhythms equivalence.

Coefficient	Frequency band (Hz)	EEG rhythm	Decomposition level
D1	50 - 100	Noise	1
D2	25 - 50	Beta – Gamma	2
D3	12.50 - 25	Beta	3
D4	6.25 - 12.50	Theta – Alpha	4
A4	0 - 6.25	Delta – Theta	4

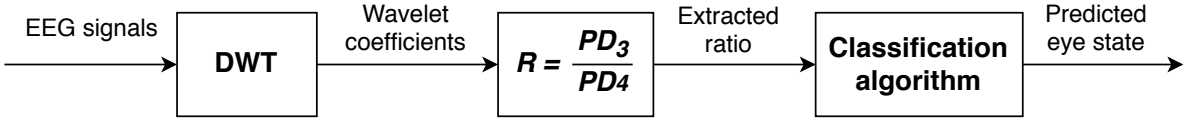

Figure 6.2: Flow chart for experiments based on feature extraction from DWT.

rhythms, D3 and D4 detail coefficients are employed to calculate the R ratio as feature to train and test classification algorithms. In this case, instead of the ratio between alpha and beta average powers, it is calculated between the D3 and D4 average powers. Let PD_3 be the average power of wavelet coefficients at D3 and PD_4 the corresponding for the wavelet coefficients at D4. Therefore, the ratio is computed as $R = \text{PD}_3/\text{PD}_4$. Figure 6.2 shows the flow chart for experiments based on feature extraction from DWT.

6.1.3 Feature Classification

In order to classify the extracted features, two widely used algorithms in the development of BCI applications, such as Linear Discriminant Analysis (LDA) and Support Vector Machine (SVM), are applied for the detection of the user's eye state.

As described in Section 4.2.1, LDA is a linear classifier that seeks to minimize the variance within each class and maximize the distance between the means of these classes. It assumes a normal distribution of data and uses hyperplanes to separate data corresponding to different classes. Similarly, SVM also employs hyperplanes for data separation, although the main difference between them is that SVM seeks for an optimal hyperplane that maximizes the distance between itself and boundary points of each class, i.e., Support Vectors (SVs). SVM achieves a higher generalization for classification, thus becoming more robust. Conversely, LDA has lower computational requirements and faster classification rates, which makes it suitable for the development of online BCI systems [17], [172]. For a more detailed description of both classifiers, please see Section 4.2 of the Chapter 4.

6.2 Experimental Results with Two-Sensor Data

In this section, we show the results obtained when the two schemes for feature extraction described in the previous section are applied on two-channel data combined with LDA and SVM for feature classification. The same EEG recordings presented and used in Chapter 5 are also employed in the experiments conducted in this chapter. These recordings are composed of 10 minutes of brain activity of 7 different subjects, where 5 minutes correspond to open eyes (oE) state and the remaining 5 minutes to closed eyes (cE) state. EEG data is acquired from two electrodes located at O1 and O2 positions. In this case, only the data recorded by the proposed EEG device is employed. For more detailed information about the practical procedure and the EEG recordings, please consult Section 5.3.

The two schemes presented in Sections 6.1.1 and 6.1.2 for feature extraction are assessed and compared using overlapped windows with a duration of 10 s and a delay of $D - d = 2$ s for all of them.

An essential feature of our proposed system is its ease of use and the users' comfort. Therefore, short training periods must be provided. To this end, as was done in the experiments with one sensor (see Section 5.3), 4 minutes are employed for the training step, where 2 of them correspond to the oE state and 2 to the cE one. Thus, the remaining 6 minutes of the recordings, composed by 3 minutes of each eye state, are employed for the test step. From this data, R ratio is extracted for each channel and each window, and used to train and test the classification algorithms.

With the goal of avoiding classification bias, each experiment has been repeated ten times, each time implementing a cross-validation process i.e., a different combination of training and test recordings is implemented for each of them. For example, the first execution uses recordings 1 and 2 of each eye state for classifier training purposes, and recordings 3, 4 and 5 for testing; the second execution uses recordings 1 and 3 for training and 2, 4 and 5 for testing and so on, until all training combinations are reached. Therefore, the results shown throughout this work correspond to an average of all these executions.

Additionally, for the training step, an inner 5-fold cross-validation is performed for tuning the hyperparameters of the classifiers, which is carried out by the Bayesian optimization algorithm [216].

6.2.1 Results from Sliding Transforms for Two-Sensor Data

Figure 6.3 shows the mean accuracy and the standard deviation achieved by LDA and SVM for each user and eye state when the STs are applied on raw EEG data of both channels for feature extraction. The first row of this figure, i.e., Figures (a) and (b), depicts the results obtained by LDA for oE and cE states, respectively, while the second row, i.e., Figures (c) and (d), shows the results achieved by SVM. As can be seen, the LDA classifier does not achieve a good performance for oE state, where 4 of the 7 subjects are below $90\,\%$. The subject 6 obtains

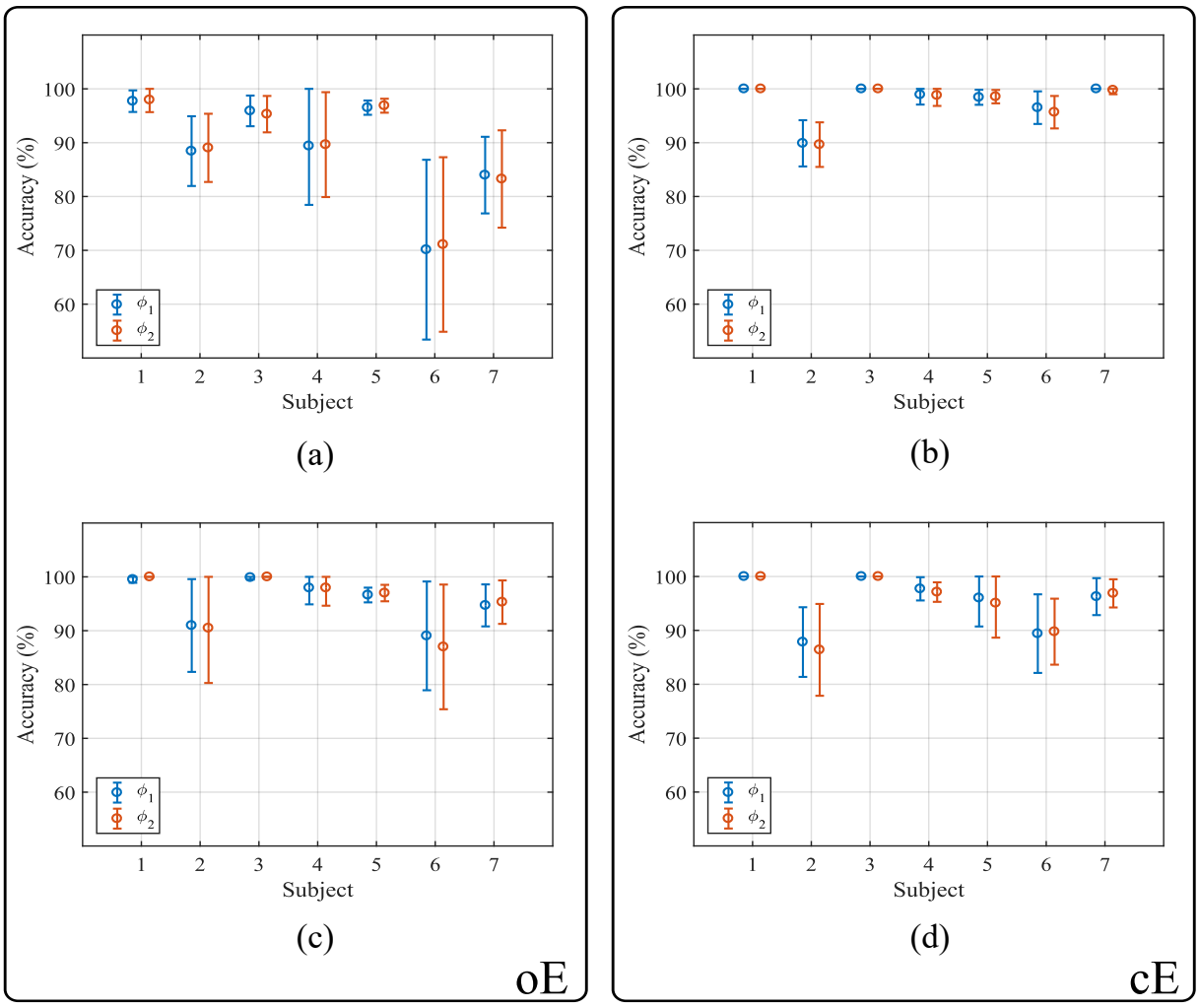

Figure 6.3: Mean classification accuracies and standard deviation per user obtained from STs applying ϕ_1 and ϕ_2 as feature extractors on raw EEG data: (a) oE with LDA; (b) cE with LDA; (c) oE with SVM and; (d) cE with SVM.

a specially low classification rate with a mean accuracy of $70.12\,\%$ and $71.08\,\%$ for ϕ_1 and ϕ_2, respectively. However, for the cE state its performance is significantly higher and more accurate, where all the subjects but one (subject 2), exhibits a mean accuracy higher than $95\,\%$.

On the other hand, we can appreciate that SVM offers more robust results, since the subjects achieve similar accuracies for both eye states. In addition, only one subject, subject 6, is below $90\,\%$ for both eye states, which obtains a mean accuracy using ϕ_1 of $89.04\,\%$ and $89.40\,\%$ for oE and cE, respectively. Subject 2 is below $90\,\%$ only in the cE case. Both subjects present large standard deviations values, with their maximum at $11\,\%$ for subject 6, oE state, and ϕ_2 transform. All other subjects present high classification rates that exceed a percentage of $94\,\%$ and reduced standard deviations.

Table 6.2: Comparison of the classification accuracy (in %) as a function of wavelet type. Bold values indicate the best result for each classifier.

	Open Eyes		Closed Eyes	
Wavelet	SVM	LDA	SVM	LDA
db2	77.57	72.63	83.96	86.39
db4	80.50	79.28	86.63	89.00
db8	87.06	83.22	**88.71**	91.64
coif1	77.68	72.56	84.04	88.30
coif4	**87.38**	**83.77**	88.04	91.76
haar	77.35	69.83	80.79	87.56
sym2	78.14	72.67	82.82	86.27
sym4	82.91	77.76	83.89	88.62
sym10	86.85	81.86	88.62	**93.80**

6.2.2 Results from Discrete Wavelet Transforms for Two-Sensor Data

Table 6.2 shows the mean classification accuracies obtained as a function of wavelet type for all the subjects and both eye states. It can be appreciated that, for the oE case, the performance achieved by each pair of wavelets and classifier is low, since none of them exceeds an $88\,\%$ of average accuracy. Slightly better results are achieved for the cE state. However, most of them remain below a percentage of $90\,\%$. It can also be seen that the best results are achieved by three wavelet types, particularly coif4 offers the highest accuracies in the oE case, while db8 and sym10 are the wavelets that best perform for the cE state.

For robustness analysis, Figure 6.4 shows the results obtained for each subject, eye state, wavelet type and classifier. The first row depicts the results obtained by LDA, while the second one shows those obtained by SVM. It can be seen that the three types of wavelets and both classifiers offer similar results, with large standard deviations and accuracies below $90\,\%$ for most of the subjects, especially for the oE state. For the cE case, slightly better results are achieved, especially by the LDA classifier. It can also be appreciated that there are significant differences in the accuracy obtained for each subject. Subjects 1 and 3 show high accuracies and short deviations for both eye states. Conversely, subjects 2 and 5 show lower results, particularly for the oE case, where none of them exceeds $86\,\%$ and, for example, subject 5 achieves accuracies close, and even below, to $60\,\%$.

6.2.3 Comparison between Results for One-Sensor and Two-Sensor Data

As previously described, one of the main features of the proposed system is to guarantee its ease of use and user's comfort. In order to achieve these goals, there are two main aspects that the system must fulfill. On the one hand, the system should offer good performance levels by

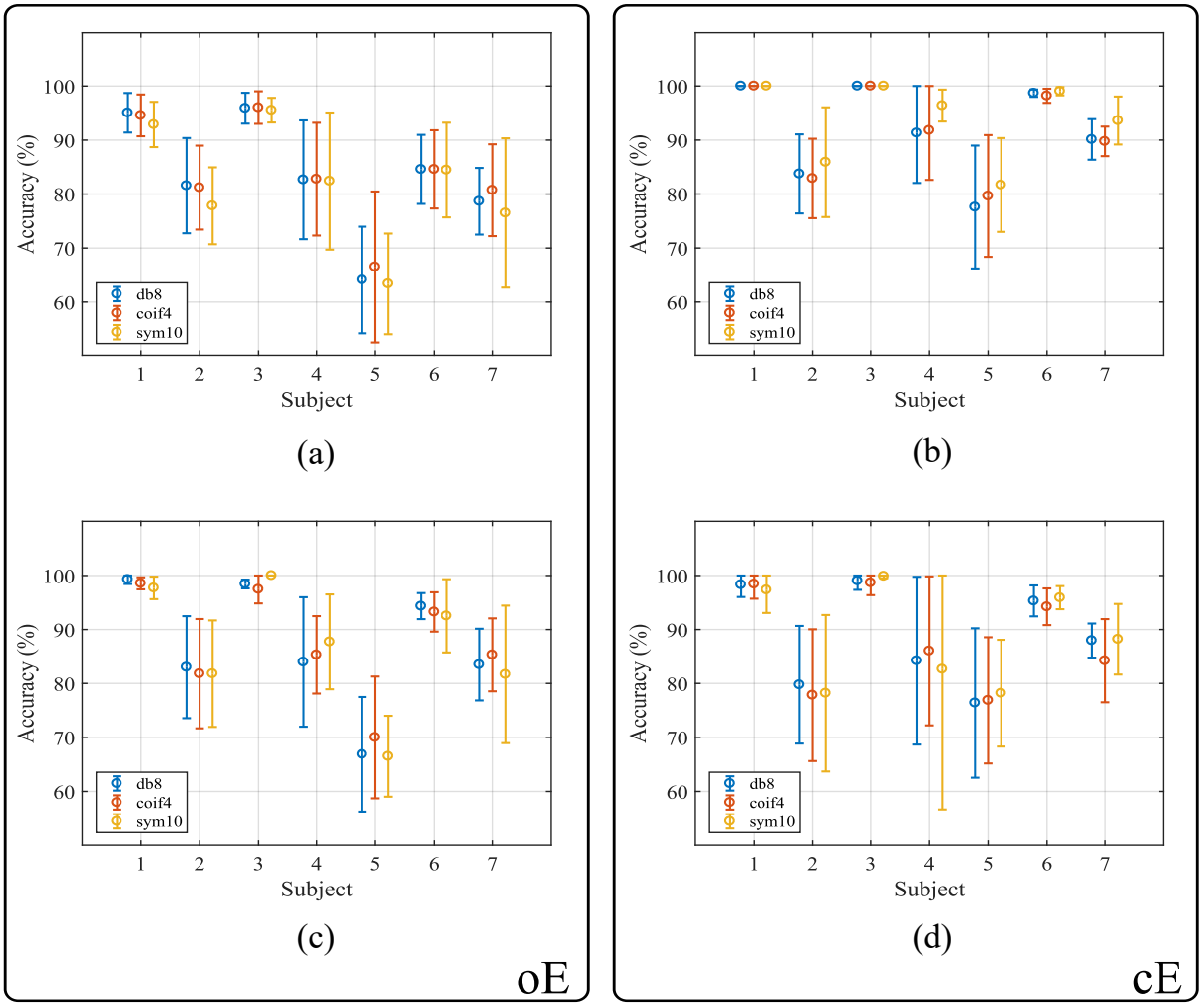

Figure 6.4: Mean classification accuracies and standard deviation per user obtained from three different types of wavelets as feature extractors on raw EEG data: (a) oE with LDA; (b) cE with LDA; (c) oE with SVM and; (d) cE with SVM.

using short training periods. This reduces its setup time and facilitates its use, otherwise, the user may lose his/her interest in the system if it requires long configuration and start-up times. On the other hand, the system should be operated with as few electrodes as possible to provide high performance. This will affect the usability of the BCI and the comfort of the user, since wearing electrodes may be cumbersome and uncomfortable.

In this section, this latter issue is analyzed comparing the results obtained using one and two sensors data for classifying user's eye states. In this regard, all the feature extraction methods as well as the classification algorithms, including threshold-based classifier, are assessed.

Tables 6.3 and 6.4 show the average accuracy per subject obtained for each classifier from ϕ_1 and ϕ_2 STs applied on raw EEG data from one and two channels. It can be appreciated that LDA is not reliable for open eyes detection, since it presents low mean accuracies and high standard deviations (see also Figures 5.11, 5.12 and 6.3). Conversely, the SVM classifier offers high accuracy results for both eye states, regardless of the number of channels used. We can

Table 6.3: Comparison of the classification accuracy (in %) using one and two sensors and the ϕ_1 transform. Bold values indicate the best accuracy per subject.

(a) Accuracy for oE

	Two Sensors		One sensor					
			Threshold classif.		LDA classif.		SVM classif.	
Subject	SVM	LDA	O1	O2	O1	O2	O1	O2
1	99.52	97.71	99.40	99.52	97.47	97.59	99.64	**99.76**
2	90.96	88.43	88.92	93.98	85.54	88.80	88.43	**94.82**
3	**99.88**	95.90	96.99	98.67	93.37	95.06	99.40	**99.88**
4	**97.95**	89.40	91.20	96.63	82.53	85.90	93.13	97.35
5	96.63	96.51	97.11	**98.55**	96.51	93.49	96.99	97.83
6	**89.04**	70.12	84.58	88.55	67.47	71.57	83.13	88.55
7	94.70	83.98	93.37	93.49	81.93	83.37	**96.14**	92.29
Mean	95.52	88.86	93.08	95.63	86.40	87.97	93.84	**95.78**

(b) Accuracy for cE

	Two Sensors		One sensor					
			Threshold classif.		LDA classif.		SVM classif.	
Subject	SVM	LDA	O1	O2	O1	O2	O1	O2
1	100.00	100.00	100.00	100.00	100.00	100.00	100.00	100.00
2	87.83	89.88	85.06	89.04	89.16	**91.08**	86.27	88.19
3	100.00	100.00	100.00	100.00	100.00	100.00	100.00	100.00
4	97.71	98.92	85.18	99.28	95.54	**100.00**	88.67	98.31
5	96.02	98.43	96.63	92.89	97.95	**98.55**	95.30	93.61
6	89.40	96.51	87.35	89.88	94.82	**97.59**	87.83	91.20
7	96.27	**100.00**	99.04	89.64	**100.00**	97.83	97.59	90.48
Mean	95.32	97.68	93.32	94.39	96.78	**97.87**	93.67	94.54

appreciate that SVM using only one channel obtains similar accuracies and, for some subjects, higher than those achieved with two channels. However, the channel that offers the best results is not always the same. For example, for cE and ϕ_1, subject 4 obtains greater accuracy with channel O2 than with O1 or both channels together. However, subject 7 achieves higher results with O1.

The same phenomenon occurs if we compare two-channel SVM with the threshold-based algorithm. SVM from two sensor data offers better results than the threshold classifier for most of the subjects, but not in all of them. Subjects 5 and 7 with ϕ_1 transform, for example, achieve higher classification accuracies for cE state using the threshold-based classifier and channel O1 than using the SVM algorithm, obtaining a percentage of $96.63\,\%$ and $99.04\,\%$ versus

Table 6.4: Comparison of the classification accuracy (in %) using one and two sensors and the ϕ_2 transform. Bold values indicate the best accuracy per subject.

(a) Accuracy for oE

	Two Sensors		One sensor					
			Threshold classif.		LDA classif.		SVM classif.	
Subject	SVM	LDA	O1	O2	O1	O2	O1	O2
1	**100.00**	97.95	99.64	**100.00**	97.83	97.23	**100.00**	**100.00**
2	90.48	89.04	88.67	94.10	85.30	89.76	87.83	**95.54**
3	**100.00**	95.30	96.99	99.16	92.65	94.46	99.64	99.76
4	97.95	89.64	91.57	96.87	82.89	85.78	90.60	**98.07**
5	96.99	96.87	97.11	**98.19**	96.27	93.73	96.99	97.47
6	86.99	71.08	84.10	**89.88**	67.83	72.17	82.65	87.59
7	**95.30**	83.25	93.73	93.25	81.93	83.37	94.94	91.57
Mean	95.39	89.02	93.12	**95.92**	86.39	88.07	93.24	95.71

(b) Accuracy for cE

	Two Sensors		One sensor					
			Threshold classif.		LDA classif.		SVM classif.	
Subject	SVM	LDA	O1	O2	O1	O2	O1	O2
1	100.00	100.00	100.00	100.00	100.00	100.00	100.00	100.00
2	86.39	**89.64**	84.22	88.19	89.40	90.72	86.51	87.11
3	100.00	100.00	100.00	100.00	100.00	100.00	100.00	100.00
4	97.11	98.80	84.82	**99.28**	95.06	100.00	88.55	98.80
5	95.06	98.55	96.02	93.49	98.19	**98.67**	95.06	92.77
6	89.76	95.66	86.27	88.43	94.46	**96.99**	86.75	90.84
7	96.87	99.76	98.80	89.16	**100.00**	97.35	98.19	90.60
Mean	95.03	97.49	92.87	94.08	96.73	**97.68**	93.58	94.30

$96.02\,\%$ and $96.27\,\%$, respectively. Subject 2 also presents higher results with the threshold-based classifier, although for the oE state and with the O2 channel data. As can be seen, the threshold classifier outperforms SVM in very specific cases, for a particular channel and eye state.

Table 6.5 shows the average accuracies per subject obtained by the different classifiers using one and two sensor data and the coif4 wavelet for the signal decomposition into detail and approximation coefficients. It can be appreciated, again, that LDA offers high, and in most of the cases, the highest accuracies for cE state. However, its performance for oE state is poor. The same behavior is presented by LDA with one and two sensor data. Moreover, it can be seen that the threshold-based classifier with channel O2 presents the best mean accuracy for the oE case,

and a higher mean accuracy than the two-channel SVM for cE. Nevertheless, its performance with subject 5 for cE state is the lowest, with an accuracy below $70\,\%$. On the other hand, both one- and two-channel SVM, although in some cases it does not offer the highest accuracies, it shows stable results between both eye states for all the subjects.

Table 6.5: Mean classification accuracies (in %) per subject obtained by different classifiers using one and two sensor data and the coif4 wavelet for signal decomposition. Bold values indicate the best accuracy per subject.

(a) Accuracy for oE

	Two Sensors		One sensor					
			Threshold classif.		LDA classif.		SVM classif.	
Subject	SVM	LDA	O1	O2	O1	O2	O1	O2
1	98.55	94.58	97.71	97.95	93.37	91.81	**98.67**	98.31
2	81.81	81.20	83.13	83.37	78.43	80.24	**83.73**	81.81
3	97.47	96.02	97.47	97.47	91.93	96.27	**98.80**	97.71
4	85.30	82.77	79.64	**86.02**	74.70	80.96	77.11	84.46
5	**70.00**	66.51	68.19	**70.00**	65.30	62.77	66.51	59.88
6	93.25	84.58	90.60	91.93	79.64	86.87	91.93	**94.58**
7	85.30	80.72	79.40	**88.55**	73.01	84.10	79.04	86.39
Mean	87.38	83.77	85.16	**87.90**	79.48	83.29	85.11	86.16

(b) Accuracy for cE

	Two Sensors		One sensor					
			Threshold classif.		LDA classif.		SVM classif.	
Subject	SVM	LDA	O1	O2	O1	O2	O1	O2
1	98.43	**100.00**	99.52	98.31	**100.00**	**100.00**	98.55	97.95
2	77.83	82.89	79.04	80.00	**83.25**	82.89	79.64	80.72
3	98.67	**100.00**	99.28	**100.00**	99.88	**100.00**	97.11	99.76
4	86.02	91.81	77.59	91.45	83.61	**96.27**	78.80	92.65
5	76.87	79.64	71.45	69.40	74.46	78.92	72.17	**81.69**
6	94.22	98.19	96.63	97.59	**98.55**	**98.55**	94.46	96.99
7	84.22	**89.76**	75.54	87.83	86.39	**89.76**	67.59	87.95
Mean	88.04	91.76	85.58	89.23	89.45	**92.34**	84.04	91.10

6.2.4 Discussion

In this chapter, we have proposed an extension of the BCI application presented in Chapter 5, by using two EEG channels instead of one, for controlling household devices in a smart home

environment. For this purpose, we have compared different classification algorithms and feature extraction methods to estimate the eye state of the subjects using data acquired from both EEG electrodes. At this point, it is important to remember the requirements we have considered for the implementation of the final system:

- The oE detection is usually more important to guarantee comfort.
- The accuracy must be high to avoid undesired situations when devices turn off/on needlessly.
- Robustness against environment changes and the user's brain activity.
- Ready-to-use application, with short training times that facilitate its usability and integration in our daily life.

The system is trained using two minutes for each eye state and tested with three minutes per state. Figures 6.3 and 6.4 show the mean accuracy and the standard deviation obtained for each subject when using STs and the DWT as feature extraction techniques, respectively. From these figures, we can observe that DWT is the method that offers the worst results. In this regard, it is important to note that alpha and beta frequency ranges, defined by the detail levels of the wavelet decomposition, do not match those used by the STs algorithms. In particular, the frequency band used in this technique for beta rhythm is significantly wider than the one used by the other techniques. Moreover, the frequency range used for alpha band, which corresponds to the detail coefficients of level 4, also includes frequencies that belong to the theta EEG rhythm (see Table 6.1). Thus, these factors may influence the ratio calculation and its subsequent classification, which provides less accurate results.

Table 6.6 presents the mean accuracies obtained from each classifier and feature extraction technique for both eye states and data from both channels. In this case, ϕ_1 was employed as ST and coif4 as wavelet for the DWT. From this table, and also from Tables 6.3 to 6.5, we can appreciate that SVM offers significantly better results than LDA for the oE case but slightly lower for the cE state. For this reason, we can conclude that the use of SVM is preferable, since it presents more stable results with high accuracies for both eye states.

On the other hand, Tables 6.3 to 6.5 present the comparison between the results achieved by SVM and LDA using two-sensor data and the threshold-based classifier, LDA and SVM using only one-sensor data. According to these results, it can be appreciated that the threshold-based classifier and SVM using one-dimensional data outperforms SVM with two-channel data in specific cases, for a particular channel and eye state, so it is not possible to find a general solution that properly works for all of them. Moreover, as was already explained, LDA, for both one- and two-sensor data, offers high results for cE that, in some cases, outperforms SVM, but its bad performance for oE states makes it a bad solution for the implementation of a BCI. Therefore, the use of SVM with two-sensor data, although in some cases it does not offer the best accuracy, is a suitable option for the implementation of a BCI application, since it presents a general solution that offers a high performance for all the subjects and eye states. However, it is also important to highlight that the threshold-based classifier and the one-channel SVM offer

Table 6.6: Mean classification accuracies (in %) obtained from different feature extraction methods and classifiers for both eye states. ST ϕ_1, coif4 wavelet and data from both channels are employed.

	Open Eyes		Closed Eyes	
Technique	SVM	LDA	SVM	LDA
STs	95.52	88.86	95.32	97.68
DWT	87.38	83.77	88.04	91.76

good results for most subjects and would also be an adequate solution for the implementation of the BCI if the minimum number of electrodes has to be used.

6.3 Conclusions

The integration of BCIs into Internet of Things (IoT) environments is an emerging and promising area. In this chapter, the low-cost EEG device proposed by the authors is employed to capture the brain activity of the subjects and to detect their eye state. For this purpose, in order to properly estimate the eye state, we compare several feature extraction methods, such as STs or DWT, and classifiers, such as SVM and LDA. Moreover, data extracted from one and two channels are also compared to prove if high system performances can be achieved using the minimum number of electrodes. The obtained results show that STs, such as the Discrete Fourier Transform (DFT) and its binary representation, applied on two-sensor data, and combined with the SVM classifier, are the most suitable solutions for the implementation of the BCI, since they offer high accuracies and robust results for both eye states. However, the threshold-based and the SVM classifiers applied on one-electrode data also achieve high performances for most subjects, so both of them could be an adequate solution if the minimum number of electrodes has to be used.

Chapter VII

EEG and EOG Human-Machine Interfaces

During the last decades, several brain signal patterns have been assessed and employed in different Brain-Computer Interfaces (BCIs) as control signals, where Motor Imagery (MI) synchronization/desynchronization, Steady-State Visual Evoked Potential (SSVEP) and P300 Evoked Potential (EP) are the most common approaches [18] (see Section 3.4). In this chapter, we present a P300-based single-channel BCI for controlling home devices and compare it with a Human-Machine Interface (HMI) based on Electrooculography (EOG) .

As described in Section 3.4.3, the P300 EP is a positive deflection located in the parietal area of the cortex that occurs in the Electroencephalography (EEG) brain activity 300 ms after an infrequent or surprising auditory, visual or somatosensory stimuli [4], [126], [132]. The most common way to employ the P300 EP in the BCIs is through the "oddball" paradigm and visual stimulation, where the different elements which the user can interact with are, usually, randomly presented on a screen. The user must focus its attention in one of these infrequent elements, so that when it appears, it will elicit the P300 potential that the BCI can detect and execute the associated action.

As we analyzed in Section 2.3, numerous works can be found in the literature of recent years proposing the use of the P300 for building assistive systems in order to facilitate communication and environmental control for patients with severe motor and neurological damages [18]. For instance, the P300 speller proposed by Donchin and Farwell [4] is a well-known BCI for communications purposes, where a virtual keyboard that contains the letters of the alphabet and also 1-word command are displayed on a screen. The user can select these commands and spell words through the P300 EP. Following this speller approach, several works have been presented in order to improve the performance of the system. For example, different configurations of the characters were proposed, such as region-based or checkerboard paradigms [50], [59]. Moreover, several preprocessing techniques were assessed to improve the P300 detection [226]. Xu et al. [144] proposed an algorithm based on Independent Component Analysis (ICA) for EEG decomposition and a reconstruction of the signal according to spatio-temporal patterns that

enhance the P300 peak. They achieved 100% accuracy for the dataset IIb of BCI Competition 2003. Donchin et al. [227] assessed a P300-based BCI over ten subjects employing the Discrete Wavelet Transform (DWT) with Daubechies wavelet and four level of decomposition. Their results indicate that, using a bootstrapping approach, an offline version of the system can achieve a communication rate of 7.8 characters per minute with an $80\,\%$ accuracy. Several classification algorithms have been also applied for P300 detection, such as Stepwise Linear Discriminant Analysis (SWLDA) [227], Linear Discriminant Analysis (LDA) [228] or Support Vector Machine (SVM) [135], [176], among others [226], [229].

Furthermore, although the original P300 Speller proposed by Donchin and Farwell [4] consisted of only one input channel, it was discovered that the use of multiple channels improved the classification accuracy [230], therefore most modern spellers employ several recording electrodes. A large number of channels require complex and expensive EEG recording devices, where each electrode must be individually placed and calibrated. Such conditions represent a limitation for home users and daily BCIs. However, reduced works using single-channel P300 systems have been developed. Xie et al. [231] propose a single-channel single-trial P300 detection with a new method, Extreme Machine Learning (EML). Their algorithm is tested on 8 subjects and an average accuracy above $85\,\%$ is obtained. In this regard, a single-channel and single-trial P300 detection algorithm is also proposed in [232]. In this work, DWT and ICA algorithms are combined to extract the features on the dataset II of the BCI Competition III, which is based on the P300 speller paradigm. Their results show an average accuracy of $65\,\%$ in single trial P300 detection.

Moreover, the matrix-based paradigm for stimuli presentation introduced by the speller has been widely applied in the P300-based BCIs for environmental control [135]. In this case, both the letters of the alphabet and the 1-word commands of the speller are replaced by device icons of the user's environment which are associated to a control function. So, instead of selecting a character to write, the user chooses an action to be executed in the selected device. For example, Carabalona et al. proposed a P300-based BCI for disabled people in a real smart home environment [133], [134]. In the study, they presented a 6×6 matrix with icons corresponding to the smart home devices and compared its performance with the standard-character speller. Their results reported lower accuracy for the icon tasks than for the character tasks, possibly due to cognitive effort in using icons. Aloise et al. [233] proposed an asynchronous P300-based BCI for home devices control such as DVD player or phone calls, among others, which were presented in a 4×4 matrix. They introduce a threshold-based classification approach that allows the interface to understand user's intents when the user is engaged in another task or is distracted by the surrounding events, avoiding false positive selections. In a more recent study, Corralejo et al. [234] propose an assistive tool for operating electronic devices at home through a P300-based BCI. The interface is tested in a real scenario with 15 severely impaired subjects, which could manage 8 real devices by means of 113 control commands. Ten out of the fifteen subjects achieved an accuracy higher than 75%, and eight out of them an accuracy above 95%. Schettini

et al. [235] presented a P300-based BCI for Amyotrophic Lateral Sclerosis (ALS) patients to manage communication and environmental control applications. The results showed that the BCI could be used as an assistive technology with no significant reduction of usability compared to other communication interfaces such as screens or buttons. In a recent work, Kim et al. [135] developed an online BCI for home appliances control such as the TV channels, electric lights and a digital lock system. They propose to present the stimuli employing a Graphical User Interface (GUI) that jointly displays a control icon and a real time image of corresponding appliances to verify if the proposed GUI correctly works in a P300-based BCI even with the introduced distractions due to the live image of the appliances. For this purpose, the P300 and N200 potentials were analyzed to overcome visual distractions. The results show that healthy participants could control the appliances via BCIs with an accuracy ranging from 78.70% to 83% on average. Moreover, different stimuli configuration and flashing methods have been also applied in the P300-based BCI for environmental control. For instance, Hoffman et al. [228] presented a BCI where home appliances images flashed one at a time to elicit the P300 potential or Aydin et al. [236] proposed an internet-based asynchronous P300 BCI for environmental control applying a region-based paradigm instead of using the standard row-column paradigm.

On the other hand, voluntary eye movements such as blinking, saccades or fixation have been also used as control signals in different HMIs. The electrical signal produced by the eye activity can be measured using the EOG technique which, like EEG, is a non-invasive, portable, easy to use and affordable technology [12]. EOG signals are stronger in amplitude than the EEG ones, so they are easier to detect and more stable across subjects [237], which could be an advantage to improve the accuracy of the interface. Consequently, several HMIs have been proposed employing blinking movements as control signals [14], [237]. The eye can be modelled as a dipole with its positive pole at the cornea and its negative pole at the retina [12]. Therefore, when closing and opening the eyelids, i.e., blinking, a vertical movement is produced in the eye, which causes a change in the dipole orientation and a subsequent change in the electric potential field measured by the EOG. As a consequence, a blink presents a specific pattern in the captured EOG signal, characterized by two consecutive large peaks, one of them a negative peak and another one positive, corresponding to the closing and opening of the eye. These two large peaks are easily recognized in the recorded signal, so HMIs can detect them in order to execute the associated actions.

Several HMIs based on EOG and eye movements have been proposed in recent years. In this regard, He et al. [14] present a single-channel EOG-based HMI that allows users to spell by only blinking. Forty characters were displayed to the subjects, which were randomly flashed. In order to select a character, the subject should blink as the target character is flashed. The results showed that eight healthy subjects achieved an average accuracy of 94.40% for selecting a character in synchronous mode and 93.43% in asynchronous mode. Deng et al. [13] proposed a multi-purpose EOG-based HMI where different eye movements (horizontal and vertical) were detected by the system to control, for example, a TV view by shifting the channels or adjusting

the volume. The authors claim that the precision of the system after adjustment can get above 90%. Also employing eye movements and the generated EOG signal, Barea et al. [15] designed a system for controlling and guiding an electric wheelchair. The users of the system could adjust the direction and speed of the wheelchair only by the movement of their eyes. The study showed successfully results with reduced learning and training times. In a recent study, Guo et al. [238] presented a single-channel HMI that recorded the EOG activity using a patchable sensor designed by the authors. Captured eye movements were converted into computer commands including scroll up, scroll down, and close. Eight subjects were trained to use the system, which was capable of making continuous controls with an average accuracy of $84\,\%$. Heo et al. [239] also designed a wearable forehead EOG measurement system for HMIs. In this case, vertical and horizontal movements of the eye were detected. The system was tested in three applications: a virtual keyboard using a modified Bremen BCI speller, an automatic sequential row-column scanner, and a drivable power wheelchair. The results showed a typing speed of 10.81 and 7.74 letters per minute for the BCI speller and the row-column scanner, and an accuracy of $91.25\,\%$ and $95.12\,\%$, respectively. For the wheelchair experiment, the user drove through an 8-shape course without collision with obstacles.

The use of EEG and EOG signals for interaction with home elements is a current challenge. Some previous work developed multi-sensor systems to capture the brain or eye activity and detect user's intentions [133]–[135], [228], [233], [236]. However, multi-sensor recording devices are usually large and cumbersome, which becomes a problem when using it for several hours a day. Therefore, single-channel solutions have been also proposed in order to overcome this issue by reducing the complexity of the system [14], [231], [232], [238]. As have been shown in Chapters 5 and 6, low-cost systems with reduced input electrodes are really useful for developing Internet of Things (IoT) applications in a smart-home environment [203]. Keeping up with this idea, in this chapter we present and compare two systems oriented to the interaction between the user and home elements. The first system is based on the P300 EP while the second system uses eye blinks as control signals. For this purpose, we developed a GUI where home elements are displayed in a matrix-form and presented using two different paradigms: 1) home elements are presented one-by-one or; 2) the elements of the same row-column are presented together. Our objective is to determine which system and paradigm offer the best performance in terms of accuracy and time delay. The proposed system has been presented in [240].

7.1 Proposed Architectures

Two different systems have been developed in this study. Figure 7.1 depicts the architecture of the EEG control system based on the P300 potential and Figure 7.2 shows the EOG system based on eye blinks. It can be seen that both systems are made up of 4 main parts. A GUI for the presentation of the stimuli, a hardware device for the recording of EEG/EOG signals, the HMI that analyzes the captured signal and converts it into an action command and, finally, household

devices that execute this action. The following sections describe each of these components.

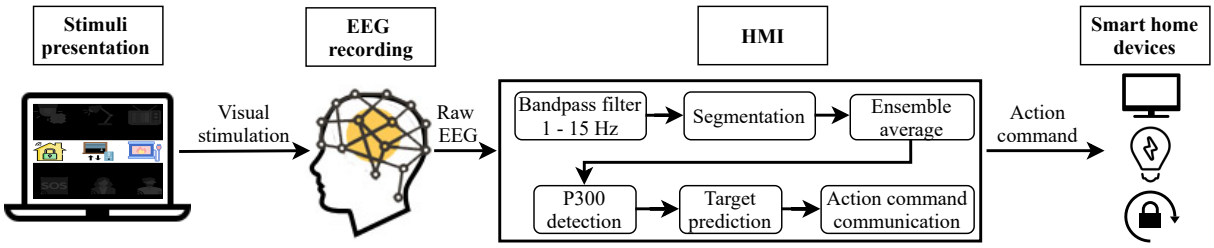

Figure 7.1: Proposed EEG system based on the P300 potential.

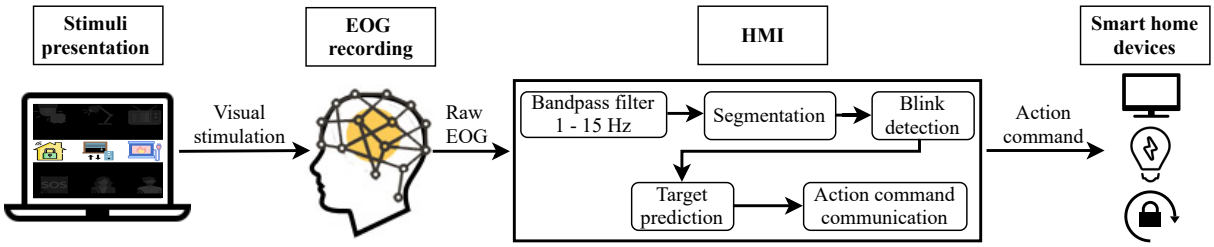

Figure 7.2: Proposed EOG system based on eye blinks.

7.1.1 Graphical User Interface

As depicted in Figures 7.1 and 7.2, in both developed systems, the objects that the user can interact with are presented on a laptop screen using a GUI. This stimulation program was designed and developed in Python employing the PsychoPy package [241].

Figure 7.3 shows an example of the GUI, composed by a 3×3 matrix containing 9 images describing the objects and control functions that the user can execute. The first two rows correspond to home devices such as the TV, digital house lock or electric lights, among others, which the user can switch its state (e.g., on/off or up/down) by selecting them with the HMI. The last row is composed of three possible phone calls. The first one is the emergency call, i.e., SOS call, while the last two calls would be related to the user's favourite contacts in his/her phone-book. Two stimulation paradigms were assessed in the experiments.

In the first paradigm, each element of the matrix is intensified one by one. These intensifications are randomly performed, but all the elements are intensified the same number of times. Therefore, all the elements of the matrix present equal probability to be intensified, $p = 1/9$. Moreover, the same element cannot be intensified two consecutive times.

In the second paradigm, instead of element by element, each row and column of the matrix is intensified. These intensifiactions are also randomly performed, and all the rows and columns are intensified the same number of times. Therefore, the probability of one element to be intensified is $p = 2/6$. Figure 7.3 shows both stimulation paradigms: on the left side, the 1-by-1

paradigm with all the elements intensified and, on the right side, the row-column paradigm with the second row intensified.

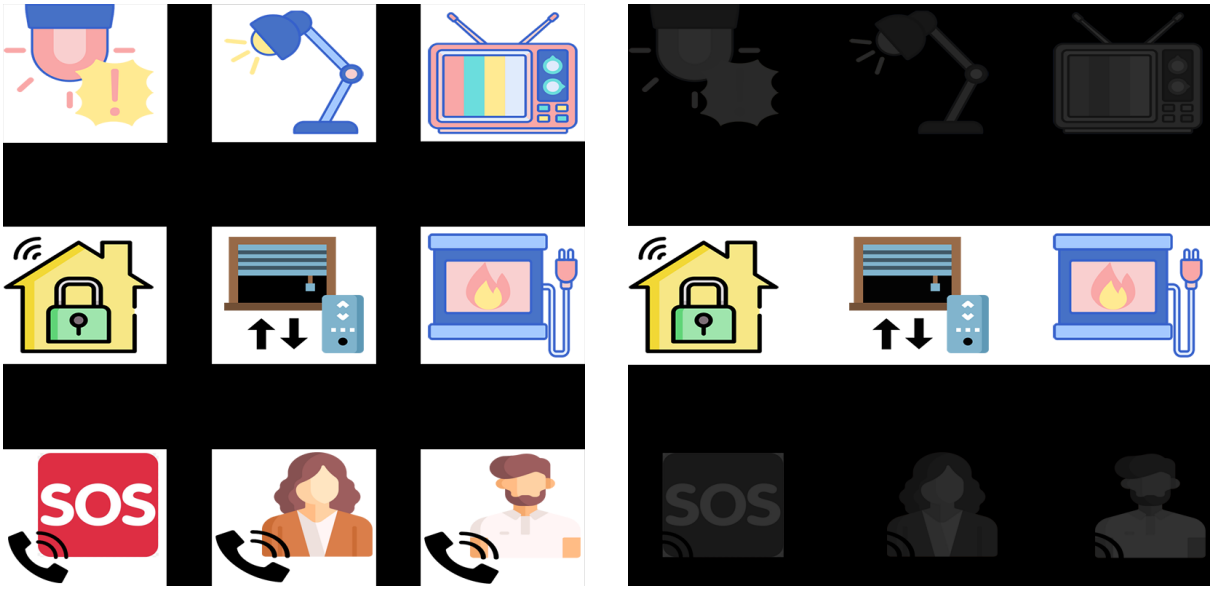

(a) (b)

Figure 7.3: GUI for the two stimulation paradigms. Figure (a) represents the 1-by-1 stimulation paradigm with all the elements intensified, while Figure (b) corresponds to row-column stimulation paradigm only with the second row intensified.

The developed application for stimuli presentation is configurable and it can be adapted to the requirements of each user. However, in order to obtain comparable results, we have selected the same parameters for all the participants of the study. Figure 7.4 shows the stimulation procedure for one run of the experiment. It can be appreciated that each run starts with a preview period of t_{p} seconds for all the elements of the matrix, so the user can locate its target before the instensifications begin. Following this first step, a dark matrix is presented to the user during t_{r} seconds. At this stage, the target must be located and the user must focus its gaze on it for the rest of the run. Once this preparation ends, the instesification step starts. The duration of this stage will be conditioned by the selected stimulation paradigm (i.e., 1-by-1 or row-column) and also by the recording modality (i.e., EEG or EOG) since the number of the intensifications and times will vary for each of them. The intensifications are randomly performed, i.e., the user does not know the order in which the object or column/row will be intensified. These parameters are explained in detail in the following sections.

7.1.2 Hardware

EEG and EOG data were recorded using the OpenBCI Cyton Board [96] with a sampling frequency of 250 Hz . The Cyton board allows simultaneous recording from 8 channels, but only 1 of them is employed in this study. For this purpose, gold cup electrodes were placed in

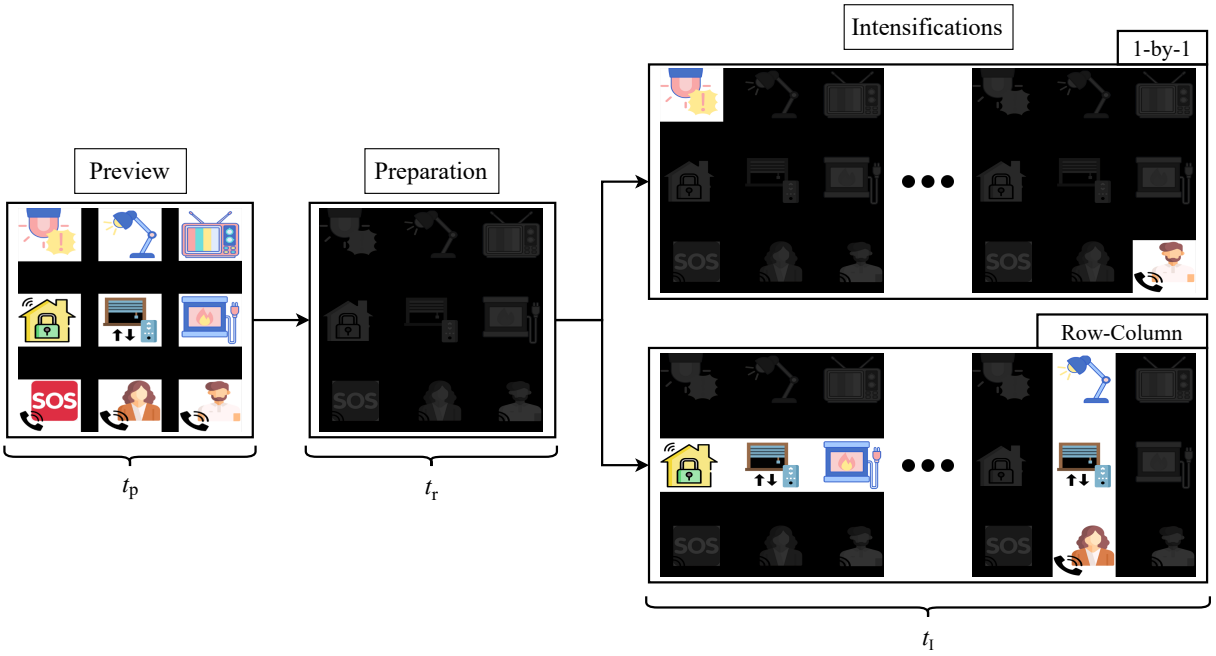

Figure 7.4: Sequence of steps in the two stimulation paradigms.

accordance with the 10–20 international system for electrode placement [86] and attached to the subjects scalp using a conductive paste. Electrode-skin impedance were checked to be below 15kΩ at all electrodes. For the EEG recordings, as the objective is to detect the P300 potential, the electrode for the input channel was located in the Cz position. Conversely, in the EOG recordings, the electrode was placed at Fp2 in order to detect activity related to eye blinks. Both recording modalities shared reference and ground electrodes, placed at Right Mastoid (RM) and left earlobe (A1), respectively. Figure 7.5 shows electrode placement for the experiments.

7.1.3 EEG Recording and Signal Processing

Classical electrode location for P300-based EEG applications generally contains three typical positions: Fz, Cz and Pz [25], [242], since the P300 potential is maximally recorded from the midline centroparietal regions [243]. Therefore, the only channel used by the proposed EEG system, shown in Figure 7.1, is placed at position Cz. The input signal is filtered using a 16th-order Butterworth infinite response filter between 1 and 15 Hz.

Evoked potentials appear as event-related responses from the brain to sensory stimulation, such as, for example, the one used in this study: visual stimulation. The main challenge to overcome when working with these brain responses is that individual EPs present very low amplitude values, ranging from 0.1 to 10 μV, while the EEG background activity ranges from 10 to 100 μV, and hence, EPs are hidden among this background information. Luckily, EPs are time-locked to the stimulus, i.e., it usually occurs at the same latency from the stimulus onset and, conversely, background EEG not related to the stimulus will fluctuate randomly. Therefore, a widely applied technique to solve this issue is the ensemble averaging, which

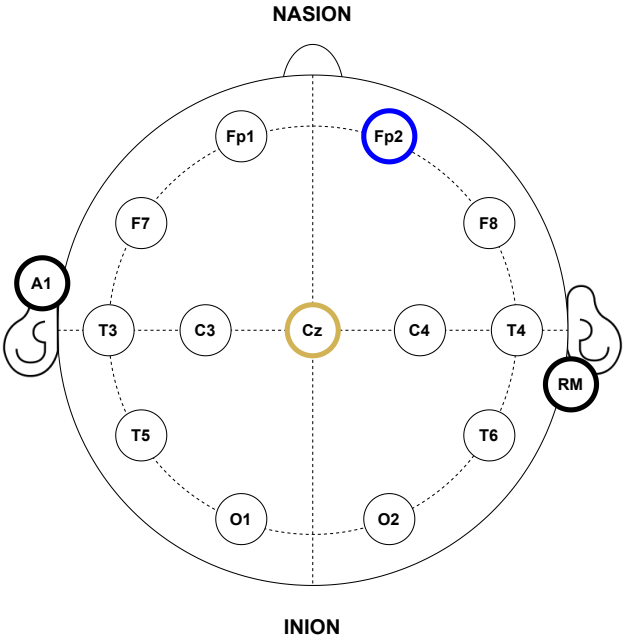

Figure 7.5: Anatomical electrode distribution in accordance with the standard 10–20 placement system used during the experiments. The yellow circle represents the input channel for EEG recordings, while the blue one corresponds to the EOG recordings. Black bordered circles represent reference and ground electrodes.

consists of averaging all brain responses related to the stimulus presentation. In this procedure, the activity time-locked to the stimulus onset will remain robust, while the random background EEG will not, so the Event-related Potentials (ERPs) will clearly appear and the noise will be cancelled [244], [245].

Consequently, this processing technique is the one chosen in this study to obtain the ERPs and detect the P300. For this purpose, firstly, the EEG signal is segmented into epochs time-locked to the stimuli. Following the criteria introduced by Farewell and Donchin in the original P300-speller [4] which states that the useful data consisted of the recorded EEG for $600\,\text{ms}$ after the onset of each intensification, epochs of this duration are extracted after each stimulus presentation. Once all the epochs have been extracted, an ensemble average is performed, i.e., the average of all the epochs for each stimuli is calculated. That is, the recorded EEG signal, $\mathbf{x}$, can be segmented according to stimulus, k, to obtain an ensemble of M epochs, which, in the discrete domain, would be represented by N samples as given

$$x_{k,i}(n), \quad i = 1, \ldots, M;\ n = 0, \ldots, N-1;\ k = 1, \ldots, K. \tag{7.1}$$

Taking this into account, the ensemble of epochs for the k^{th} stimulus can be represented in a matrix form, $\mathbf{X}_k$, where each row vector represents the different epochs and each column vector

the samples of the recorded EEG in this way

$$\mathbf{X}_k = \begin{bmatrix} x_{k,1}(0) & \cdots & x_{k,1}(N-1) \\ \vdots & \ddots & \vdots \\ x_{k,M}(0) & \cdots & x_{k,M}(N-1) \end{bmatrix}. \tag{7.2}$$

The size of the resulting matrix will be $M \times N$, where each element $x_{k,i}(n)$ represents the n^{th} sample of the i^{th} epoch for the k^{th} stimulus.

At this point, the ensemble average for each stimulus, $\mathbf{s}_k$, can be easily calculated by averaging all its epochs as follows

$$\mathbf{s}_k = \frac{\mathbf{x}_{k,1} + \mathbf{x}_{k,2} + \cdots + \mathbf{x}_{k,M}}{M}. \tag{7.3}$$

Once the ensemble average for each stimulus has been obtained, the P300 potential should clearly appear in the resulting averaged signal for the target stimulus. Therefore, if the HMI is able to automatically detect this P300, it would be predicting the user's will without any physical intervention. Several methods have been proposed for detecting the P300 potential [55]. In this study, we define a P300 window that contains and surrounds the potential, the peak and area of the averaged signal in this window can be used for prediction [144]. Those elements with the highest area inside the P300 window were considered as the possible targets.

In order to detect the target element, one prediction criteria was applied for each stimulation paradigm. On the one hand, on the 1-by-1 paradigm, the element with the highest area inside the P300 window was selected as the target. However, on the row-column paradigm, the row and column with the highest area were selected, and the target element was identified as the element at the intersection of the selected row and the selected column.

7.1.4 EOG Recording and Signal Processing

In the EOG system shown in Figure 7.2, the data is captured employing only one input channel placed on the forehead at position Fp2. This electrode location is selected due to blinking activity concentrates at frontal regions [237]. Data captured is filtered using a 4th-order Butterworth infinite response filter between 1 and 15 Hz.

Taking into account that EOG activity and specially blinking movements present consistent patterns with large potentials, they become easier to detect than EEG brain responses [237], [246], so there is no need to present the stimulus a large number of times to reduce the background noise.

The user must blink when its target element is intensified. The purpose of this action is to communicate the objective element to the HMI so it can execute its associated action. As a consequence, this voluntary blink is time-locked to the stimulus, since it must appear right after the intensification onset of the target element and before the onset of the next intensification. Taking this into account, the recorded EOG signal can be segmented into epochs

of 1 s according to each intensification. Therefore, an ensemble of the epochs for the stimulus k can be represented in a matrix form, $\mathbf{X}_k$, as in Eq. (7.2), where each row vector of the matrix represents the epoch for stimulus k and each column vector the samples of the recorded EOG signal. Hence, the element $x_{k,i}(n)$ corresponds to the n^{th} sample of the i^{th} epoch for the k^{th} stimulus.

Once the recorded signal has been segmented, the HMI must detect the blinks in the extracted epochs in order to predict the user's will and execute the desired action. Fortunately, blink movements present clear and characterized patterns in the EOG signals with two consecutive large peaks, negative and positive, respectively, corresponding to the closing and opening of the eyes. These large peaks can be easily recognized from the background EEG activity, which presents smaller amplitude values [12], [247]. Consequently, a threshold-based detection algorithm is proposed in this study. For this purpose, two specific threshold values are defined, th_n, for the negative peak and, th_p, for the positive one. Hence, each epoch can be analyzed and a resulting vector $\mathbf{v}$ can be constructed, where its n^{th} sample follows this criteria

$$v_{k,i}(n) = \begin{cases} -1, & x_{k,i}(n) < th_n, \\ 1, & x_{k,i}(n) > th_p, \\ 0, & th_n \leq x_{k,i}(n) \leq th_p, \end{cases} \tag{7.4}$$

which represents the threshold vector for the i^{th} epoch of the k^{th} stimulus.

According to Eq. (7.4), the observed epochs can be divided into blinking and non-blinking intervals. Blinking intervals will be those between $v_{k,i}(n) = -1$ and $v_{k,i}(n) = 1$, i.e., between the closing and opening of the eyes, while non-blinking intervals will be those outside these values. In addition, as average duration for blinking movements ranges from 100 to 400 ms [12], [248], blinking intervals longer than 400 ms are discarded. As a result, it will be considered that a blink is produced in a specific epoch when it contains a valid blinking interval, i.e., the closing and opening of the eyes have been detected in the lapse of 400 ms. Taking this into account, the BCI can predict the target element by counting the blinks produced on each of its epochs. According to the stimulation paradigm, two prediction criteria were applied. On the one hand, in the 1-by-1 paradigm, the element with the same number of blinks as runs of the experiment will be considered as the target. However, in the row-column paradigm, the row and column with the same number of blinks as runs were selected, and the target element was determined as the one that falls on its intersection.

7.2 Experimental Results

The participant group included a total of nine volunteers who agreed to participate in the research. The participants indicated that they did not have hearing or visual impairments. Participation was voluntary and informed consent was obtained for each participant in order

to employ their data in our study. Table 7.1 summarizes the information of each subject that participated in the experiments.

Table 7.1: Information of each subject that participated in the experiments.

Subject	Age	Gender
1	26	Male
2	26	Female
3	26	Male
4	50	Female
5	53	Male
6	26	Male
7	26	Male
8	27	Male
9	26	Male

The experiments were carried out in a sound-attenuated room where the participants were asked to sit in a comfortable chair while focusing their attention on a 15.6-inch laptop screen where stimuli were presented. Figure 7.6 shows a participant during the P300 recording session, the electrode placement for both experiments and the recording device.

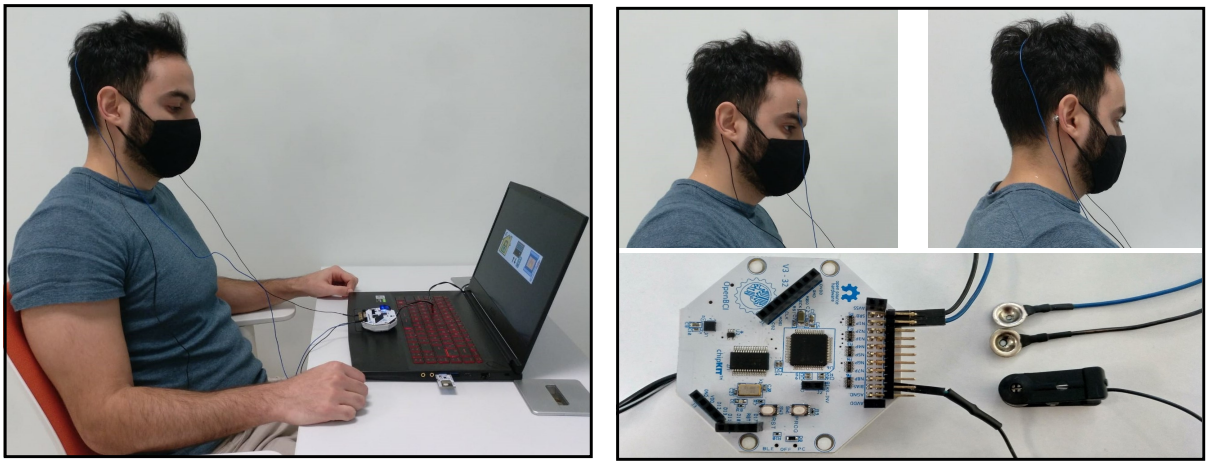

(a) (b)

Figure 7.6: Recording session from one participant of the study, electrode placement for the experiments and recording device: (a) P300 recording session; (b) electrode locations for blinking experiments depicted in the upper left corner; electrode locations for P300 experiments depicted in the upper right corner, and the Cyton board employed for recording the data shown on the bottom.

Recording sessions for each participant were divided into 4 experiments, one per each stimulation paradigm and recording modality, i.e., one experiment for the 1-by-1 paradigm and EEG signals, another experiment for row-column paradigm and EEG signals, another for

EOG signals and the 1-by-1 paradigm and, lastly, one experiment for the row-column paradigm and EOG data.

As shown in Figure 7.4, each experiment was divided into runs consisting of three stages: preview, preparation and intensifications. The graphical user interface described in Section 7.1.1 was used to present the stimuli and configured with $t_{\mathrm{p}} = 5\,\mathrm{s}$ and $t_{\mathrm{r}} = 2\,\mathrm{s}$. The duration of the intensifications stage, t_{I}, is conditioned by four different parameters:

- The number of possible stimuli (NS), that will be 9 in the 1-by-1 paradigm (one per each element of the matrix) and 6 in the row-column paradigm (one per each row and column of the matrix).
- The number of instensifications (NI), i.e., the number of times that each stimulus is presented to the user.
- The intensification time (IT), i.e., the time that a stimulus remains intensified.
- The inter-stimulus interval (ISI), that is, the elapsed time from the end of stimulus intensification to the onset of the next one. During the ISI, no element of the matrix is intensified, i.e., all of them stay dark.

Consequently, $t_{\mathrm{I}} = \mathrm{NS} \times \mathrm{NI} \times (\mathrm{IT} + \mathrm{ISI})$. Table 7.2 summarizes the different configurations selected for each experiment type. The same parameters were used for all the participants in the study.

Table 7.2: Parameters selected for each experiment performed during the recording sessions. NS: number of possible stimuli; NI: number of intensification; IT: intensification time; ISI: inter-stimulus interval; t_{I}: time of the intensification stage.

Experiment	Recorded Signal	Stimulation Paradigm	Runs	NS	NI	IT (ms)	ISI (ms)	t_{I} (s)
1	EEG	1-by-1	8	9	50	70	130	90
2	EEG	Row-Column	8	6	50	100	200	90
3	EOG	1-by-1	8	9	3	500	500	27
4	EOG	Row-Column	8	6	3	500	500	18

After each run, a rest interval of at least $30\,\mathrm{s}$ was allowed. The entire experiment session lasted approximately 90 minutes. Moreover, as the analysis of the collected data is performed offline, no visual feedback is provided to the user at the end of each run.

7.2.1 Signal Analysis

Captured EEG signals from all the participants in the study are analyzed and visually inspected in order to verify that the recordings were correctly performed and that the P300 EP is elicited when the target element is intensified. As previously described, EEG signal is filtered, epoched and averaged for this purpose.

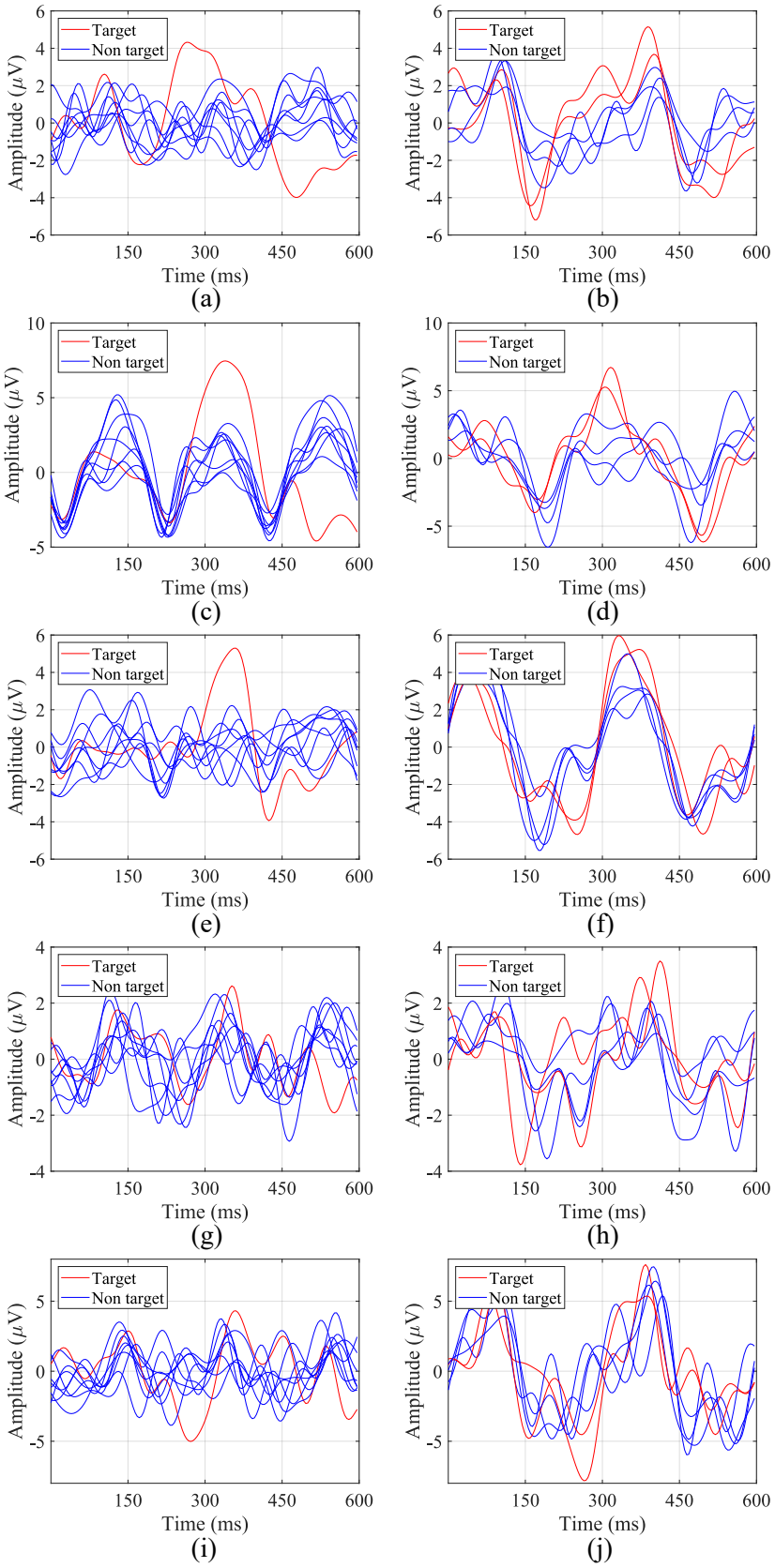

Figure 7.7: Averaged ERPs for the first 5 subjects for both stimulation paradigms. The left column contains the ERPs for the 1-by-1 paradigm, while the right one represents ERPs for the row-column paradigm.

Figure 7.7 shows the averaged ERPs of the first 5 subjects for both intensification paradigms of one run of the experiment. The left column contains the ERPs for the 1-by-1 paradigm, while the right one represents the averaged signal for the row-column paradigm.

The P300 potential clearly appears around 300 ms for subjects 1, 2 and 3 when the target element is intensified, whereas for subjects 4 and 5, although the potential appears, it is more difficult to distinguish. In addition, it can be observed that the latency, i.e., the elapsed time from the stimulus onset to the highest value of the P300 potential curve, varies from one participant to another. For example, for the 1-by-1 paradigm, the first subject (Figure 7.7(a)) reaches his/her highest value at 264 ms, whereas for the third subject (Figure 7.7(e)) this happens at 360 ms. For the first subject, the delay also varies for each paradigm, since for the row-column the peak appears closer to 400 ms (Figure 7.7(b)).

Taking this analysis into account, the P300 window, defined by the BCI for the P300 detection and the subsequent target identification, will depend on the latency of the participants for each paradigm. Therefore, the BCI must define a P300 window adapted to each participant and condition, since a general common window would offer poor results.

EOG recordings were also analyzed and visually inspected in order to verify that the data were correctly captured and that the blinks were well represented in the signals. Figure 7.8 shows data from the first 5 subjects for one run of the blinking experiment and both stimulation paradigms. The left column contains the signal for the 1-by-1 paradigm, while the right one corresponds to the row-column one. The blinks, which are represented by two consecutive large peaks, negative and positive, are clearly distinguishable from the background EEG data captured by the electrode. These voluntary blinks appear right after the intensification onset of the target element, so the user is communicating to the HMI the element that he/she wants to select. It is important to note that the amplitude of these blinks varies for each participant. For example, for the first subject, blink peaks are above $300\,\mu$V, while for the second subject they appear from 80 to $200\,\mu$V.

Taking this amplitude variation into account, the threshold value employed by the blink detection algorithm must be subject-dependent. That is, the BCI must define a threshold value for each participant in order to detect the produced blinks in the epochs.

7.2.2 Classification

High classification accuracy when detecting the element selected by the user is of primary importance for the correct performance of the HMI. Low accuracies would imply to execute the wrong action in the user's environment, which could be frustrating, annoying and, in some cases, it could be even a risk for him/her, for example, if the user needs to call emergencies but the interface can not detect the user's will. Consequently, the accuracy of the classification algorithms presented in this study is assessed and analyzed in order to determine if their results are suitable for the implementation of a reliable HMI with practical applications in a smart-

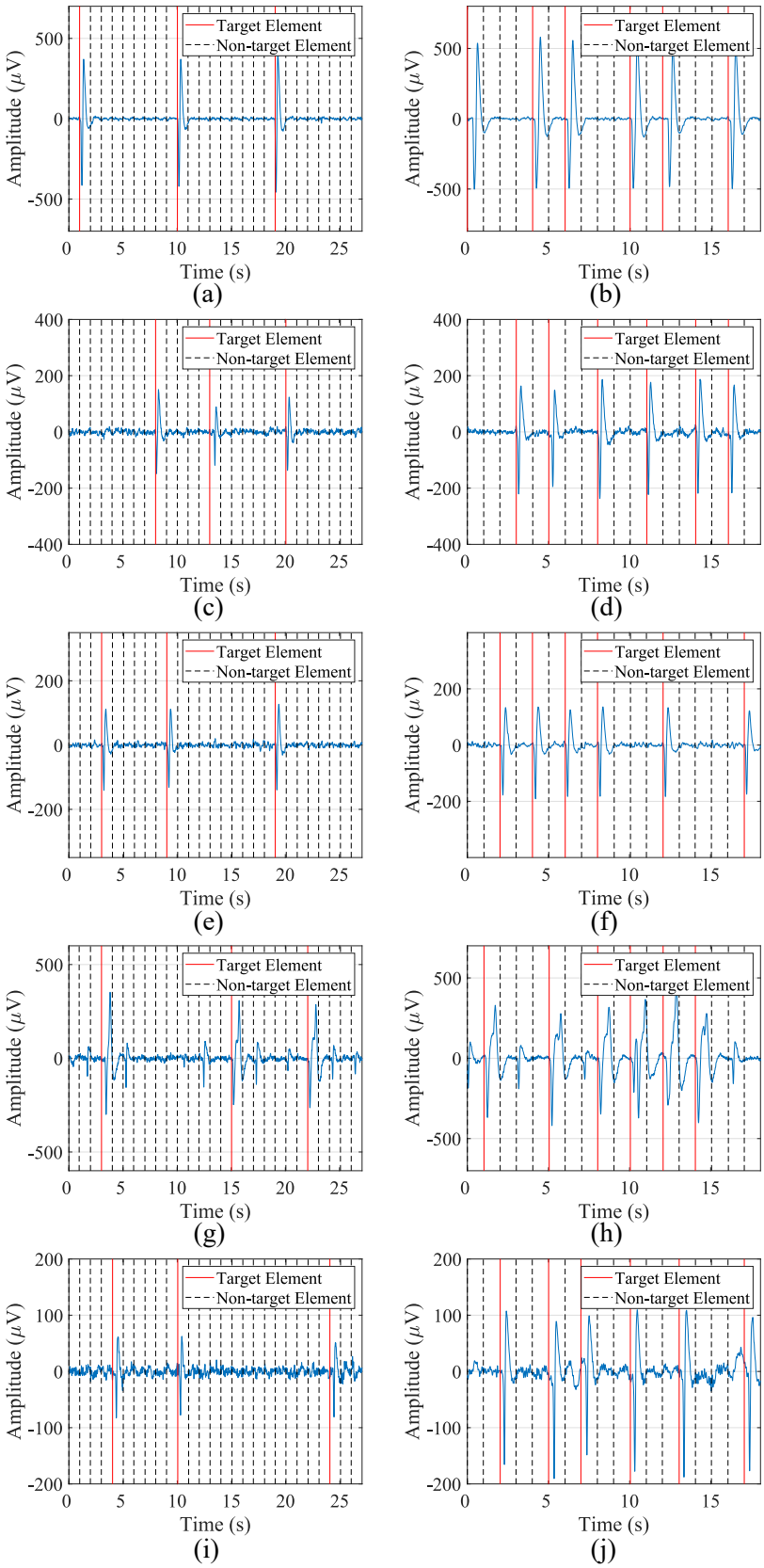

Figure 7.8: Data of the first 5 subjects for one run of the blinking experiment for both stimulation paradigms. The left column contains the signals for the 1-by-1 paradigm, while the right one corresponds to the row-column paradigm.

home environment.

Table 7.3 shows the classification accuracy for each subject, stimulation paradigm and both control signals. This accuracy is calculated according to the number of runs that were correctly classified by the HMI. An accuracy of $100\,\%$ is achieved when the interface is able to correctly predict each target element in the eight runs of the experiment.

For the P300 experiments, the 1-by-1 stimulation paradigm presents significantly higher results than the row-column one, with all the participants above $75\,\%$ and 5 of them reaching $100\,\%$ of accuracy. Conversely, the row-column paradigm offers very poor results, with 5 out of the 9 subjects below $63\,\%$. In the blinking case, both paradigms achieve similar results, offering high classification rates with comparable average accuracy.

Table 7.3: Classification accuracy (in %) for each subject, stimulation paradigm and control signal.

	P300		Blink	
Subjects	1-by-1	Row-column	1-by-1	Row-column
1	100	62.50	87.50	100
2	100	100	100	100
3	100	100	100	100
4	100	62.50	100	87.50
5	87.50	62.50	100	100
6	75	75	87.50	100
7	87.50	100	100	100
8	100	62.50	100	100
9	75	50	100	100
Average	91.67	75	97.22	98.61

7.2.3 Response Time

The response time of the HMI is also an important feature to be evaluated. Long response times will produce fatigue, frustration and anxiety in the users, which can lead to a bad performance of the interface and a loss of interest in the system. We must find the shortest response time for the HMI that does not compromise the classification accuracy. Thus, the time response of each stimulation paradigm and control signal was assessed.

Figure 7.9 shows the average classification accuracy obtained for each participant as a function of the number of intensifications performed for each stimulus, which is directly related to response time. Figures 7.9(a) and 7.9(b) show the accuracy obtained from the P300 experiments. Figure 7.9(a) shows the results obtained from the 1-by-1 paradigm, while Figure 7.9(b) shows those from the row-column paradigm. It is apparent that exists a trade-off between NI and accuracy of the HMI, i.e., as NI increases the obtained accuracy improves, and vice

versa. This is due to the fact that a higher number of intensifications implies a larger number of epochs for the ensemble average and, therefore, the P300 EP becomes easier to detect. As a consequence, a higher classification accuracy means longer response times.

From Figure 7.9(a) it can be observed that, for the 1-by-1 paradigm, subjects 3 and 5 achieved their highest accuracy with 40 NI at $72\,\mathrm{s}$. A significant improvement can be seen for subject 2, who reaches $100\,\%$ accuracy at $27\,\mathrm{s}$ with only 15 intensifications, and for subject 8, who achieves a stable $100\,\%$ accuracy at 30 NI. Subject 6 also achieves a stable accuracy with 30 intensifications, but with poorer results. Conversely, for subjects 1, 4 and 9, all or almost all the possible intensifications are needed to achieve a high and stable performance. In the case of the row-column paradigm (Figure 7.9(b)), lower results are obtained and more time is required to achieve the best performance. Subject 7 is the only one that shows an improvement over the 1-by-1 paradigm in short NI. Subject 2 exhibits excellent results, but slower response time than for the 1-by-1 paradigm. Subject 3 also reaches a good accuracy, but the other subjects do not show a stable behaviour, since their performance drop even when the elapsed time and the number of intensifications increase. Therefore, it becomes difficult to determine which specific response time offers the best accuracy.

Blinking experiments can be also analyzed in order to evaluate the response time of the system. In this case, the delay in the response is also dependent on the number of intensifications performed for each stimulus. It should be noted that, for these experiments, every time the target stimulus is presented, the user must blink in order to communicate its selection to the HMI. Therefore, the higher the NI, the larger the response time and the number of blinks required to select the target element. We must take into account that if a very low number of blinks is employed for this purpose, the false positive rate will increase, since non-voluntary blinks can be misinterpreted as control signals sent by users. If the number of blinks needed to pick the target is higher (e.g., 2 or 3 blinks), the interface can employ a double or triple verification system and non-voluntary blinks will probably not be interpreted as voluntary control signals. Therefore, for EOG there also exists a trade-off between response time and reliability, since a large number of blinks for target selection implies a longer response time and a lower false positive rate.

Figures 7.9(c) and 7.9(d) show the accuracy of the HMI obtained for EOG experiments as a function of NI and the response time. Figure 7.9(c) shows the results for the 1-by-1 paradigm and Figure 7.9(d) those corresponding to the row-column paradigm. For both cases, some subjects achieve their highest accuracy with 1 and 2 intensifications and no improvement is produced when using the maximum NI. However, it can be observed that for 1 intensification (i.e., only 1 blink for target selection), several subjects show a lower accuracy due to non-voluntary blinks mistaken as control signals. Therefore, 2 intensifications seems the most suitable option, since mistakes produced by non-voluntary blinks can be avoided and the response time of the system is kept low.

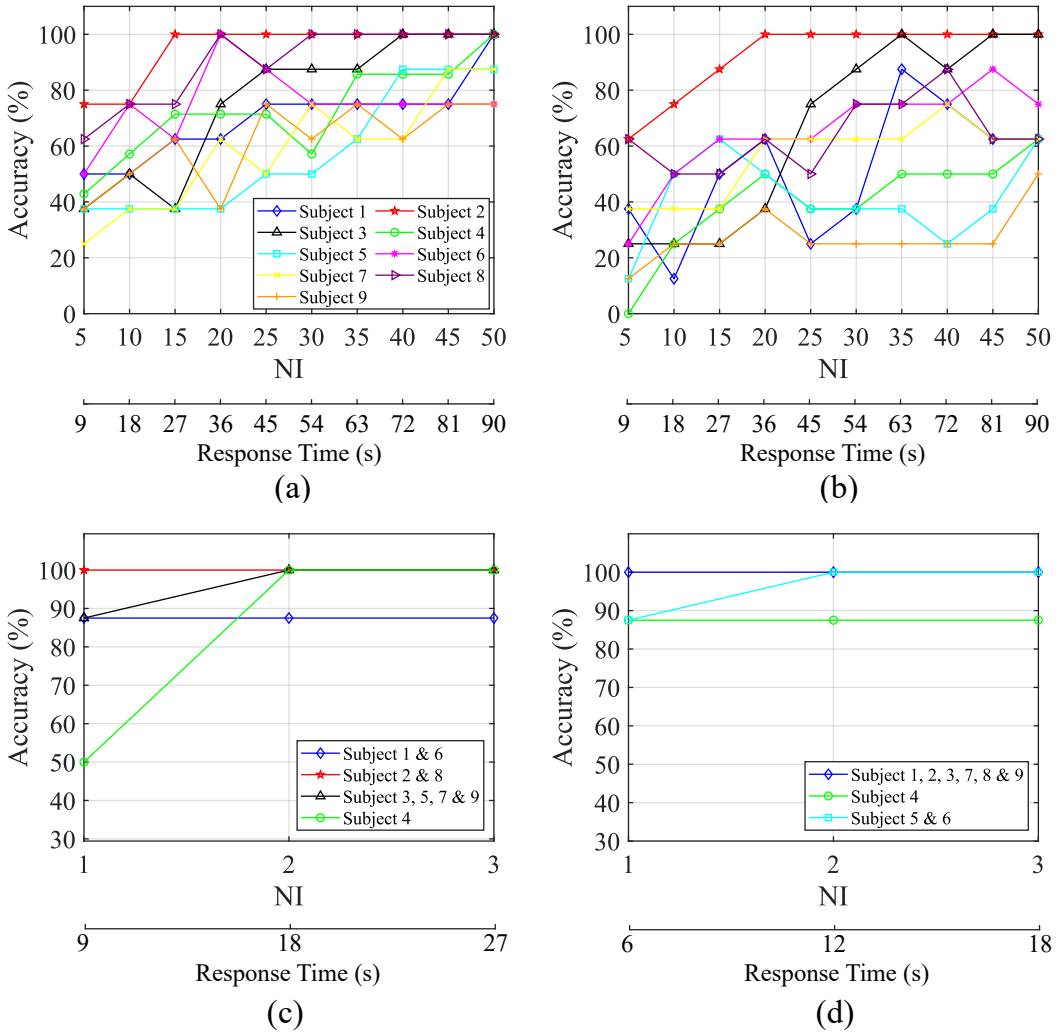

Figure 7.9: Accuracy obtained for each participant as a function of the elapsed time from the start of the intensifications. Figures (a) and (b) correspond to P300-based experiments while Figures (c) and (d) correspond to blink-based experiments. The left column (Figures (a) and (c)) shows the results for the 1-by-1 paradigm and the right one (Figures (b) and (d)) depicts the results for the row-column paradigm.

7.2.4 Discussion

In this study, we have developed an HMI for environmental control using a single-channel recording system. The P300 potential and eye blinks are compared as control signals in order to determine which one offers the best performance in terms of accuracy and response time. The home elements to be controlled are displayed in a GUI following a matrix-form and presented to users using two different stimulation paradigms: 1) home elements are intensified one by one or 2) all the elements of the same row/column are jointly intensified at the same time. Both interfaces, either the P300-based interface or the blink-based interface, employ only one input channel of the same EEG device to capture the brain/eye user's activity. In addition, the

GUI to show the stimuli is fully configurable and able to implement both paradigms. Thus, both interfaces exhibit similar cost and complexity for their respective implementations in real environments.

Practical and real applications of the HMIs will differ among users according to their degree of muscular control. The P300-based HMI does not require voluntary muscle activation for controlling and communicating with external devices. Thus, their immediate users will be those who suffer a complete locked-in state with a loss of all motor control or whose remaining control is easily fatigued or otherwise unreliable. This user group includes totally paralyzed patients due to, for example, terminal stages of ALS or brainstem stroke, or users suffering from movement disorders that abolish motor control caused by, for example, cerebral palsy [18]. For these patients, even the most simple HMI for turning on/off a home device is a valuable tool [126]. However, most potential users have better conventional options for communication. For example, those who retain control of only a single muscle, such as the eyelids, can use it to send control signals in a faster and more accurate way than that provided by EEG-based HMIs [126]. The results presented in this study agree with this statement, as shown in Table 7.3 and Figure 7.9, where it is apparent that the blink-based interface offers shorter response times and similar or higher accuracy in classification than the P300-based HMI.

The subjects of this study, all able-bodied with no motor disabilities, indicated their preference for the blink-based interface since it is not as mental-demanding and time-consuming as the P300-based interface. Moreover, they also pointed out they felt with greater control over the system when using blinks as control signals, by marking the target element with voluntary and conscious actions.

From the EEG recordings, depicted in Figure 7.7, it is apparent that the latency of the P300 potential varies for each subject. As has been already studied [249], individual differences on the P300 latency are related to mental function speeds and cognitive capabilities, such that a shorter latency corresponds to a higher cognitive performance [250], [251]. Moreover, the P300 latency is reduced with children and increases with normal aging [249], [252], [253]. It can also be observed in Figure 7.7 that the P300 potential clearly appears with the 1-by-1 paradigm, especially for the 3 first subjects, while for the row-column experiments the P300 curve generated by the target stimulus does not show big differences with respect to other stimuli. A possible explanation for this behaviour is the human perceptual error produced by targeting adjacent rows and columns [59]. According to this phenomenon, when rows/columns adjacent to desired elements are intensified, they also elicit a P300 potential, which can be confused with the one elicited by the target element. As a consequence, as shown in Table 7.3, the row-column paradigm offers a classification accuracy significantly lower than that obtained by the 1-by-1 paradigm, where all the participants achieve an accuracy above $75\,\%$. Notable differences can also be observed between both paradigms regarding time responses, shown in Figure 7.9, in which the 1-by-1 paradigm shows a more stable behaviour and, with 45 s, 5 of the 9 subjects are above $70\,\%$. All of the subjects were above $70\,\%$ for 81 s.

On the other hand, for the blink detection experiments, the results achieved by both stimulation paradigms are very similar, only varying for three of the subjects and with a close average accuracy of $97.22\,\%$ for the 1-by-1 paradigm and $98.61\,\%$ for the row-column paradigm (see Table 7.3). Moreover, since the number of possible stimuli for the row-column paradigm (6) is lower than for the 1-by-1 (9), the response time for row-column will be shorter, as shown in Figure 7.9. This response time can be further reduced if we analyze the reaction time of each participant, i.e., the elapsed time from the presentation of the target element to the corresponding user blink. In our experiments, the time between the onset of the intensification of one element and the onset of the next one is fixed to $1\,\mathrm{s}$ (see Table 7.2). However, if the reaction time of a particular subject is faster, the period between two consecutive intensifications can be reduced and, consequently, the final response time of the system will be shorter. Figure 7.10 shows a box plot of the reaction times for all the blinks performed by the subjects across all the blinking experiments. On each box, the average response time is marked as the central red line and the bottom and top edges of the box indicate the 25th and 75th percentiles, respectively. The whiskers extend to the maximum and minimum reaction time not considered as outliers. The outliers are individually plotted using the '+' symbol. The mean response time for all the subjects is below $0.55\,\mathrm{s}$, and no blink exceeds $0.85\,\mathrm{s}$, so the period between two consecutive instensifications could be reduced by at least $0.15\,\mathrm{s}$, which would also decrease the overall response time of the system.

The proposed HMIs should be implemented in an IoT environment for smart-home control using the shortest response times while providing a high reliability of the system. Practical applications of an HMI and their implementation in real environments are strongly conditioned by their response times and accuracies [126]. Table 7.4 shows the shortest response time for both stimulation paradigms and control signals while keeping an average accuracy higher than $80\,\%$. Note that, for the blink-based experiments, although the results achieved by the minimum number of blinks are higher than $80\,\%$, they are not taken into account due to their sensitivity to non-voluntary blinks, which could badly influence the final performance of the HMI. Both stimulation paradigms offer a similar accuracy, but shorter response times are achieved for the row-column paradigm, so it is the most suitable option for a blink-based HMI. Conversely, for the P300 experiments, the row-column paradigm does not achieve an $80\,\%$ of accuracy, so the 1-by-1 paradigm, with a response time of $63\,\mathrm{s}$ and an accuracy of $80.36\,\%$, is the preferable option.

The proposed HMI systems can be used for non-critical applications where short response times are not required. The objective of these interfaces is to control basic functions of home devices, such as on/off switching of lights or raising/lowering window blinds. Thus, ensuring that the system performs the correct action is more important than providing a fast response.

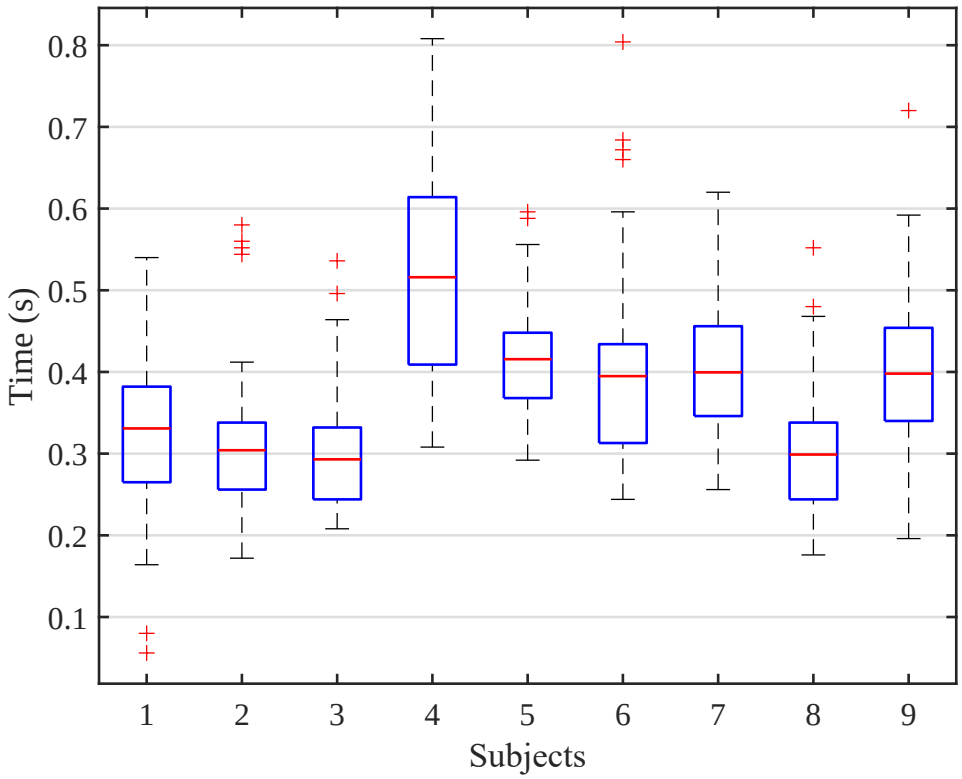

Figure 7.10: Box plot of the reaction times for all the blinks performed by the subjects across all the blinking experiments. On each box, the average response time is marked as the central red line and the bottom and top edges of the box indicate the 25th and 75th percentiles, respectively. The whiskers extend to the maximum and minimum reaction time not considered as outliers. The outliers are individually plotted using the '+' symbol.

Table 7.4: Response time for both stimulation paradigms and control signals that provides an average accuracy higher than 80 %. For the blink-based experiments, the minimum number of blinks are not taken into account due to their sensitivity to non-voluntary blinks.

	P300		Blink	
	1-by-1	row-column	1-by-1	row-column
Accuracy (%)	80.36	No value	97.22	98.61
Response time (s)	63	No value	18	12

7.3 Conclusions

We have developed an environmental control HMI using a low-cost and open-hardware recording device that captures EEG and EOG signals from one single input channel. For this purpose, eye blinks and the P300 potential are assessed and compared in order to determine which is the most suitable control signal for the HMI implementation. A fully configurable GUI

has been developed for stimuli presentation and two stimulation paradigms were evaluated: the elements to be controlled are intensified one by one, or all the elements of the same row/column are jointly intensified at the same time. The obtained results show that the blink-based HMI using the row-column paradigm offered the best performance in terms of accuracy and response time. However, this interface requires voluntary muscle activation for controlling the eyelids movement, which could be a limitation for some potential users of the interface. In this case, the P300-based HMI using the 1-by-1 stimulation paradigm proved to be the most reliable and suitable option. The analysis of the response times obtained by each system shows that the proposed HMIs can be used for non-critical applications where short response times are not required.

Chapter VIII

Conclusions and Future Work

The main objective of this work is to contribute to the Brain-Computer Interface (BCI) research field by proposing new developments based on open solutions including both hardware and software in order to make this technology accessible to anyone who needs it for improving its quality of life. We have shown that open and low-cost recording devices can be employed for implementing new interfaces for controlling elements of a smart-home environment. At the same time, we have exhibited that reliable results can be achieved when using a reduced number of electrodes that guarantees the user's comfort.

8.1 Summary of Contributions

We started by introducing the Human-Machine Interfaces (HMIs) and the variety of biological signals that can be employed for the interaction with this kind of systems. We focused on one particular type of HMI, BCI, which captures the biological signals produced by the neural activity of the user's brain and translates them into control commands for external devices. For this purpose, we examined and studied the anatomy and physiology of the human brain, the different areas where this technology can be applied and the general architecture of a BCI, which is composed by three main elements: signal acquisition, signal processing and actuator device.

Based on this architecture design, we analyze the first component, signal acquisition. Particularly, we study the most used technique for capturing the brain activity of the users in the BCI systems, the Electroencephalography (EEG) technique. EEG is a widely-known non-invasive technique for neuroimaging that captures the electric fields produced by the activity of the neurons and their synapses from outside the brain. In this regard, we review the composition of the EEG devices and compare several commercial and low-cost devices presented over the last years. Additionally, we study the EEG brain rhythms, the possible artifacts that can occur during the EEG recordings and the most popular control signals used in BCI systems for interacting with external devices.

Brain signals captured with EEG devices need to be processed for their posterior translation into commands. Therefore, we analyze the techniques that can be applied for this purpose in the second component of the BCI architecture, signal processing. To this end, we study different feature extraction methods in several domains, such as time, frequency and time-frequency domains. Later, we analyze the most common classifiers employed in the BCI systems for feature classification.

Based on the previous studies, we present an architecture for integrating a BCI application in an Internet of Things (IoT) environment for home automation. For this purpose, we have developed a low-cost open-source EEG device that acquires EEG signals from two input channels. Using the EEG data of only one channel, we propose and compare different feature extraction algorithms based on Sliding Transforms (STs) techniques for determining the user's eye states, i.e., open eyes (oE) or closed eyes (cE). The algorithms include different configurations oriented to provide accurate results with a low computational burden. Firstly, we compare real-valued and complex-valued transforms. Secondly, we consider sliding windows with overlap instead of using the traditional approach with non-overlapped windows, thus reducing the delay time between acquisition and decision. Then, we compare three classification approaches, one based on a threshold classifier and another two that implement the well known Linear Discriminant Analysis (LDA) and Support Vector Machine (SVM) algorithms. The obtained results show the advantages of using the proposed threshold-based classifier and overlapped windows to reduce decision delays and increase robustness. In this sense, we have reached high accuracies for both cE and oE detection independently of the used transform, although for some subjects the Discrete Fourier Transform (DFT) and its binary representation exhibit better results.

After that, we extended the study to the situation where the data captured by both channels is employed together in order to build a two-dimensional feature set that may provide higher and more robust results. To this end, we compare the previously analyzed feature extraction techniques with other strategies commonly used in BCI applications, such as Discrete Wavelet Transform (DWT). At the same time, results obtained with one and two channel data are also compared. We show that STs, such as the DFT and its binary representation, applied on two-sensor data, and combined with the SVM classifier, are the most suitable solutions for the implementation of the BCI, since they offer high accuracies and robust results for both eye states. However, the threshold-based and the SVM classifiers applied on one-electrode data also achieve high performances for most of the subjects, so both of them could be an adequate solution if the minimum number of electrodes has to be used.

Finally, we devoted the last chapter to present an HMI for environmental control using a single-channel recording system. The P300 Evoked Potential (EP) and eye blinks are compared as control signals in order to determine which one offers the best performance in terms of accuracy and response time. For this purpose, we developed a Graphical User Interface (GUI) that presents the home elements the user can control. Two stimulation paradigms are compared:

one of them where the elements are presented one by one and the another one where the elements of the same row/column are presented together. The results show that the blink-based HMI using the row-column paradigm achieved the best performance in terms of accuracy and response time. However, this interface requires voluntary muscle activation for controlling the eyelids movement, which could be a limitation for some potential users of the interface. In this case, the P300-based HMI using the 1-by-1 stimulation paradigm proved to be a reliable and suitable option. The analysis of the response times shows that the proposed HMIs can be used for non-critical applications where short response times are not required.

Taking into account the developed research and the obtained results, we can conclude that HMIs and specially BCIs are emerging technologies that, combined with IoT environments, can end up in useful solutions with great potential for users with severe motor and neurological damages. We have shown that such interfaces can achieve accurate and reliable results when using a reduced number of electrodes and low-cost and open devices. This can help the technology to spread and be employed by a greater number of users who need it.

8.2 Results

The work and results presented in this thesis led to the publication of several co-authored publications. The following sections detail them.

8.2.1 Journal Papers

The results presented in this dissertation have been published in several international journals:

1. Francisco Laport, Adriana Dapena, Paula M. Castro, Francisco J. Vazquez-Araujo, and Daniel Iglesia, "**A prototype of eeg system for iot**", *International journal of neural systems*, vol. 30, no. 07, p. 2 050 018, 2020.
2. Francisco Laport, Daniel Iglesia, Adriana Dapena, Paula M. Castro, and Francisco J. Vazquez-Araujo, "**Proposals and comparisons from one-sensor eeg and eog human-machine interfaces**", *Sensors*, vol. 21, no. 6, p. 2220, 2021.
3. Francisco Laport, Paula M. Castro, Adriana Dapena, Francisco J. Vazquez-Araujo, and Oscar Fresnedo, "**Eye state identification based on discrete wavelet transforms**", *Applied Sciences*, vol. 11, no. 11, p. 5051, 2021.

Note that all the journals appear in the Journal Citation Reports (JCR). The impact factor (IF), position and quartile are summarized in Table 8.1.

8.2.2 Conference Papers

The results presented in this thesis resulted in the publication of the following co-authored conference articles:

Table 8.1: Impact factor of journals.

Journal	Year	IF	Category	Position	Q.
International Journal of Neural Systems	2020	5.866	COMPUTER SCIENCE, ARTIFICIAL INTELLIGENCE	28/140	1
Sensors	2020	3.576	INSTRUMENTS & INSTRUMENTATION	14/64	1
Applied Sciences	2020	2.679	ENGINEERING, MULTIDISCIPLINARY	38/91	2

1. Francisco Laport, Paula M. Castro, Francisco J. Vazquez-Araujo, Adriana Dapena, and José Juan Lamas-Seco, "**Extracción y clasificación de características a partir de señales eeg**", *Proc. of XXXIII SIMPOSIUM NACIONAL DE LA UNIÓN CIENTÍFICA INTERNACIONAL DE RADIO (URSI 2018)*, Granada, Spain, 2018, pp. 1–4.
2. Francisco Laport, Francisco J. Vazquez-Araujo, Paula M. Castro, and Adriana Dapena, "**Brain-computer interfaces for internet of things**", *Proceedings*, vol. 2, no. 18, p. 59, 2018.
   DOI: 10.3390/proceedings2181179.
3. Francisco Laport, Francisco J. Vazquez-Araujo, Paula M. Castro, and Adriana Dapena, "**Estudio de la dft deslizante para clasificación de estados oculares con bajo retardo**", *Proc. of XXXIV SIMPOSIUM NACIONAL DE LA UNIÓN CIENTÍFICA INTERNACIONAL DE RADIO (URSI 2019)*, Sevilla, Spain, 2019, pp. 1–4.
4. Francisco Laport, Francisco J. Vazquez-Araujo, Daniel Iglesia, Paula M. Castro, and Adriana Dapena, "**A comparative study of low cost open source eeg devices**", *Proceedings*, vol. 21, no. 1, p. 116, 2019.
   DOI: 10.3390/proceedings2019021040.
5. Francisco Laport, Francisco J. Vazquez-Araujo, Paula M. Castro, and Adriana Dapena, "**Hardware and software for integrating brain–computer interface with internet of things**", *Proc. of Understanding the Brain Function and Emotions*, José Manuel Ferrández Vicente, José Ramón Álvarez-Sánchez, Félix de la Paz López, Javier Toledo Moreo, and Hojjat Adeli, Eds., Cham, Springer International Publishing, 2019, pp. 22–31, ISBN: 978-3-030-19591-5.
6. Francisco Laport, Adriana Dapena, Paula M. Castro, and Francisco J. Vazquez-Araujo, "**Comparison of sliding transforms and discrete wavelet transforms to detect eye states**", *Proc. of XXXV SIMPOSIUM NACIONAL DE LA UNIÓN CIENTÍFICA INTERNACIONAL DE RADIO (URSI 2020)*, Málaga, Spain, 2020, pp. 1–4.
7. Francisco Laport, Paula M. Castro, Adriana Dapena, Francisco J. Vazquez-Araujo, and Daniel Iglesia, "**Study of machine learning techniques for eeg eye state detection**", *Proceedings*, vol. 54, no. 1, p. 168, 2020.
   DOI: 10.3390/proceedings2020054053.

In addition, the work proposed in [240] was presented in the Maker Faire Galicia 2021,

where it obtained the third prize of the industry conferences.

8.3 Future Work

The results obtained throughout this work meet the expectations and objectives initially set. However, there are some future lines that we could explore to improve our work as well as its contribution to the BCI and HMI fields.

Regarding the work carried out for the detection of the ocular state of the users (Chapters 5 and 6), we can appreciate that the proposed system offers high results for a 2 s delay. This means that the system response time is suitable for the implementation of non-critical applications. However, for certain environments, this delay could produce user disagreements or possible artifacts and, therefore, should be reduced in future developments. In addition, better success rates must be achieved for those subjects with accuracies below $90\,\%$, since the wrong estimation of the eye state can lead to incorrect performance of the system and turn on/off external devices needlessly.

The same improvement should be studied in the HMI proposed in Chapter 7. The interface provides good results, but with slow response times. This problem should be mitigated in future developments or, on the contrary, users could end up tired of the system and giving up not using it. For this purpose, it would be interesting to record EEG signals using more than one input sensor. For example, we could employ the three electrodes located in the midline of the scalp: Fz, Cz and Pz. This would not imply a great hassle for the users and can help to detect the P300 EP from different brain areas. In addition, the system needs to be configured for each subject, which can be inconvenient for its usability. Therefore, an automatic detection algorithm would be a desirable solution, where users only have to connect the interface and, with a short training period, they calibrate it without the need for external intervention. This could be implemented using machine learning techniques, extracting relevant features from the control signals, e.g., pick-picking or sum of values, and popular classification algorithms such as LDA or Stepwise Linear Discriminant Analysis (SWLDA). Moreover, different stimulation paradigms, such as the region-based paradigm, could also be tested in order to mitigate the human perceptual error that may be produced in the row/column paradigm for the EEG recordings.

Furthermore, we recognize that both the BCI for ocular state detection and the HMI for home automation control, need to be evaluated in a larger population sample. In particular, it would be of great interest to assess the performance of these systems in subjects with mobility disorders. Additionally, these experiments should be conducted in real scenarios to study their performance under real-life conditions.

Appendix I

Resumen de la Tesis

Una casa inteligente puede definirse como una residencia equipada con una red de comunicación, sensores, dispositivos y electrodomésticos que los residentes pueden controlar, acceder y monitorizar de forma remota para satisfacer sus necesidades de la vida diaria. Representa un sistema sensible al contexto que, utilizando tecnologías como Internet de las cosas (IoT) y técnicas de inteligencia artificial, puede detectar, anticipar y responder a las actividades en el hogar. Los hogares inteligentes ofrecen herramientas útiles para las personas mayores o para las que padecen problemas motrices, ya que estos sistemas se pueden programar fácilmente para encender o apagar las luces, controlar las puertas o ajustar el termostato sin grandes movimientos y esfuerzos físicos.

Con el objetivo de mejorar la calidad de vida de aquellas personas afectadas por enfermedades motrices, a lo largo de los últimos años se han propuesto diferentes Interfaces Hombre-Máquina(HMI) basadas en señales bio-eléctricas. Estas interfaces ofrecen nuevos canales de comunicación que permiten a sus usuarios interactuar con dispositivos de su entorno empleando las señales biológicas provenientes de diferentes partes de su cuerpo como comandos de control. Es decir, las señales producidas por el cerebro, los músculos o los ojos, por ejemplo, pueden emplearse para controlar dispositivos externos, como una silla de ruedas, teclados virtuales o la prótesis de una extremidad, entre otras aplicaciones. Por lo tanto, resulta una tecnología de gran utilidad para pacientes con discapacidades motrices severas o lesiones graves en sus extremidades, ya que les permite interactuar con su entorno o controlar partes dañadas de su cuerpo sin necesidad de grandes movimientos físicos.

Una amplia variedad de señales biológicas pueden ser empleadas para interactuar con las HMI. El uso de cada una de ellas dependerá del objetivo de la interfaz y de las capacidades motrices que posea el usuario. Los tres tipos más comunes de señales biológicas son: musculares, oculares y cerebrales. En las interfaces basadas en señales musculares, la actividad eléctrica producida por la contracción de los músculos del usuario es capturada empleando técnicas como la Electromiografía (EMG). Dicha actividad es procesada y analizada y, posteriormente, traducida a un comando de control sobre un dispositivo externo. De una forma similar, las interfaces basadas en las señales oculares capturan la actividad de los ojos del

usuario, como los parpadeos, a través de técnicas como la Electrooculografía (EOG). Dicha actividad es también procesada y analizada y, posteriormente, traducida a un comando de control. Ambas interfaces, muscular y ocular, requieren que el usuario posea cierto grado de control muscular, aunque sea mínimo, como por ejemplo, los párpados, mandíbula o músculos del cuello. Sin embargo, las interfaces basadas en señales cerebrales no requieren ningún tipo de control muscular, ya que la interacción con la interfaz se realiza a través de la actividad neuronal del usuario. Son, por lo tanto, las interfaces con mayor potencial, ya que abarcan a todo tipo de usuarios, independientemente de sus capacidades motrices. Por esta razón, centramos nuestro trabajo en el estudio y desarrollo de nuevas interfaces basadas en señales cerebrales, también conocidas como Interfaces Cerebro-Ordenador (BCI).

Las interfaces BCI pueden definirse como la combinación de hardware y software de un sistema de comunicación que monitoriza la actividad cerebral del usuario y traduce ciertas características, correspondientes a las intenciones del usuario, a comandos de control sobre dispositivos externos. Estas interfaces presentan un nuevo canal de comunicación sin involucrar nervios y músculos periféricos, donde los usuarios pueden interactuar con su entorno sin ninguna actividad física, solo usando sus pensamientos.

La población objetivo de las aplicaciones BCI se puede dividir en tres grupos principales. El primer grupo está compuesto por pacientes que han perdido todo el control motor y presentan un estado de bloqueo completo. El segundo grupo incluye a pacientes con un estado de bloqueo parcial, que solo conservan movimientos motrices residuales, como parpadeos, movimientos oculares o pequeños movimientos de los labios. El grupo objetivo final está compuesto por personas que padecen ciertas discapacidades motrices, pero que aún conservan funcionalidades motoras importantes, como el habla o los movimientos de las manos.

Esta tecnología puede ser empleada en una gran variedad de dominios, pero su aplicación más relevante es la de proporcionar herramientas y soluciones útiles a personas con enfermedades motrices severas, como por ejemplo, pacientes con esclerosis lateral amiotrófica, amputaciones o deformaciones musculares. En estos casos, la comunicación directa con dispositivos externos, como un teclado o un ratón, no es posible, por lo que la BCI proporciona hardware y software específico para reconocer los pensamientos e intenciones del usuario que permitan la interacción con el dispositivo. Además, representan un fuerte apoyo para los cuidadores y familiares del paciente, ya que permiten reducir las tareas y gastos derivados del cuidado. En concreto, estas interfaces han sido empleadas en áreas como la comunicación humana, donde las BCI permiten a los usuarios comunicarse con su entorno a través de, por ejemplo, un teclado virtual, donde el sujeto selecciona cada una de las letras que componen el mensaje final que quiere transmitir y, posteriormente, el sistema se encarga de enviar o reproducir dicho mensaje. Asimismo, las BCI han sido utilizadas para el control del entorno, donde a través de la interfaz el usuario puede manejar elementos de su hogar, como por ejemplo, la televisión, el termostato o la alarma de su casa. También han sido empleadas en aplicaciones para el transporte y la locomoción de sus usuarios, permitiendo que estos se muevan en su

ambiente mediante el control de medios de transporte como, por ejemplo, las sillas de ruedas. Además, se han utilizado también en áreas del entretenimiento, donde los usuarios pueden interactuar con videojuegos a través de su actividad neuronal.

Diferentes técnicas de neuroimagen pueden ser empleadas para capturar la actividad cerebral de los usuarios, como por ejemplo, Electrocorticografía (ECoG), Magnetoencefalografía (MEG) o Electroencefalografía (EEG), entre otras. Esta última, la EEG, es la técnica más popular para el desarrollo de interfaces BCI. Esta preferencia se basa en su carácter no invasivo, su bajo coste, su alta portabilidad y resolución temporal así como su facilidad para emplearla y su bajo riesgo para los usuarios. Este método emplea un conjunto de electrodos colocados sobre el cuero cabelludo del usuario que captura señales de electroencefalografía de diferentes partes del cerebro.

La actividad neuronal capturada por los dispositivos EEG se compone de un conjunto de señales que se pueden dividir según su frecuencia y amplitud en distintos ritmos cerebrales. Dichos ritmos se corresponderán con estados mentales concretos y con una distribución espacial específica en el cuero cabelludo del usuario. Estos ritmos se conocen como: *Delta* (por debajo de 4 Hz), *Theta* (entre 4 Hz y 7 Hz), *Alpha* (entre 8 Hz y 12 Hz), *Beta* (entre 12 Hz y 30 Hz) y *Gamma* (entre 30 Hz y 100 Hz).

Además, existen distintos tipos de señales cerebrales que los usuarios pueden modular para emplearlas como señales de control sobre la interfaz BCI. Un gran número de señales han sido estudiadas y analizadas en las últimas décadas, pero entre las más empleadas encontramos, por ejemplo, los Potenciales Evocados Visuales (VEP), los cuales aparecen en la corteza visual como la respuesta del usuario a la estimulación visual externa. Una BCI basada en VEP puede identificar el objetivo al que está mirando el usuario tras analizar las señales de EEG registradas. Cada uno de los objetivos está representado por una secuencia de estimulación única que, a su vez, también evoca un patrón de potenciales VEP únicos. Por lo tanto, el objetivo que el usuario desea seleccionar puede identificarse analizando las características del VEP generado. Los Potenciales Corticales Lentos (SCP) también han sido utilizados como señales de control. Estos son potenciales de baja frecuencia producidos en la parte central y frontal de la corteza cerebral que pueden ser modulados por el usuario para controlar la interfaz BCI. Además, el Potencial Evocado P300 es otra de las respuestas cerebrales que han sido ampliamente empleadas como señales de control. Este potencial es una respuesta que aparece como una desviación positiva en la señal EEG tras 300 ms de producirse un estímulo visual, auditivo o somatosensorial poco frecuente o sorprendente. Las BCI basadas en este potencial se encargarán de detectar dicha desviación para identificar las intenciones del usuario. Por último, los ritmos sensoriomotores pueden ser modulados por el usuario cuando realiza tareas de imaginación motora (MI), es decir, cuando el usuario se imagina que realiza un movimiento pero, en realidad, no se realiza ningún movimiento físico real. De esta manera, el usuario puede realizar dicha modulación para comunicarle sus intenciones a la interfaz.

La técnica de EEG ha sido tradicionalmente empleada para el desarrollo de aplicaciones

médicas, por lo que los dispositivos empleados para este fin son de un precio elevado y constan de un gran número de electrodos, lo cual no favorece su uso en aplicaciones domésticas. Sin embargo, los recientes avances producidos en tecnologías biomédicas, integración de circuitos, sensores y técnicas de análisis de datos, han llevado al desarrollo de nuevos dispositivos portátiles de EEG que pueden utilizarse tanto en aplicaciones clínicas como no clínicas. La reducción del coste, su mayor facilidad de uso, la menor necesidad de intervención humana experta y su menor mantenimiento, han propiciado que estos nuevos dispositivos se empleen fuera del laboratorio y utilicen esta tecnología en entornos reales como hogares y escuelas.

Durante los últimos años se han presentado diferentes dispositivos comerciales de EEG. Dos de los dispositivos de bajo coste más conocidos son Epoc + y MindWave que, aunque requieren el uso de software y hardware propietario, han sido evaluados en numerosos trabajos de investigación y aplicaciones BCI. Por otro lado, también se han propuesto dispositivos de software y hardware abiertos para capturar señales cerebrales. En este caso, las placas presentadas por la empresa OpenBCI (placas Cyton y Ganglion) son soluciones abiertas muy conocidas, también empleadas en diferentes trabajos de investigación y aplicaciones domésticas.

A pesar de todos estos avances logrados en los últimos años, la tecnología BCI debe enfrentar y resolver varios desafíos para convertirse en una herramienta más útil y confiable para los usuarios. Dichos desafíos incluyen aspectos relacionados con la necesidad de reducir los períodos de entrenamiento, probar las aplicaciones en entornos no controlados o el desarrollo de dispositivos listos para usar que puedan monitorizar la actividad cerebral del usuario sin necesidad de conocimiento experto y sin causar molestias al usuario. Por lo tanto, en el trabajo realizado en esta tesis nos centramos en el desarrollo de nuevas interfaces BCI, basadas en dispositivos de bajo coste y abiertos, que puedan ser empleadas de forma fiable por los usuarios y con un número reducido de electrodos para el control de elementos de una casa inteligente. Dos arquitecturas y sistemas distintos han sido propuestos, los cuales se detallan a continuación.

A.1 Detección del Estado Ocular

Como primera propuesta, presentamos una arquitectura que integra una aplicación BCI en un entorno de IoT para el control de una casa inteligente. Para este propósito, hemos desarrollado un dispositivo EEG abierto y de bajo coste que captura señales cerebrales de dos canales de entrada. Haciendo uso únicamente de un canal, proponemos y comparamos distintos algoritmos de extracción de características basados en Transformadas Deslizantes (ST) para determinar el estado ocular del usuario, es decir, ojos abiertos (oE) u ojos cerrados (cE). Los algoritmos incluyen diferentes configuraciones orientadas a proporcionar resultados precisos con baja carga computacional. En primer lugar, comparamos transformadas reales y complejas. Posteriormente, consideramos ventanas deslizantes con solapamiento en lugar de emplear el enfoque tradicional con ventanas no solapadas, reduciendo así el retraso entre la adquisición de

la señal y la toma de decisión. Además, comparamos tres algoritmos de clasificación diferentes: uno basado en umbrales, y otros dos basados en el Análisis Discriminante Lineal (LDA) y en las Máquinas de Vectores de Soporte (SVM).

Para el desarrollo de este sistema, hemos definido varios requisitos que han de cumplirse en la implementación final:

- La detección de ojos abiertos es, por lo general, más importante para garantizar el confort del usuario.
- La precisión del sistema debe ser elevada para evitar situaciones indeseadas en las que los dispositivos del hogar se apagan o encienden de manera innecesaria.
- Robustez ante cambios en el entorno y en la actividad cerebral del usuario.
- Aplicación lista para ser usada, con tiempos de entrenamiento cortos que faciliten su uso e integración en la vida cotidiana del usuario.

El sistema ha sido probado sobre siete sujetos, los cuales accedieron voluntariamente a participar en el estudio. La actividad cerebral de cada uno de estos voluntarios fue recogida empleando el dispositivo de EEG desarrollado así como con la placa Cyton de la empresa OpenBCI, con el objetivo de comparar el rendimiento de nuestro dispositivo con uno comercial. Todos los experimentos se llevaron a cabo en un entorno controlado. Los participantes fueron sentados en una silla cómoda y se les pidió que estuvieran relajados y concentrados en la tarea, tratando de evitar cualquier distracción o estímulo externo. Los experimentos se compusieron de dos tareas: la primera, $60\,\mathrm{s}$ de ojos abiertos, y la segunda, $60\,\mathrm{s}$ de ojos cerrados. Para simular una situación de la vida real, los sujetos podían mover libremente la mirada durante las tareas con los ojos abiertos, sin necesidad de mantenerla en un punto fijo. El procedimiento se explicó convenientemente con antelación, lo que permitió a los participantes sentirse cómodos y familiarizados con el entorno de la prueba. Se registraron de forma continua un total de 10 tareas (es decir, $10\,\mathrm{minutos}$) para cada participante, lo que corresponde a cinco tareas de ojos abiertos y otras cinco de ojos cerrados. Cada tarea estaba separada por una alerta sonora, la cual indicaba al usuario que debía cambiar de estado ocular. Todos los experimentos comenzaron con los ojos abiertos como estado inicial. Las grabaciones fueron monitorizadas y analizadas para detectar artefactos o ruidos introducidos en las señales.

El sistema propuesto es entrenado con 2 minutos para cada estado ocular y probado con 3 minutos por estado. Los resultados obtenidos muestran que las ventanas deslizantes ofrecen precisiones más elevadas que las no deslizantes, sobre todo cuando se requieren tiempos de respuesta cortos. Además, las cuatro transformadas propuestas para la extracción de características ofrecen buenos resultados para ambos estados oculares, siendo la Transformada Discreta de Fourier (DFT) y su representación binaria las que mejores precisiones alcanzan.

En cuanto a los algoritmos de clasificación, el clasificador basado en umbrales y SVM ofrecen resultados similares, obteniendo un rendimiento alto para ambos estados oculares. Por el contrario, LDA obtiene altas precisiones para los ojos cerrados, pero significativamente más bajas para los ojos abiertos, por lo que no es una opción adecuada para la implementación

final del sistema. Es importante resaltar que el funcionamiento del sistema es altamente dependiente el sujeto. Es decir, para cada uno de los sujetos existe una configuración óptima de canal, transformada y tiempo de retraso que consigue los mejores resultados. Sin embargo, dicha configuración no es compartida por el resto de usuarios. Esto nos indica que no es posible obtener una configuración general del sistema que funcione correctamente para todos los usuarios, lo cual dificulta su implementación. Con el objetivo de resolver este problema, proponemos extender la arquitectura inicial para que emplee los datos de ambos canales de entrada y construir así un conjunto de características más amplio que permita obtener precisiones más altas y un sistema más robusto.

En esta nueva arquitectura, las técnicas empleadas anteriormente para extraer las características son comparadas con otras estrategias comúnmente utilizadas en las aplicaciones BCI, como la Transformada Discreta Wavelet (DWT). A su vez, se comparan los resultados obtenidos empleando uno y dos canales. Estos resultados muestran que, una vez más, la DFT y su representación binaria, aplicadas sobre datos de dos sensores y combinadas con el clasificador SVM, son las soluciones más adecuadas para la implementación de la BCI, ya que ofrecen altas precisiones y resultados robustos para ambos estados del ojo. Sin embargo, los clasificadores basados en umbrales y SVM aplicados en datos de un electrodo también logran rendimientos altos para la mayoría de los sujetos, por lo que ambos clasificadores podrían ser una solución adecuada si se desea usar el mínimo número de electrodos.

A.2 Interfaz Hombre-Máquina Basada en EEG y EOG

La segunda propuesta de nuestro trabajo es una interfaz hombre-máquina para el control de un hogar inteligente empleando un dispositivo de grabación de señales biológicas de un único canal. El potencial evocado P300 y los parpadeos son comparados como señales de control, con el objetivo de determinar cuál de ellas ofrece los mejores resultados en términos de precisión y tiempos de respuesta. Los elementos del hogar que el usuario puede controlar con la HMI son presentados en una Interfaz Gráfica de Usuario (GUI). Dichos elementos son mostrados siguiendo dos paradigmas distintos de estimulación: 1) los elementos son presentados uno a uno o 2) todos los elementos de una misma fila/columna son presentados conjuntamente. Esta GUI es totalmente configurable, es decir, el usuario puede elegir qué señal de control y paradigma de estimulación desea utilizar, así como adaptar los tiempos de presentación de los objetos.

El sistema ha sido probado sobre nueve sujetos, los cuales accedieron voluntariamente a participar en el estudio. La actividad cerebral y ocular de cada uno de estos voluntarios fue recogida con la placa Cyton de la empresa OpenBCI. Los experimentos se llevaron a cabo en un entorno controlado y con los mismos parámetros de configuración para todos los sujetos. Los participantes fueron sentados en una silla cómoda y se les pidió que centraran su atención en una pantalla de ordenador situada frente a ellos, donde se presentaban los estímulos. Las sesiones de grabación para cada participante se dividieron en cuatro experimentos, uno por cada

paradigma de estimulación y señal de control, es decir, un experimento para el paradigma uno por uno y señales EEG, otro experimento para el paradigma fila-columna y señales EEG, otro para señales EOG y el paradigma uno por uno y, por último, un experimento para el paradigma fila-columna y datos EOG. Además, cada experimento se compuso de ocho ejecuciones, donde el usuario debía fijar su atención en un elemento específico a controlar. La interfaz HMI analiza cada una de estas ejecuciones para determinar las intenciones del usuario y ejercer la acción correspondiente sobre el elemento seleccionado.

Las aplicaciones prácticas de una HMI variarán entre sus usuarios de acuerdo con su grado de control muscular. La HMI basada en el potencial P300 no requiere la activación muscular voluntaria para controlar o interactuar con dispositivos externos. Por lo tanto, sus usuarios inmediatos serán aquellos que sufren una pérdida completa del control motor. Para este tipo de sujetos, incluso un sistema tan simple como una interfaz que le permita apagar o encender elementos de su casa, se convierte en una herramienta de gran utilidad y valor. Sin embargo, la mayoría de los usuarios potenciales de una HMI tienen mejores opciones para la comunicación. Por ejemplo, aquellos que retienen el control de un único músculo, como los párpados, pueden usarlos para enviar señales de control de una forma más rápida y precisa que la proporcionada por una interfaz basada únicamente en la actividad cerebral. Los resultados obtenidos en este estudio ratifican esta afirmación, donde la HMI basada en parpadeos obtiene resultados más precisos y tiempos de respuesta más cortos que los alcanzados con el potencial evocado P300.

En esta interfaz basada en parpadeos, ambos paradigmas de estimulación ofrecen precisiones similares. Sin embargo, el tiempo de respuesta obtenido por el paradigma de fila-columna es menor que el de uno por uno, por lo que esta será la opción más adecuada para realizar la implementación de la HMI. Como ya se ha explicado, este tipo de interfaces requieren un control muscular voluntario de los párpados, lo que puede suponer una limitación para algunos usuarios. En este caso, la interfaz basada en el potencial P300 empleando el paradigma de estimulación de uno por uno ha demostrado ser la opción más fiable y adecuada. Además, el análisis de los tiempos de respuesta de ambos sistemas muestra que las HMI propuestas pueden ser empleadas en aplicaciones no críticas donde no se requieren tiempos de respuesta cortos.

Appendix II

List of Acronyms

AC Alternating Current
ADC Analog-to-Digital Converter
ALS Amyotrophic Lateral Sclerosis
ANN Artificial Neural Network
BCI Brain-Computer Interface
BMI Brain-Machine Interface
BLE Bluetooth Low Energy
cE closed eyes
CAD Computer-Aided-Diagnosis
CLS Complete Locked-In State
CMS Common Mode Sense
CNN Convolutional Neural Network
CP Control Packet
CSP Common Spatial Pattern
CWT Continuous Wavelet Transform
DFT Discrete Fourier Transform
DNN Deep Neural Networks
DRL Driven Right Leg
DWT Discrete Wavelet Transform
EEG Electroencephalography
ECG Electrocardiogram
ECoG Electrocorticography
EMG Electromyography
EOG Electrooculography
EML Extreme Machine Learning
EP Evoked Potential
ERD Event-related Desynchronization
ERS Event-related Synchronization

ERP Event-related Potential
FES Functional Electrical Stimulation
FT Fourier transform
FFT Fast Fourier Transform
fMRI Functional Magnetic Resonance Imaging
GUI Graphical User Interface
HMI Human-Machine Interface
IAL Incremental Attribute Learning
ICA Independent Component Analysis
IF impact factor
IoT Internet of Things
ISI inter-stimulus interval
IT intensification time
JCR Journal Citation Reports
LDA Linear Discriminant Analysis
LFP Local Field Potential
LIS Locked-In State
LR Logistic Regression
MEMD Multivariate Empirical Mode Decomposition
MEG Magnetoencephalography
MI Motor Imagery
MUA Multi-Unit Activity
MQTT Message Queue Telemetry Transport
NI number of instensifications
NIRS Near Infrared Spectroscopy
NS number of possible stimuli
oE open eyes
PCA Principal Component Analysis
PSDA Power Spectral Density Analysis
PSD Power Spectral Density
RBF Radial Basis Function
RM Right Mastoid
RNN Recurrent Neural Network
ROC Receiver Operating Characteristic
SCP Slow Cortical Potential
SDFT sliding Discrete Fourier Transform
SSVEP Steady-State Visual Evoked Potential
ST Sliding Transform
STFT Short-Time Fourier Transform

SUA Single-Unit Activity
SVM Support Vector Machine
SV Support Vector
SWLDA Stepwise Linear Discriminant Analysis
TVEP Transient Visual Evoked Potential
TTD Thought Translation Device
VEP Visual Evoked Potential
WT Wavelet Transform

References

[1] Nazmiye Balta-Ozkan, Benjamin Boteler, and Oscar Amerighi, "**European smart home market development: Public views on technical and economic aspects across the united kingdom, germany and italy**", *Energy Research & Social Science*, vol. 3, pp. 65–77, 2014.

[2] Andre Ferreira, Wanderley C Celeste, Fernando A Cheein, Teodiano F Bastos-Filho, Mario Sarcinelli-Filho, and Ricardo Carelli, "**Human-machine interfaces based on emg and eeg applied to robotic systems**", *Journal of NeuroEngineering and Rehabilitation*, vol. 5, no. 1, pp. 1–15, 2008.

[3] Ferran Galán, Marnix Nuttin, Eileen Lew, Pierre W Ferrez, Gerolf Vanacker, Johan Philips, and J del R Millán, "**A brain-actuated wheelchair: Asynchronous and non-invasive brain–computer interfaces for continuous control of robots**", *Clinical neurophysiology*, vol. 119, no. 9, pp. 2159–2169, 2008.

[4] Lawrence Ashley Farwell and Emanuel Donchin, "**Talking off the top of your head: Toward a mental prosthesis utilizing event-related brain potentials**", *Electroencephalography and clinical Neurophysiology*, vol. 70, no. 6, pp. 510–523, 1988.

[5] Rupert Ortner, Brendan Z Allison, Gerd Korisek, Herbert Gaggl, and Gert Pfurtscheller, "**An ssvep bci to control a hand orthosis for persons with tetraplegia**", *IEEE transactions on neural systems and rehabilitation engineering*, vol. 19, no. 1, pp. 1–5, 2010.

[6] Mamun Bin Ibne Reaz, M Sazzad Hussain, and Faisal Mohd-Yasin, "**Techniques of emg signal analysis: Detection, processing, classification and applications**", *Biological procedures online*, vol. 8, no. 1, pp. 11–35, 2006.

[7] Gwo-Ching Chang, Wen-Juh Kang, Jer-Junn Luh, Cheng-Kung Cheng, Jin-Shin Lai, Jia-Jin J Chen, and Te-Son Kuo, "**Real-time implementation of electromyogram pattern recognition as a control command of man-machine interface**", *Medical engineering & physics*, vol. 18, no. 7, pp. 529–537, 1996.

[8] Jaime Gomez-Gil, Israel San-Jose-Gonzalez, Luis Fernando Nicolas-Alonso, and Sergio Alonso-Garcia, "**Steering a tractor by means of an emg-based human-machine interface**", *Sensors*, vol. 11, no. 7, pp. 7110–7126, 2011.

[9] Pradeep Shenoy, Kai J Miller, Beau Crawford, and Rajesh PN Rao, "**Online electromyographic control of a robotic prosthesis**", *IEEE transactions on biomedical engineering*, vol. 55, no. 3, pp. 1128–1135, 2008.

[10] Matthew R Williams and Robert F Kirsch, "**Evaluation of head orientation and neck muscle emg signals as command inputs to a human–computer interface for individuals with high tetraplegia**", *IEEE Transactions on Neural Systems and Rehabilitation Engineering*, vol. 16, no. 5, pp. 485–496, 2008.

[11] Lai Wei and Huosheng Hu, "**Emg and visual based hmi for hands-free control of an intelligent wheelchair**", *Proc. of 2010 8th World Congress on Intelligent Control and Automation*, IEEE, 2010, pp. 1027–1032.

[12] Andreas Bulling, Jamie A Ward, Hans Gellersen, and Gerhard Troster, "**Eye movement analysis for activity recognition using electrooculography**", *IEEE transactions on pattern analysis and machine intelligence*, vol. 33, no. 4, pp. 741–753, 2010.

[13] Lawrence Y Deng, Chun-Liang Hsu, Tzu-Ching Lin, Jui-Sen Tuan, and Shih-Ming Chang, "**Eog-based human–computer interface system development**", *Expert Systems with Applications*, vol. 37, no. 4, pp. 3337–3343, 2010.

[14] Shenghong He and Yuanqing Li, "**A single-channel eog-based speller**", *IEEE Transactions on Neural Systems and Rehabilitation Engineering*, vol. 25, no. 11, pp. 1978–1987, 2017.

[15] Rafael Barea, Luciano Boquete, Manuel Mazo, and E López, "**Wheelchair guidance strategies using eog**", *Journal of intelligent and robotic systems*, vol. 34, no. 3, pp. 279–299, 2002.

[16] G. Pfurtscheller and C. Neuper, "**Motor imagery and direct brain-computer communication**", *Proceedings of the IEEE*, vol. 89, no. 7, pp. 1123–1134, 2001. DOI: 0.1109/5.939829.

[17] Alexis Ortiz-Rosario and Hojjat Adeli, "**Brain-computer interface technologies: From signal to action**", *Reviews in the Neurosciences*, vol. 24, no. 5, pp. 537–552, 2013.

[18] Luis Fernando Nicolas-Alonso and Jaime Gomez-Gil, "**Brain computer interfaces, a review**", *Sensors*, vol. 12, no. 2, pp. 1211–1279, 2012.

[19] Rabie A Ramadan and Athanasios V Vasilakos, "**Brain computer interface: Control signals review**", *Neurocomputing*, vol. 223, pp. 26–44, 2017.

[20] Niels Birbaumer, Nimr Ghanayim, Thilo Hinterberger, Iver Iversen, Boris Kotchoubey, Andrea Kübler, Juri Perelmouter, Edward Taub, and Herta Flor, "**A spelling device for the paralysed**", *Nature*, vol. 398, no. 6725, pp. 297–298, 1999.

[21] Gert Pfurtscheller, Christof Guger, Gernot Müller, Gunther Krausz, and Christa Neuper, "**Brain oscillations control hand orthosis in a tetraplegic**", *Neuroscience letters*, vol. 292, no. 3, pp. 211–214, 2000.

[22] Inc. Neuralink, **Neuralink**, https://neuralink.com/.

[23] David A Moses, Matthew K Leonard, Joseph G Makin, and Edward F Chang, "**Real-time decoding of question-and-answer speech dialogue using human cortical activity**", *Nature communications*, vol. 10, no. 1, pp. 1–14, 2019.

[24] John P Donoghue, "**Bridging the brain to the world: A perspective on neural interface systems**", *Neuron*, vol. 60, no. 3, pp. 511–521, 2008.

[25] Eric W Sellers and Emanuel Donchin, "**A p300-based brain–computer interface: Initial tests by als patients**", *Clinical neurophysiology*, vol. 117, no. 3, pp. 538–548, 2006.

[26] Femke Nijboer, EW Sellers, Jürgen Mellinger, Mary Ann Jordan, Tamara Matuz, Adrian Furdea, Sebastian Halder, Ursula Mochty, DJ Krusienski, TM Vaughan, *et al.*, "**A p300-based brain–computer interface for people with amyotrophic lateral sclerosis**", *Clinical neurophysiology*, vol. 119, no. 8, pp. 1909–1916, 2008.

[27] Hans Berger, "**Über das elektroenkephalogramm des menschen**", *Archiv für psychiatrie und nervenkrankheiten*, vol. 87, no. 1, pp. 527–570, 1929.

[28] Chang S Nam, Anton Nijholt, and Fabien Lotte, ***Brain–computer interfaces handbook: technological and theoretical advances***. CRC Press, 2018.

[29] Joseph Kamiya, "**Conscious control of brain waves**", *Psychology Today*, vol. 1, 1968.

[30] Thelma Estrin, "**On-line electroencephalographic digital computing system**", *Electroencephalography and Clinical Neurophysiology*, vol. 19, no. 5, pp. 524–526, 1965.

[31] Andrea Kübler, "**The history of bci: From a vision for the future to real support for personhood in people with locked-in syndrome**", *Neuroethics*, vol. 13, no. 2, pp. 163–180, 2020.

[32] Jacques J Vidal, "**Toward direct brain-computer communication**", *Annual review of Biophysics and Bioengineering*, vol. 2, no. 1, pp. 157–180, 1973.

[33] Graz University of Technology, **Bnci research groups**, http://bnci-horizon-2020.eu/community/research-groups/.

[34] Graz University of Technology, **Bnci research companies**, http://bnci-horizon-2020.eu/community/companies/.

[35] Minkyu Ahn, Mijin Lee, Jinyoung Choi, and Sung Chan Jun, "**A review of brain-computer interface games and an opinion survey from researchers, developers and users**", *Sensors*, vol. 14, no. 8, pp. 14 601–14 633, 2014.

[36] Yongtian He, David Eguren, José M Azorín, Robert G Grossman, Trieu Phat Luu, and Jose L Contreras-Vidal, "**Brain–machine interfaces for controlling lower-limb powered robotic systems**", *Journal of neural engineering*, vol. 15, no. 2, p. 021 004, 2018.

[37] Sarah N Abdulkader, Ayman Atia, and Mostafa-Sami M Mostafa, "**Brain computer interfacing: Applications and challenges**", *Egyptian Informatics Journal*, vol. 16, no. 2, pp. 213–230, 2015.

[38] Wikimedia Commons, **Structure of the brain.** https://commons.wikimedia.org/wiki/File:Cerebrum_lobes.svg.

[39] Dean J Krusienski and Jerry J Shih, "**Control of a visual keyboard using an electrocorticographic brain–computer interface**", *Neurorehabilitation and neural repair*, vol. 25, no. 4, pp. 323–331, 2011.

[40] Simon P Levine, Jane E Huggins, Spencer L BeMent, Ramesh K Kushwaha, Lori A Schuh, Erasmo A Passaro, Mitchell M Rohde, and Donald A Ross, "**Identification of electrocorticogram patterns as the basis for a direct brain interface**", *Journal of clinical neurophysiology*, vol. 16, no. 5, p. 439, 1999.

[41] G Schalk, J Kubanek, KJ Miller, NR Anderson, EC Leuthardt, JG Ojemann, Dave Limbrick, D Moran, LA Gerhardt, and JR Wolpaw, "**Decoding two-dimensional movement trajectories using electrocorticographic signals in humans**", *Journal of neural engineering*, vol. 4, no. 3, p. 264, 2007.

[42] Abdulhamit Subasi and M Ismail Gursoy, "**Eeg signal classification using pca, ica, lda and support vector machines**", *Expert systems with applications*, vol. 37, no. 12, pp. 8659–8666, 2010.

[43] Arnaud Delorme, Terrence Sejnowski, and Scott Makeig, "**Enhanced detection of artifacts in eeg data using higher-order statistics and independent component analysis**", *Neuroimage*, vol. 34, no. 4, pp. 1443–1449, 2007.

[44] Herbert Ramoser, Johannes Muller-Gerking, and Gert Pfurtscheller, "**Optimal spatial filtering of single trial eeg during imagined hand movement**", *IEEE transactions on rehabilitation engineering*, vol. 8, no. 4, pp. 441–446, 2000.

[45] Steven Lemm, Benjamin Blankertz, Gabriel Curio, and K-R Muller, "**Spatio-spectral filters for improving the classification of single trial eeg**", *IEEE transactions on biomedical engineering*, vol. 52, no. 9, pp. 1541–1548, 2005.

[46] Hasan Ocak, "**Automatic detection of epileptic seizures in eeg using discrete wavelet transform and approximate entropy**", *Expert Systems with Applications*, vol. 36, no. 2, pp. 2027–2036, 2009.

[47] Dean J Krusienski, Dennis J McFarland, and Jonathan R Wolpaw, "**An evaluation of autoregressive spectral estimation model order for brain-computer interface applications**", *Proc. of 2006 International Conference of the IEEE Engineering in Medicine and Biology Society*, IEEE, 2006, pp. 1323–1326.

[48] Jiang Wang, Guizhi Xu, Lei Wang, and Huiyuan Zhang, "**Feature extraction of brain-computer interface based on improved multivariate adaptive autoregressive models**", *Proc. of 2010 3rd International Conference on Biomedical Engineering and Informatics*, IEEE, vol. 2, 2010, pp. 895–898.

[49] Fabien Lotte, Marco Congedo, Anatole Lécuyer, Fabrice Lamarche, and Bruno Arnaldi, "**A review of classification algorithms for eeg-based brain–computer interfaces**", *Journal of neural engineering*, vol. 4, no. 2, R1, 2007.

[50] George Townsend, Brandon K LaPallo, Chadwick B Boulay, Dean J Krusienski, GE Frye, CKea Hauser, Nicholas Edward Schwartz, Theresa M Vaughan, Jonathan R Wolpaw, and Eric W Sellers, "**A novel p300-based brain–computer interface stimulus presentation paradigm: Moving beyond rows and columns**", *Clinical neurophysiology*, vol. 121, no. 7, pp. 1109–1120, 2010.

[51] Vladimir Bostanov, "**Bci competition 2003-data sets ib and iib: Feature extraction from event-related brain potentials with the continuous wavelet transform and the t-value scalogram**", *IEEE Transactions on Biomedical engineering*, vol. 51, no. 6, pp. 1057–1061, 2004.

[52] Carmen Vidaurre, Nicole Krämer, Benjamin Blankertz, and Alois Schlögl, "**Time domain parameters as a feature for eeg-based brain–computer interfaces**", *Neural Networks*, vol. 22, no. 9, pp. 1313–1319, 2009.

[53] Gary N Garcia, Touradj Ebrahimi, and J-M Vesin, "**Support vector eeg classification in the fourier and time-frequency correlation domains**", *Proc. of First International IEEE EMBS Conference on Neural Engineering, 2003.*, IEEE, 2003, pp. 591–594.

[54] M.V.M. Yeo, X. Li, K. Shen, and E.P.V. Wilder-Smith, "**Can svm be used for automatic EEG detection of drowsiness during car driving?**", *Safety Science*, vol. 47, no. 1, pp. 115–124, 2009.
DOI: 10.1016/j.ssci.2008.01.007.

[55] Dean J Krusienski, Eric W Sellers, François Cabestaing, Sabri Bayoudh, Dennis J McFarland, Theresa M Vaughan, and Jonathan R Wolpaw, "**A comparison of classification techniques for the p300 speller**", *Journal of neural engineering*, vol. 3, no. 4, p. 299, 2006.

[56] Aya Rezeika, Mihaly Benda, Piotr Stawicki, Felix Gembler, Abdul Saboor, and Ivan Volosyak, "**Brain–computer interface spellers: A review**", *Brain sciences*, vol. 8, no. 4, p. 57, 2018.

[57] Febo Cincotti, Donatella Mattia, Fabio Aloise, Simona Bufalari, Gerwin Schalk, Giuseppe Oriolo, Andrea Cherubini, Maria Grazia Marciani, and Fabio Babiloni, "**Non-invasive brain–computer interface system: Towards its application as assistive technology**", *Brain research bulletin*, vol. 75, no. 6, pp. 796–803, 2008.

[58] Jiahui Xu and Baichang Zhong, "**Review on portable eeg technology in educational research**", *Computers in Human Behavior*, vol. 81, pp. 340–349, 2018.

[59] Reza Fazel-Rezai and Kamyar Abhari, "**A region-based p300 speller for brain-computer interface**", *Canadian Journal of Electrical and Computer Engineering*, vol. 34, no. 3, pp. 81–85, 2009.

[60] Brijil Chambayil, Rajesh Singla, and Rameshwar Jha, "**Virtual keyboard bci using eye blinks in eeg**", *Proc. of 2010 IEEE 6th International Conference on Wireless and Mobile Computing, Networking and Communications*, IEEE, 2010, pp. 466–470.

[61] J. Gubbi, R. Buyya, S. Marusic, and M. Palaniswami, "**Internet of things (iot): A vision, architectural elements, and future directions**", *Future Generation Computer Systems*, vol. 29, no. 7, pp. 1645–1660, 2013.
DOI: 10.1016/j.future.2013.01.010.

[62] Dietrich D., Bruckner D., Zucker G., and Palensky P., "**Communication and computation in buildings: A short introduction and overview**", *IEEE Transactions on Industrial Electronics*, vol. 57, no. 11, pp. 3577–3584, 2010.
DOI: 10.1109/TIE.2010.2046570.

[63] Jesus Minguillon, Miguel Angel Lopez-Gordo, Christian Morillas, and Francisco Pelayo, "**A mobile brain-computer interface for clinical applications: From the lab to the ubiquity**", *Proc. of International Work-Conference on the Interplay Between Natural and Artificial Computation*, Springer, 2017, pp. 68–76.

[64] B. Jagadish, M. P. R. S. Kiran, and P. Rajalakshmi, "**A novel system architecture for brain controlled iot enabled environments**", *Proc. of 2017 IEEE 19th International Conference on e-Health Networking, Applications and Services (Healthcom)*, 2017, pp. 1–5.
DOI: 10.1109/HealthCom.2017.8210814.

[65] E. Mathe and E. Spyrou, "**Connecting a consumer brain-computer interface to an internet-of-things ecosystem**", *Proc. of 9th ACM International Conference on Pervasive Technologies Related to Assistive Environments*, vol. article n.90, 2016.

[66] Inc. NeuroSky, **Neurosky mindwave**, http://neurosky.com/biosensors/eeg-sensor/biosensors/.

[67] Kazuo Tanaka, Kazuyuki Matsunaga, and Hua O Wang, "**Electroencephalogram-based control of an electric wheelchair**", *IEEE transactions on robotics*, vol. 21, no. 4, pp. 762–766, 2005.

[68] Brice Rebsamen, Cuntai Guan, Haihong Zhang, Chuanchu Wang, Cheeleong Teo, Marcelo H Ang, and Etienne Burdet, "**A brain controlled wheelchair to navigate in familiar environments**", *IEEE Transactions on Neural Systems and Rehabilitation Engineering*, vol. 18, no. 6, pp. 590–598, 2010.

[69] Brice Rebsamen, Etienne Burdet, Cuntai Guan, Chee Leong Teo, Qiang Zeng, Marcelo Ang, and Christian Laugier, "**Controlling a wheelchair using a bci with low information transfer rate**", *Proc. of 2007 IEEE 10th International Conference on Rehabilitation Robotics*, IEEE, 2007, pp. 1003–1008.

[70] Iñaki Iturrate, Javier M Antelis, Andrea Kubler, and Javier Minguez, "**A noninvasive brain-actuated wheelchair based on a p300 neurophysiological protocol and automated navigation**", *IEEE transactions on robotics*, vol. 25, no. 3, pp. 614–627, 2009.

[71] Gert Pfurtscheller, Gernot R Müller, Jörg Pfurtscheller, Hans Jürgen Gerner, and Rüdiger Rupp, "**'thought'–control of functional electrical stimulation to restore hand grasp in a patient with tetraplegia**", *Neuroscience letters*, vol. 351, no. 1, pp. 33–36, 2003.

[72] Gernot R Müller-Putz, Reinhold Scherer, Gert Pfurtscheller, and Rüdiger Rupp, "**Eeg-based neuroprosthesis control: A step towards clinical practice**", *Neuroscience letters*, vol. 382, no. 1-2, pp. 169–174, 2005.

[73] Gernot R Muller-Putz and Gert Pfurtscheller, "**Control of an electrical prosthesis with an ssvep-based bci**", *IEEE Transactions on Biomedical Engineering*, vol. 55, no. 1, pp. 361–364, 2007.

[74] Bojan Kerous, Filip Skola, and Fotis Liarokapis, "**Eeg-based bci and video games: A progress report**", *Virtual Reality*, vol. 22, no. 2, pp. 119–135, 2018.

[75] Athanasios Vourvopoulos and Sergi Bermúdez i Badia, "**Motor priming in virtual reality can augment motor-imagery training efficacy in restorative brain-computer interaction: A within-subject analysis**", *Journal of neuroengineering and rehabilitation*, vol. 13, no. 1, p. 69, 2016.

[76] Darius A Rohani and Sadasivan Puthusserypady, "**Bci inside a virtual reality classroom: A potential training tool for attention**", *EPJ Nonlinear Biomedical Physics*, vol. 3, no. 1, p. 12, 2015.

[77] Andrea Finke, Alexander Lenhardt, and Helge Ritter, "**The mindgame: A p300-based brain–computer interface game**", *Neural Networks*, vol. 22, no. 9, pp. 1329–1333, 2009.

[78] Edmund C Lalor, Simon P Kelly, Ciarán Finucane, Robert Burke, Ray Smith, Richard B Reilly, and Gary Mcdarby, "**Steady-state vep-based brain-computer interface control in an immersive 3d gaming environment**", *EURASIP Journal on Advances in Signal Processing*, vol. 2005, no. 19, p. 706 906, 2005.

[79] Laurent Bonnet, Fabien Lotte, and Anatole Lécuyer, "**Two brains, one game: Design and evaluation of a multiuser bci video game based on motor imagery**", *IEEE Transactions on Computational Intelligence and AI in games*, vol. 5, no. 2, pp. 185–198, 2013.

[80] Inc. Emotive, **Emotiv epoch+ 14 channel mobile eeg**, https://www.emotiv.com/product/emotiv-epoc-14-channel-mobile-eeg/.

[81] Jonathan Wolpaw and Elizabeth Winter Wolpaw, ***Brain-computer interfaces: principles and practice***. Oxford University Press, 2012.

[82] Sylvain Baillet, John C Mosher, and Richard M Leahy, "**Electromagnetic brain mapping**", *IEEE Signal processing magazine*, vol. 18, no. 6, pp. 14–30, 2001.

[83] Niels Birbaumer, "**Brain–computer-interface research: Coming of age**", *Clinical Neurophysiology*, vol. 117, no. 3, pp. 479–483, 2006, ISSN: 1388-2457.
DOI: https://doi.org/10.1016/j.clinph.2005.11.002. Online access: http://www.sciencedirect.com/science/article/pii/S138824570500461X.

[84] S.Y. Bookheimer, M.H. Strojwas, M.S. Cohen, A.M. Saunders, M.A. Pericak-Vance, J.C. Mazziotta, and G.W. Small, "**Patterns of brain activation in people at risk for alzheimer's disease**", *New England journal of medicine*, vol. 343, no. 7, pp. 450–456, 2000.
DOI: 10.1056/NEJM200008173430701.

[85] R.S. Fisher, W.V. Boas, W. Blume, C. Elger, P. Genton, P. Lee, and J. Engel, "**Epileptic seizures and epilepsy: Definitions proposed by the international league against epilepsy (ilae) and the international bureau for epilepsy (ibe)**", *Epilepsia*, vol. 46, no. 4, pp. 470–472, 2005.
DOI: 10.1111/j.0013-9580.2005.66104.x.

[86] Herbert H Jasper, "**The ten-twenty electrode system of the international federation**", *Electroencephalogr. Clin. Neurophysiol.*, vol. 10, pp. 370–375, 1958.

[87] Jiawei Xu, Srinjoy Mitra, Chris Van Hoof, Refet Firat Yazicioglu, and Kofi AA Makinwa, "**Active electrodes for wearable eeg acquisition: Review and electronics design methodology**", *IEEE reviews in biomedical engineering*, vol. 10, pp. 187–198, 2017.

[88] Mark O'Sullivan, Andriy Temko, Andrea Bocchino, Conor O'Mahony, Geraldine Boylan, and Emanuel Popovici, "**Analysis of a low-cost eeg monitoring system and dry electrodes toward clinical use in the neonatal icu**", *Sensors*, vol. 19, no. 11, p. 2637, 2019.

[89] Rytis Maskeliunas, Robertas Damasevicius, Ignas Martisius, and Mindaugas Vasiljevas, "**Consumer-grade eeg devices: Are they usable for control tasks?**", *PeerJ*, vol. 4, e1746, 2016.

[90] Chih-Ming Chen, Jung-Ying Wang, and Chih-Ming Yu, "**Assessing the attention levels of students by using a novel attention aware system based on brainwave signals**", *British Journal of Educational Technology*, vol. 48, no. 2, pp. 348–369, 2017.

[91] Georgios Patsis, Hichem Sahli, Werner Verhelst, and Olga De Troyer, "**Evaluation of attention levels in a tetris game using a brain computer interface**", *Proc. of International conference on user modeling, adaptation, and personalization*, Springer, 2013, pp. 127–138.

[92] Athanasios Vourvopoulos and Fotis Liarokapis, "**Evaluation of commercial brain–computer interfaces in real and virtual world environment: A pilot study**", *Computers & Electrical Engineering*, vol. 40, no. 2, pp. 714–729, 2014.

[93] Oliver Röesler, Lucas Bader, Jan Forster, Yoshikatsu Hayashi, Stefan Heßler, and David Suendermann-Oeft, "**Comparison of eeg devices for eye state classification**", *Proc. of the AIHLS*, 2014.

[94] Ramla Ghali, Sébastien Ouellet, and Claude Frasson, "**Lewispace: An exploratory study with a machine learning model in an educational game**", *Journal of Education and Training Studies*, vol. 4, no. 1, pp. 192–201, 2015.

[95] Ioana Ghergulescu and Cristina Hava Muntean, "**Totcompute: A novel eeg-based timeontask threshold computation mechanism for engagement modelling and monitoring**", *International Journal of Artificial Intelligence in Education*, vol. 26, no. 3, pp. 821–854, 2016.

[96] Inc. OpenBCI, **Openbci**, https://openbci.com/.

[97] Valer Jurcak, Daisuke Tsuzuki, and Ippeita Dan, "**10/20, 10/10, and 10/5 systems revisited: Their validity as relative head-surface-based positioning systems**", *Neuroimage*, vol. 34, no. 4, pp. 1600–1611, 2007.

[98] Rustam Shadiev, Ting-Ting Wu, and Yueh-Min Huang, "**Enhancing learning performance, attention, and meditation using a speech-to-text recognition application: Evidence from multiple data sources**", *Interactive Learning Environments*, vol. 25, no. 2, pp. 249–261, 2017.

[99] Alireza Sahami Shirazi, Mariam Hassib, Niels Henze, Albrecht Schmidt, and Kai Kunze, "**What's on your mind? mental task awareness using single electrode brain computer interfaces**", *Proc. of 5th augmented human international conference*, 2014, pp. 1–4.

[100] Matthieu Duvinage, Thierry Castermans, Mathieu Petieau, Thomas Hoellinger, Guy Cheron, and Thierry Dutoit, "**Performance of the emotiv epoc headset for p300-based applications**", *Biomedical engineering online*, vol. 12, no. 1, p. 56, 2013.

[101] Nikolay Chumerin, Nikolay V Manyakov, Marijn van Vliet, Arne Robben, Adrien Combaz, and Marc M Van Hulle, "**Steady-state visual evoked potential-based computer gaming on a consumer-grade eeg device**", *IEEE transactions on computational intelligence and ai in games*, vol. 5, no. 2, pp. 100–110, 2012.

[102] Yuan-Pin Lin, Yijun Wang, and Tzyy-Ping Jung, "**Assessing the feasibility of online ssvep decoding in human walking using a consumer eeg headset**", *Journal of neuroengineering and rehabilitation*, vol. 11, no. 1, p. 119, 2014.

[103] Hatma Suryotrisongko and Febriliyan Samopa, "**Evaluating openbci spiderclaw v1 headwear's electrodes placements for brain-computer interface (bci) motor imagery application**", *Procedia Computer Science*, vol. 72, pp. 398–405, 2015.

[104] Shivanthan AC Yohanandan, Isabell Kiral-Kornek, Jianbin Tang, Benjamin S Mshford, Umar Asif, and Stefan Harrer, "**A robust low-cost eeg motor imagery-based brain-computer interface**", *Proc. of 2018 40th Annual International Conference of the IEEE Engineering in Medicine and Biology Society (EMBC)*, IEEE, 2018, pp. 5089–5092.

[105] Kais Belwafi, Ridha Djemal, Fakhreddine Ghaffari, Olivier Romain, Bouraoui Ouni, and Sofien Gannouni, "**Online adaptive filters to classify left and right hand motor imagery.**" *Proc. of BIOSIGNALS*, 2016, pp. 335–339.

[106] Jérémy Frey, "**Comparison of a consumer grade EEG amplifier with medical grade equipment in BCI applications**", *Proc. of International BCI meeting*, Asilomar, United States, 2016, p. 147.

[107] Qing Wu, Wenbing Zhao, and Tessadori Jacopo, "**Towards objective assessment of movie trailer quality using human electroencephalogram and facial recognition**", *Proc. of 2018 IEEE International Conference on Electro/Information Technology (EIT)*, IEEE, 2018, pp. 0449–0452.

[108] Victoria Peterson, Catalina Galván, Hugo Hernández, and Ruben Spies, "**A feasibility study of a complete low-cost consumer-grade brain-computer interface system**", *Heliyon*, vol. 6, no. 3, e03425, 2020.

[109] Andrey Parfenov, **Brainflow library**, https://brainflow.readthedocs.io/.

[110] R.J. Barry, A.R. Clarke, S.J. Johnstone, C.A. Magee, and J.A. Rushby, "**EEG differences between eyes-closed and eyes-open resting conditions**", *Clinical Neurophysiology*, vol. 118, no. 12, pp. 2765–2773, 2007.
DOI: 10.1016/j.clinph.2007.07.028.

[111] Jaime A Pineda, "**The functional significance of mu rhythms: Translating "seeing" and "hearing" into "doing"**", *Brain research reviews*, vol. 50, no. 1, pp. 57–68, 2005.

[112] Jose Antonio Urigüen and Begoña Garcia-Zapirain, "**Eeg artifact removal—state-of-the-art and guidelines**", *Journal of neural engineering*, vol. 12, no. 3, p. 031 001, 2015.

[113] Leif Sörnmo and Pablo Laguna, ***Bioelectrical signal processing in cardiac and neurological applications***. Academic Press, 2005, vol. 8.

[114] Irina I Goncharova, Dennis J McFarland, Theresa M Vaughan, and Jonathan R Wolpaw, "**Emg contamination of eeg: Spectral and topographical characteristics**", *Clinical neurophysiology*, vol. 114, no. 9, pp. 1580–1593, 2003.

[115] Manish N Tibdewal, M Mahadevappa, Ajoy Kumar Ray, Monika Malokar, and Himanshu R Dey, "**Power line and ocular artifact denoising from eeg using notch filter and wavelet transform**", *Proc. of 2016 3rd International Conference on Computing for Sustainable Global Development (INDIACom)*, IEEE, 2016, pp. 1654–1659.

[116] Sergio Romero, Miguel A Mañanas, and Manel J Barbanoj, "**A comparative study of automatic techniques for ocular artifact reduction in spontaneous eeg signals based on clinical target variables: A simulation case**", *Computers in biology and medicine*, vol. 38, no. 3, pp. 348–360, 2008.

[117] Tzyy-Ping Jung, Scott Makeig, Marissa Westerfield, Jeanne Townsend, Eric Courchesne, and Terrence J Sejnowski, "**Removal of eye activity artifacts from visual event-related potentials in normal and clinical subjects**", *Clinical Neurophysiology*, vol. 111, no. 10, pp. 1745–1758, 2000.

[118] Xiao Jiang, Gui-Bin Bian, and Zean Tian, "**Removal of artifacts from eeg signals: A review**", *Sensors*, vol. 19, no. 5, p. 987, 2019.

[119] David Regan, "**Some characteristics of average steady-state and transient responses evoked by modulated light**", *Electroencephalography and clinical neurophysiology*, vol. 20, no. 3, pp. 238–248, 1966.

[120] David Regan, ***Human brain electrophysiology: Evoked potentials and evoked magnetic fields in science and medicine***. New York: Elsevier, 1989.

[121] Guangyu Bin, Xiaorong Gao, Yijun Wang, Bo Hong, and Shangkai Gao, "**Vep-based brain-computer interfaces: Time, frequency, and code modulations [research frontier]**", *IEEE Computational Intelligence Magazine*, vol. 4, no. 4, pp. 22–26, 2009.

[122] Brendan Z Allison, Dennis J McFarland, Gerwin Schalk, Shi Dong Zheng, Melody Moore Jackson, and Jonathan R Wolpaw, "**Towards an independent brain–computer interface using steady state visual evoked potentials**", *Clinical neurophysiology*, vol. 119, no. 2, pp. 399–408, 2008.

[123] Xiaorong Gao, Dingfeng Xu, Ming Cheng, and Shangkai Gao, "**A bci-based environmental controller for the motion-disabled**", *IEEE Transactions on neural systems and rehabilitation engineering*, vol. 11, no. 2, pp. 137–140, 2003.

[124] Pablo F Diez, Vicente A Mut, Enrique M Avila Perona, and Eric Laciar Leber, "**Asynchronous bci control using high-frequency ssvep**", *Journal of neuroengineering and rehabilitation*, vol. 8, no. 1, p. 39, 2011.

[125] Niels Birbaumer, Thomas Elbert, Anthony G Canavan, and Brigitte Rockstroh, "**Slow potentials of the cerebral cortex and behavior.**" *Physiological reviews*, vol. 70, no. 1, pp. 1–41, 1990.

[126] J.R. Wolpaw, N. Birbaumer, D.J. McFarland, G. Pfurtscheller, and T.M. Vaughan, "**Brain-computer interfaces for communication and control**", *Clinical neurophysiology*, vol. 113, no. 6, pp. 767–791, 2002. DOI: 10.1016/s1388-2457(02)00057-3.

[127] Niels Birbaumer, Andrea Kubler, Nimr Ghanayim, Thilo Hinterberger, Jouri Perelmouter, Jochen Kaiser, Iver Iversen, Boris Kotchoubey, Nicola Neumann, and Herta Flor, "**The thought translation device (ttd) for completely paralyzed patients**", *IEEE Transactions on rehabilitation Engineering*, vol. 8, no. 2, pp. 190–193, 2000.

[128] Andrea Kübler, Nicola Neumann, Jochen Kaiser, Boris Kotchoubey, Thilo Hinterberger, and Niels P Birbaumer, "**Brain-computer communication: Self-regulation of slow cortical potentials for verbal communication**", *Archives of physical medicine and rehabilitation*, vol. 82, no. 11, pp. 1533–1539, 2001.

[129] Andrea Kübler, Boris Kotchoubey, Thilo Hinterberger, Nimr Ghanayim, Juri Perelmouter, Margarete Schauer, Christoph Fritsch, Edward Taub, and Niels Birbaumer, "**The thought translation device: A neurophysiological approach to communication in total motor paralysis**", *Experimental brain research*, vol. 124, no. 2, pp. 223–232, 1999.

[130] IH Iversen, N Ghanayim, A Kübler, N Neumann, N Birbaumer, and J Kaiser, "**A brain–computer interface tool to assess cognitive functions in completely paralyzed patients with amyotrophic lateral sclerosis**", *Clinical neurophysiology*, vol. 119, no. 10, pp. 2214–2223, 2008.

[131] Ioulietta Lazarou, Spiros Nikolopoulos, Panagiotis C Petrantonakis, Ioannis Kompatsiaris, and Magda Tsolaki, "**Eeg-based brain–computer interfaces for communication and rehabilitation of people with motor impairment: A novel approach of the 21st century**", *Frontiers in human neuroscience*, vol. 12, p. 14, 2018.

[132] Emanuel Donchin and David BD Smith, "**The contingent negative variation and the late positive wave of the average evoked potential**", *Electroencephalography and clinical Neurophysiology*, vol. 29, no. 2, pp. 201–203, 1970.

[133] Roberta Carabalona, Ferdinando Grossi, Adam Tessadri, Antonio Caracciolo, Paolo Castiglioni, and Ilaria De Munari, "**Home smart home: Brain-computer interface control for real smart home environments**", *Proc. of 4th International Convention on Rehabilitation Engineering & Assistive Technology (iCREATe'10). Singapore Therapeutic, Assistive & Rehabilitative Technologies (START) Centre, Kaki Bukit TechPark II,, Singapore,, Article*, vol. 51, 2010.

[134] Roberta Carabalona, Ferdinando Grossi, Adam Tessadri, Paolo Castiglioni, Antonio Caracciolo, and Ilaria de Munari, "**Light on! real world evaluation of a p300-based brain–computer interface (bci) for environment control in a smart home**", *Ergonomics*, vol. 55, no. 5, pp. 552–563, 2012.

[135] Minju Kim, Min-Ki Kim, Minho Hwang, Hyun-Young Kim, Jeongho Cho, and Sung-Phil Kim, "**Online home appliance control using eeg-based brain–computer interfaces**", *Electronics*, vol. 8, no. 10, p. 1101, 2019.

[136] Carolina B Tabernig, Lucía C Carrere, Camila A Lopez, and Carlos Ballario, "**Eeg event-related desynchronization of patients with stroke during motor imagery of hand movement**", *Proc. of Journal of Physics: Conference Series*, IOP Publishing, vol. 705, 2016, p. 012 059.

[137] Gert Pfurtscheller, Ch Neuper, Doris Flotzinger, and Martin Pregenzer, "**Eeg-based discrimination between imagination of right and left hand movement**", *Electroencephalography and clinical Neurophysiology*, vol. 103, no. 6, pp. 642–651, 1997.

[138] Jonathan R Wolpaw, Dennis J McFarland, and Theresa M Vaughan, "**Brain-computer interface research at the wadsworth center**", *IEEE Transactions on Rehabilitation Engineering*, vol. 8, no. 2, pp. 222–226, 2000.

[139] Gert Pfurtscheller, Christa Neuper, GR Muller, Bernhard Obermaier, Gunter Krausz, A Schlogl, Reinhold Scherer, Bernhard Graimann, Claudia Keinrath, Dimitris Skliris, *et al.*, "**Graz-bci: State of the art and clinical applications**", *IEEE Transactions on neural systems and rehabilitation engineering*, vol. 11, no. 2, pp. 1–4, 2003.

[140] Benjamin Blankertz, Florian Losch, Matthias Krauledat, Guido Dornhege, Gabriel Curio, and Klaus-Robert Müller, "**The berlin brain-computer interface: Accurate performance from first-session in bci-naive subjects**", *IEEE transactions on biomedical engineering*, vol. 55, no. 10, pp. 2452–2462, 2008.

[141] Fabien Lotte, "A tutorial on eeg signal-processing techniques for mental-state recognition in brain–computer interfaces", *Guide to Brain-Computer Music Interfacing*, Eduardo Reck Miranda and Julien Castet, Eds. London, Springer London, 2014, pp. 133–161. DOI: 10.1007/978-1-4471-6584-2_7.

[142] Vahid Abootalebi, Mohammad Hassan Moradi, and Mohammad Ali Khalilzadeh, "**A new approach for eeg feature extraction in p300-based lie detection**", *Computer methods and programs in biomedicine*, vol. 94, no. 1, pp. 48–57, 2009.

[143] Ioannis Kalatzis, Nikolaos Piliouras, Eric Ventouras, Charalabos C Papageorgiou, Andreas D Rabavilas, and D Cavouras, "**Design and implementation of an svm-based computer classification system for discriminating depressive patients from healthy controls using the p600 component of erp signals**", *Computer Methods and Programs in Biomedicine*, vol. 75, no. 1, pp. 11–22, 2004.

[144] Neng Xu, Xiaorong Gao, Bo Hong, Xiaobo Miao, Shangkai Gao, and Fusheng Yang, "**Bci competition 2003-data set iib: Enhancing p300 wave detection using ica-based subspace projections for bci applications**", *IEEE transactions on biomedical engineering*, vol. 51, no. 6, pp. 1067–1072, 2004.

[145] D Puthankattil Subha, Paul K Joseph, Rajendra Acharya, and Choo Min Lim, "**Eeg signal analysis: A survey**", *Journal of medical systems*, vol. 34, no. 2, pp. 195–212, 2010.

[146] Nasser Kehtarnavaz, ***Digital signal processing system design: LabVIEW-based hybrid programming***. Elsevier, 2011.

[147] Tom Springer, "Sliding fft computes frequency spectra in real time", *Electronic Circuits, Systems and Standards*, Elsevier, 1991, pp. 40–46.

[148] E. Jacobsen and R. Lyons, "**The sliding dft**", *IEEE Signal Processing Magazine*, vol. 20, no. 2, pp. 74–80, 2003.
DOI: 10.1109/MSP.2003.1184347.

[149] Hojjat Adeli, Ziqin Zhou, and Nahid Dadmehr, "**Analysis of eeg records in an epileptic patient using wavelet transform**", *Journal of neuroscience methods*, vol. 123, no. 1, pp. 69–87, 2003.

[150] Vincent J Samar, Ajit Bopardikar, Raghuveer Rao, and Kenneth Swartz, "**Wavelet analysis of neuroelectric waveforms: A conceptual tutorial**", *Brain and language*, vol. 66, no. 1, pp. 7–60, 1999.

[151] Tapan Gandhi, Bijay Ketan Panigrahi, and Sneh Anand, "**A comparative study of wavelet families for eeg signal classification**", *Neurocomputing*, vol. 74, no. 17, pp. 3051–3057, 2011.

[152] Noor Kamal Al-Qazzaz, Sawal Hamid Bin Mohd Ali, Siti Anom Ahmad, Mohd Shabiul Islam, and Javier Escudero, "**Selection of mother wavelet functions for multi-channel eeg signal analysis during a working memory task**", *Sensors*, vol. 15, no. 11, pp. 29 015–29 035, 2015.

[153] Charles K. Chui, ***An Introduction to Wavelets***. USA, Academic Press Professional, Inc., 1992, ISBN: 0121745848.

[154] Stephane G Mallat, "**A theory for multiresolution signal decomposition: The wavelet representation**", *IEEE transactions on pattern analysis and machine intelligence*, vol. 11, no. 7, pp. 674–693, 1989.

[155] EA Bartnik, Katarzyna J Blinowska, and Piotr J Durka, "**Single evoked potential reconstruction by means of wavelet transform**", *Biological cybernetics*, vol. 67, no. 2, pp. 175–181, 1992.

[156] R Quian Quiroga, OW Sakowitz, E Basar, and M Schürmann, "**Wavelet transform in the analysis of the frequency composition of evoked potentials**", *Brain Research Protocols*, vol. 8, no. 1, pp. 16–24, 2001.

[157] R Quian Quiroga and H Garcia, "**Single-trial event-related potentials with wavelet denoising**", *Clinical Neurophysiology*, vol. 114, no. 2, pp. 376–390, 2003.

[158] Thilo Hinterberger, Andrea Kübler, Jochen Kaiser, Nicola Neumann, and Niels Birbaumer, "**A brain–computer interface (bci) for the locked-in: Comparison of different eeg classifications for the thought translation device**", *Clinical neurophysiology*, vol. 114, no. 3, pp. 416–425, 2003.

[159] Tamer Demiralp, Juliana Yordanova, Vasil Kolev, Ahmet Ademoglu, Müge Devrim, and Vincent J Samar, "**Time–frequency analysis of single-sweep event-related potentials by means of fast wavelet transform**", *Brain and Language*, vol. 66, no. 1, pp. 129–145, 1999.

[160] Wei-Yen Hsu and Yung-Nien Sun, "**Eeg-based motor imagery analysis using weighted wavelet transform features**", *Journal of neuroscience methods*, vol. 176, no. 2, pp. 310–318, 2009.

[161] Lei Qin and Bin He, "**A wavelet-based time–frequency analysis approach for classification of motor imagery for brain–computer interface applications**", *Journal of neural engineering*, vol. 2, no. 4, p. 65, 2005.

[162] Steven J Schiff, Akram Aldroubi, Michael Unser, and Susumu Sato, "**Fast wavelet transformation of eeg**", *Electroencephalography and clinical neurophysiology*, vol. 91, no. 6, pp. 442–455, 1994.

[163] Florian Mormann, Juergen Fell, Nikolai Axmacher, Bernd Weber, Klaus Lehnertz, Christian E Elger, and Guillén Fernández, "**Phase/amplitude reset and theta–gamma interaction in the human medial temporal lobe during a continuous word recognition memory task**", *Hippocampus*, vol. 15, no. 7, pp. 890–900, 2005.

[164] Atsuo Murata, "**An attempt to evaluate mental workload using wavelet transform of eeg**", *Human Factors*, vol. 47, no. 3, pp. 498–508, 2005.

[165] Tatjana Zikov, Stephane Bibian, Guy A Dumont, Mihai Huzmezan, and Craig R Ries, "**A wavelet based de-noising technique for ocular artifact correction of the electroencephalogram**", *Proc. of Second Joint 24th Annual Conference and the Annual Fall Meeting of the Biomedical Engineering Society][Engineering in Medicine and Biology*, IEEE, vol. 1, 2002, pp. 98–105.

[166] Nazareth P Castellanos and Valeri A Makarov, "**Recovering eeg brain signals: Artifact suppression with wavelet enhanced independent component analysis**", *Journal of neuroscience methods*, vol. 158, no. 2, pp. 300–312, 2006.

[167] Keinosuke Fukunaga, *Introduction to statistical pattern recognition*, 1990.

[168] Richard O Duda, Peter E Hart, and David G Stork, ***Pattern classification and scene analysis***. Wiley New York, 1973, vol. 3.

[169] Benjamin Blankertz, Steven Lemm, Matthias Treder, Stefan Haufe, and Klaus-Robert Müller, "**Single-trial analysis and classification of erp components—a tutorial**", *NeuroImage*, vol. 56, no. 2, pp. 814–825, 2011.

[170] Christa Neuper, Gernot R Müller-Putz, Reinhold Scherer, and Gert Pfurtscheller, "**Motor imagery and eeg-based control of spelling devices and neuroprostheses**", *Progress in brain research*, vol. 159, pp. 393–409, 2006.

[171] Gert Pfurtscheller, Teodoro Solis-Escalante, Rupert Ortner, Patricia Linortner, and Gernot R Muller-Putz, "**Self-paced operation of an ssvep-based orthosis with and without an imagery-based "brain switch:" a feasibility study towards a hybrid bci**", *IEEE transactions on neural systems and rehabilitation engineering*, vol. 18, no. 4, pp. 409–414, 2010.

[172] Alberto Dellacasa Bellingegni, Emanuele Gruppioni, Giorgio Colazzo, Angelo Davalli, Rinaldo Sacchetti, Eugenio Guglielmelli, and Loredana Zollo, "**Nlr, mlp, svm, and lda: A comparative analysis on emg data from people with trans-radial amputation**", *Journal of neuroengineering and rehabilitation*, vol. 14, no. 1, pp. 1–16, 2017.

[173] Vladimir N Vapnik, ***The nature of statistical learning theory***. Springer, 1995.

[174] Christopher JC Burges, "**A tutorial on support vector machines for pattern recognition**", *Data mining and knowledge discovery*, vol. 2, no. 2, pp. 121–167, 1998.

[175] S. Sanei and J.A. Chambers, ***EEG signal processing***. John Wiley & Sons, 2013.

[176] Manoj Thulasidas, Cuntai Guan, and Jiankang Wu, "**Robust classification of eeg signal for brain-computer interface**", *IEEE Transactions on Neural Systems and Rehabilitation Engineering*, vol. 14, no. 1, pp. 24–29, 2006.

[177] Alain Rakotomamonjy and Vincent Guigue, "**Bci competition iii: Dataset ii-ensemble of svms for bci p300 speller**", *IEEE transactions on biomedical engineering*, vol. 55, no. 3, pp. 1147–1154, 2008.

[178] Matthias Kaper, Peter Meinicke, Ulf Grossekathoefer, Thomas Lingner, and Helge Ritter, "**Bci competition 2003-data set iib: Support vector machines for the p300 speller paradigm**", *IEEE Transactions on biomedical Engineering*, vol. 51, no. 6, pp. 1073–1076, 2004.

[179] Alois Schlögl, Felix Lee, Horst Bischof, and Gert Pfurtscheller, "**Characterization of four-class motor imagery eeg data for the bci-competition 2005**", *Journal of neural engineering*, vol. 2, no. 4, p. L14, 2005.

[180] Siuly Siuly and Yan Li, "**Improving the separability of motor imagery eeg signals using a cross correlation-based least square support vector machine for brain–computer interface**", *IEEE Transactions on Neural Systems and Rehabilitation Engineering*, vol. 20, no. 4, pp. 526–538, 2012.

[181] Ignas Martišius and Robertas Damaševičius, "**A prototype ssvep based real time bci gaming system**", *Computational intelligence and neuroscience*, vol. 2016, 2016.
DOI: 10.1155/2016/3861425.

[182] Yuanqing Li, Jiahui Pan, Fei Wang, and Zhuliang Yu, "**A hybrid bci system combining p300 and ssvep and its application to wheelchair control**", *IEEE Transactions on Biomedical Engineering*, vol. 60, no. 11, pp. 3156–3166, 2013.

[183] Jinyi Long, Yuanqing Li, Tianyou Yu, and Zhenghui Gu, "**Target selection with hybrid feature for bci-based 2-d cursor control**", *IEEE Transactions on biomedical engineering*, vol. 59, no. 1, pp. 132–140, 2011.

[184] Chong Sun Hong, "**Optimal threshold from roc and cap curves**", *Communications in Statistics-Simulation and Computation*, vol. 38, no. 10, pp. 2060–2072, 2009.

[185] Zhenchong Zhao and Xiaodan Wang, "**A research of optimal rejection thresholds based on roc curve**", *Proc. of 2014 12th International Conference on Signal Processing (ICSP)*, IEEE, 2014, pp. 1403–1407.

[186] Ignazio Pillai, Giorgio Fumera, and Fabio Roli, "**Threshold optimisation for multi-label classifiers**", *Pattern Recognition*, vol. 46, no. 7, pp. 2055–2065, 2013.

[187] L. Kirkup, A. Searle, A. Craig, P. McIsaac, and P. Moses, "**EEG-based system for rapid on-off switching without prior learning**", *Medical and Biological Engineering and Computing*, vol. 35, no. 5, pp. 504–509, 1997.
DOI: 10.1007/BF02525531.

[188] Ping Wan, Chaozhong Wu, Yingzi Lin, and Xiaofeng Ma, "**Optimal threshold determination for discriminating driving anger intensity based on eeg wavelet features and roc curve analysis**", *Information*, vol. 7, no. 3, p. 52, 2016.

[189] J. Ma, Y. Zhang, A. Cichocki, and F. Matsuno, "**A novel EOG/EEG hybrid human–machine interface adopting eye movements and erps: Application to robot control**", *IEEE Transactions on Biomedical Engineering*, vol. 62, no. 3, pp. 876–889, 2015.
DOI: 10.1109/TBME.2014.2369483.

[190] T.K. Reddy and L. Behera, "**Online eye state recognition from EEG data using deep architectures**", *Proc. of 2016 IEEE International Conference on Systems, Man, and Cybernetics (SMC)*, 2016, pp. 712–717.
DOI: 10.1109/SMC.2016.7844325.

[191] T. Wang, S.U. Guan, K.L. Man, and T.O. Ting, "**Time series classification for EEG eye state identification based on incremental attribute learning**", *Proc. of 2014 International Symposium on Computer, Consumer and Control (IS3C)*, 2014, pp. 158–161.
DOI: 10.1109/IS3C.2014.52.

[192] P.A. Estévez, C.M. Held, C.A. Holzmann, C.A. Perez, J.P. Pérez, J. Heiss, M. Garrido, and P. Peirano, "**Polysomnographic pattern recognition for automated classification of sleep-waking states in infants**", *Medical and Biological Engineering and Computing*, vol. 40, no. 1, pp. 105–113, 2002.
DOI: 10.1007/bf02347703.

[193] N. Sulaiman, M.N. Taib, S. Lias, Z. Hj Murat, S.A.M. Aris, and N.H.A. Hamid, "**Novel methods for stress features identification using EEG signals**", *International Journal of Simulation: Systems, Science and Technology*, vol. 12, no. 1, pp. 27–33, 2011.
DOI: 10.5013/IJSSST.a.12.01.04.

[194] E.D. Adrian and B.H.C. Matthews, "**The berger rhythm: Potential changes from the occipital lobes in man**", *Brain*, vol. 57, no. 4, pp. 355–385, 1934.
DOI: 10.1093/brain/57.4.355.

[195] T. Cao, F. Wan, C.M. Wong, da Cruz J.N., and Y. Hu, "**Objective evaluation of fatigue by EEG spectral analysis in steady-state visual evoked potential-based brain-computer interfaces**", *BioMedical Engineering*, vol. 13, 28, pp. 1–13, 2014.
DOI: 10.1186/1475-925X-13-28.

[196] J.B. Barry and F.M. De Blasio, "**EEG differences between eyes-closed and eyes-open resting remain in healthy ageing**", *Biological Psychology*, vol. 129, pp. 293–304, 2017.
DOI: 10.1016/j.biopsycho.2017.09.010.

[197] Mohammad Ali Naderi and Homayoun Mahdavi-Nasab, "**Analysis and classification of eeg signals using spectral analysis and recurrent neural networks**", *Proc. of 2010 17th Iranian Conference of Biomedical Engineering (ICBME)*, IEEE, 2010, pp. 1–4.

[198] U Rajendra Acharya, Shu Lih Oh, Yuki Hagiwara, Jen Hong Tan, and Hojjat Adeli, "**Deep convolutional neural network for the automated detection and diagnosis of seizure using eeg signals**", *Computers in biology and medicine*, vol. 100, pp. 270–278, 2018.

[199] Oliver Rösler and David Suendermann, "**A first step towards eye state prediction using eeg**", *Proc. of the AIHLS*, vol. 1, pp. 1–4, 2013.

[200] A. Saghafi, C.P. Tsokos, M. Goudarzi, and H. Farhidzadeh, "**Random eye state change detection in real-time using eeg signals**", *Expert Systems with Applications*, vol. 72, no. 1, pp. 42–48, 2017.
DOI: 10.1016/j.eswa.2016.12.010.

[201] Cameron R Hamilton, Shervin Shahryari, and Khaled M Rasheed, "**Eye state prediction from eeg data using boosted rotational forests**", *Proc. of 2015 IEEE 14th International Conference on Machine Learning and Applications (ICMLA)*, IEEE, 2015, pp. 429–432.

[202] Francisco Laport, Francisco J. Vazquez-Araujo, Paula M. Castro, and Adriana Dapena, "**Hardware and software for integrating brain–computer interface with internet of things**", *Proc. of Understanding the Brain Function and Emotions*, José Manuel Ferrández Vicente, José Ramón Álvarez-Sánchez, Félix de la Paz López, Javier Toledo Moreo, and Hojjat Adeli, Eds., Cham, Springer International Publishing, 2019, pp. 22–31, ISBN: 978-3-030-19591-5.

[203] Francisco Laport, Adriana Dapena, Paula M. Castro, Francisco J. Vazquez-Araujo, and Daniel Iglesia, "**A prototype of eeg system for iot**", *International journal of neural systems*, vol. 30, no. 07, p. 2 050 018, 2020.

[204] Francisco Laport, Francisco J. Vazquez-Araujo, Paula M. Castro, and Adriana Dapena, "**Brain-computer interfaces for internet of things**", *Proceedings*, vol. 2, no. 18, p. 59, 2018.
DOI: 10.3390/proceedings2181179.

[205] Francisco Laport, Francisco J. Vazquez-Araujo, Daniel Iglesia, Paula M. Castro, and Adriana Dapena, "**A comparative study of low cost open source eeg devices**", *Proceedings*, vol. 21, no. 1, p. 116, 2019.
DOI: 10.3390/proceedings2019021040.

[206] Francisco Laport, Paula M. Castro, Adriana Dapena, Francisco J. Vazquez-Araujo, and Daniel Iglesia, "**Study of machine learning techniques for eeg eye state detection**", *Proceedings*, vol. 54, no. 1, p. 168, 2020.
DOI: 10.3390/proceedings2020054053.

[207] Francisco Laport, Adriana Dapena, Paula M. Castro, and Francisco J. Vazquez-Araujo, "**Comparison of sliding transforms and discrete wavelet transforms to detect eye states**", *Proc. of XXXV SIMPOSIUM NACIONAL DE LA UNIÓN CIENTÍFICA INTERNACIONAL DE RADIO (URSI 2020)*, Málaga, Spain, 2020, pp. 1–4.

[208] Francisco Laport, Francisco J. Vazquez-Araujo, Paula M. Castro, and Adriana Dapena, "**Estudio de la dft deslizante para clasificación de estados oculares con bajo retardo**", *Proc. of XXXIV SIMPOSIUM NACIONAL DE LA UNIÓN CIENTÍFICA INTERNACIONAL DE RADIO (URSI 2019)*, Sevilla, Spain, 2019, pp. 1–4.

[209] R.P. Sallen and E.L. Key, "**A practical method of designing rc active filters**", *IRE Transactions on Circuit Theory*, vol. 2, no. 1, pp. 74–85, 1955.
DOI: 10.1109/TCT.1955.6500159.

[210] CO. ESPRESSIF SYSTEMS (SHANGHAI), **Esp32-wroom-32 datasheet**, https://www.espressif.com/sites/default/files/documentation/esp32-wroom-32_datasheet_en.pdf/.

[211] Park C.S., "**Recursive algorithm for sliding walsh hadamard transform**", *IEEE Transactions on Signal Processing*, vol. 62, no. 11, pp. 2827–2836, 2014.
DOI: 10.1109/TSP.2014.2316146.

[212] J.M. Robinson, J.G. Frey, A.J. Stanford-Clark, A.D. Reynolds, and B.V. Bedi, "**Sensor networks and grid middleware for laboratory monitoring**", *Proc. of First International Conference on e-Science and Grid Computing*, 2005, p. 8.
DOI: 10.1109/E-SCIENCE.2005.73.

[213] Daria La Rocca, Patrizio Campisi, and Gaetano Scarano, "**Eeg biometrics for individual recognition in resting state with closed eyes**", *Proc. of 2012 International Conference of Biometrics Special Interest Group (BIOSIG)*, IEEE, 2012, pp. 1–12.

[214] Anthony Gale, Naomi Dunkin, and Michael Coles, "**Variation in visual input and the occipital eeg**", *Psychonomic Science*, vol. 14, no. 6, pp. 262–263, 1969.

[215] Mikito Ogino and Yasue Mitsukura, "**Portable drowsiness detection through use of a prefrontal single-channel electroencephalogram**", *Sensors*, vol. 18, no. 12, p. 4477, 2018.

[216] Jasper Snoek, Hugo Larochelle, and Ryan P Adams, "**Practical bayesian optimization of machine learning algorithms**", *Proc. of Advances in neural information processing systems*, 2012, pp. 2951–2959.

[217] Inc. Eclipse Foundation, **Eclipse mosquitto**, https://mosquitto.org/.

[218] OASIS Standard, **Mqtt version 3.1.1**, http://docs.oasis-open.org/mqtt/mqtt/v3.1.1/mqtt-v3.1.1.html.

[219] Oliver Faust, U Rajendra Acharya, Hojjat Adeli, and Amir Adeli, "**Wavelet-based eeg processing for computer-aided seizure detection and epilepsy diagnosis**", *Seizure*, vol. 26, pp. 56–64, 2015.

[220] Wu Ting, Yan Guo-Zheng, Yang Bang-Hua, and Sun Hong, "**Eeg feature extraction based on wavelet packet decomposition for brain computer interface**", *Measurement*, vol. 41, no. 6, pp. 618–625, 2008.

[221] F Sherwani, Shahnoor Shanta, BSKK Ibrahim, and M Saiful Huq, "**Wavelet based feature extraction for classification of motor imagery signals**", *Proc. of 2016 IEEE EMBS Conference on Biomedical Engineering and Sciences (IECBES)*, IEEE, 2016, pp. 360–364.

[222] Abdulhamit Subasi, "**Eeg signal classification using wavelet feature extraction and a mixture of expert model**", *Expert Systems with Applications*, vol. 32, no. 4, pp. 1084–1093, 2007.

[223] Sravanth K Ramakuri, Chinmay Chakraborty, Sanchita Ghosh, and Bharat Gupta, "**Performance analysis of eye-state charecterization through single electrode eeg device for medical application**", *Proc. of 2017 Global Wireless Summit (GWS)*, IEEE, 2017, pp. 1–6.

[224] H Hindarto, A Muntasa, and S Sumarno, "**Feature extraction electroencephalogram (eeg) using wavelet transform for cursor movement**", *Proc. of IOP Conference Series: Materials Science and Engineering*, IOP Publishing, vol. 434, 2018, p. 012 261.

[225] Mohd Syakir Fathillah, Rosmina Jaafar, Kalaivani Chellappan, and Rabani Remli, "**A study on eeg signals during eye-closed and eye-open using discrete wavelet transform**", *Proc. of 2016 IEEE EMBS Conference on Biomedical Engineering and Sciences (IECBES)*, IEEE, 2016, pp. 674–678.

[226] Reza Fazel-Rezai, Brendan Z Allison, Christoph Guger, Eric W Sellers, Sonja C Kleih, and Andrea Kübler, "**P300 brain computer interface: Current challenges and emerging trends**", *Frontiers in neuroengineering*, vol. 5, p. 14, 2012.

[227] Emanuel Donchin, Kevin M Spencer, and Ranjith Wijesinghe, "**The mental prosthesis: Assessing the speed of a p300-based brain-computer interface**", *IEEE transactions on rehabilitation engineering*, vol. 8, no. 2, pp. 174–179, 2000.

[228] Ulrich Hoffmann, Jean-Marc Vesin, Touradj Ebrahimi, and Karin Diserens, "**An efficient p300-based brain–computer interface for disabled subjects**", *Journal of Neuroscience methods*, vol. 167, no. 1, pp. 115–125, 2008.

[229] Hamed Mirghasemi, Reza Fazel-Rezai, and Mohammad B Shamsollahi, "**Analysis of p300 classifiers in brain computer interface speller**", *Proc. of 2006 International Conference of the IEEE Engineering in Medicine and Biology Society*, IEEE, 2006, pp. 6205–6208.

[230] KA Colwell, DB Ryan, CS Throckmorton, EW Sellers, and LM Collins, "**Channel selection methods for the p300 speller**", *Journal of neuroscience methods*, vol. 232, pp. 6–15, 2014.

[231] Songyun Xie, You Wu, Yunpeng Zhang, Juanli Zhang, and Chang Liu, "**Single channel single trial p300 detection using extreme learning machine: Compared with bpnn and svm**", *Proc. of 2014 International Joint Conference on Neural Networks (IJCNN)*, IEEE, 2014, pp. 544–549.

[232] Neda Haghighatpanah, Rasoul Amirfattahi, Vahid Abootalebi, and Behzad Nazari, "**A single channel-single trial p300 detection algorithm**", *Proc. of 2013 21st Iranian Conference on Electrical Engineering (ICEE)*, IEEE, 2013, pp. 1–5.

[233] F Aloise, F Schettini, P Aricò, F Leotta, S Salinari, D Mattia, F Babiloni, and F Cincotti, "**P300-based brain–computer interface for environmental control: An asynchronous approach**", *Journal of neural engineering*, vol. 8, no. 2, p. 025 025, 2011.

[234] Rebeca Corralejo, Luis F Nicolás-Alonso, Daniel Álvarez, and Roberto Hornero, "**A p300-based brain–computer interface aimed at operating electronic devices at home for severely disabled people**", *Medical & biological engineering & computing*, vol. 52, no. 10, pp. 861–872, 2014.

[235] Francesca Schettini, Angela Riccio, Luca Simione, Giulia Liberati, Mario Caruso, Vittorio Frasca, Barbara Calabrese, Massimo Mecella, Alessia Pizzimenti, Maurizio Inghilleri, *et al.*, "**Assistive device with conventional, alternative, and brain-computer interface inputs to enhance interaction with the environment for people with amyotrophic lateral sclerosis: A feasibility and usability study**", *Archives of physical medicine and rehabilitation*, vol. 96, no. 3, S46–S53, 2015.

[236] Eda Akman Aydin, Omer Faruk Bay, and Inan Guler, "**P300-based asynchronous brain computer interface for environmental control system**", *IEEE journal of biomedical and health informatics*, vol. 22, no. 3, pp. 653–663, 2017.

[237] Yajun Zhou, Shenghong He, Qiyun Huang, and Yuanqing Li, "**A hybrid asynchronous brain-computer interface combining ssvep and eog signals**", *IEEE Transactions on Biomedical Engineering*, vol. 67, no. 10, pp. 2881–2892, 2020.

[238] Xuhong Guo, Weihua Pei, Yijun Wang, Yuanfang Chen, He Zhang, Xian Wu, Xiaowei Yang, Hongda Chen, Yuanyuan Liu, and Ruicong Liu, "**A human-machine interface based on single channel eog and patchable sensor**", *Biomedical Signal Processing and Control*, vol. 30, pp. 98–105, 2016.

[239] Jeong Heo, Heenam Yoon, and Kwang Suk Park, "**A novel wearable forehead eog measurement system for human computer interfaces**", *Sensors*, vol. 17, no. 7, p. 1485, 2017.

[240] Francisco Laport, Daniel Iglesia, Adriana Dapena, Paula M. Castro, and Francisco J. Vazquez-Araujo, "**Proposals and comparisons from one-sensor eeg and eog human-machine interfaces**", *Sensors*, vol. 21, no. 6, p. 2220, 2021.

[241] Open Science Tools Ltd., **Psychopy python package**, https://www.psychopy.org/.

[242] Dean J Krusienski, Eric W Sellers, Dennis J McFarland, Theresa M Vaughan, and Jonathan R Wolpaw, "**Toward enhanced p300 speller performance**", *Journal of neuroscience methods*, vol. 167, no. 1, pp. 15–21, 2008.

[243] Terence W Picton, "**The p300 wave of the human event-related potential**", *Journal of clinical neurophysiology*, vol. 9, no. 4, pp. 456–479, 1992.

[244] Kara Morgan-Short and Darren Tanner, "Event-related potentials (erps)", *Research methods in second language psycholinguistics*, Routledge New York, 2013, pp. 143–168.

[245] Leif Sörnmo and Pablo Laguna, "Chapter 4 - evoked potentials", *Bioelectrical Signal Processing in Cardiac and Neurological Applications*, ser. Biomedical Engineering, Leif Sörnmo and Pablo Laguna, Eds., Burlington, Academic Press, 2005, pp. 181–336, ISBN: 978-0-12-437552-9.
DOI: 10.1016/B978-012437552-9/50004-0.

[246] Shang-Lin Wu, Lun-De Liao, Shao-Wei Lu, Wei-Ling Jiang, Shi-An Chen, and Chin-Teng Lin, "**Controlling a human–computer interface system with a novel classification method that uses electrooculography signals**", *IEEE transactions on Biomedical Engineering*, vol. 60, no. 8, pp. 2133–2141, 2013.

[247] Won-Du Chang, Ho-Seung Cha, Kiwoong Kim, and Chang-Hwan Im, "**Detection of eye blink artifacts from single prefrontal channel electroencephalogram**", *Computer methods and programs in biomedicine*, vol. 124, pp. 19–30, 2016.

[248] Craig N Karson, Karen Faith Berman, Edward F Donnelly, Wallace B Mendelson, Joel E Kleinman, and Richard Jed Wyatt, "**Speaking, thinking, and blinking**", *Psychiatry research*, vol. 5, no. 3, pp. 243–246, 1981.

[249] John Polich, "**Updating p300: An integrative theory of p3a and p3b**", *Clinical neurophysiology*, vol. 118, no. 10, pp. 2128–2148, 2007.

[250] Ivar Reinvang, "**Cognitive event-related potentials in neuropsychological assessment**", *Neuropsychology Review*, vol. 9, no. 4, pp. 231–248, 1999.

[251] Michael Houlihan, Robert Stelmack, and Kenneth Campbell, "**Intelligence and the effects of perceptual processing demands, task difficulty and processing speed on p300, reaction time and movement time**", *Intelligence*, vol. 26, no. 1, pp. 9–25, 1998.

[252] Anders M Fjell and Kristine B Walhovd, "**P300 and neuropsychological tests as measures of aging: Scalp topography and cognitive changes**", *Brain Topography*, vol. 14, no. 1, pp. 25–40, 2001.

[253] John Polich, "**Meta-analysis of p300 normative aging studies**", *Psychophysiology*, vol. 33, no. 4, pp. 334–353, 1996.

[254] Francisco Laport, Paula M. Castro, Adriana Dapena, Francisco J. Vazquez-Araujo, and Oscar Fresnedo, "**Eye state identification based on discrete wavelet transforms**", *Applied Sciences*, vol. 11, no. 11, p. 5051, 2021.

[255] Francisco Laport, Paula M. Castro, Francisco J. Vazquez-Araujo, Adriana Dapena, and José Juan Lamas-Seco, "**Extracción y clasificación de características a partir de señales eeg**", *Proc. of XXXIII SIMPOSIUM NACIONAL DE LA UNIÓN CIENTÍFICA INTERNACIONAL DE RADIO (URSI 2018)*, Granada, Spain, 2018, pp. 1–4.